Review

Carbon dioxide capture-related gas adsorption and separation in metal-organic frameworks

Jian-Rong Li[a], Yuguang Ma[b], M. Colin McCarthy[b], Julian Sculley[a], Jiamei Yu[b,c], Hae-Kwon Jeong[b,c,*], Perla B. Balbuena[b,c,*], Hong-Cai Zhou[a,c,**]

[a] Department of Chemistry, Texas A&M University, College Station, TX 77842-3012, USA
[b] Artie McFerrin Department of Chemical Engineering, Texas A&M University, College Station, TX 77843-3122, USA
[c] Materials Science and Engineering Program, Texas A&M University, College Station, TX 77843-3003, USA

Contents

* Corresponding authors at: Artie McFerrin Department of Chemical Engineering, Texas A&M University, PO Box 30012, College Station, TX 77842-3012, USA.
** Corresponding author at: Department of Chemistry, Texas A&M University, PO Box 30012, College Station, TX 77842-3012, USA. Tel.: +1 979 845 4034; fax: +1 979 845 1595.
    E-mail addresses: zhou@mail.chem.tamu.edu, zhouh@tamu.edu (H.-C. Zhou).

A B S T R A C T

Reducing anthropogenic CO_2 emission and lowering the concentration of greenhouse gases in the atmosphere has quickly become one of the most urgent environmental issues of our age. Carbon capture and storage (CCS) is one option for reducing these harmful CO_2 emissions. While a variety of technologies and methods have been developed, the separation of CO_2 from gas streams is still a critical issue. Apart from establishing new techniques, the exploration of capture materials with high separation performance and low capital cost are of paramount importance. Metal-organic frameworks (MOFs), a new class of crystalline porous materials constructed by metal-containing nodes bonded to organic bridging ligands hold great potential as adsorbents or membrane materials in gas separation. In this paper, we review the research progress (from experimental results to molecular simulations) in MOFs for CO_2 adsorption, storage, and separations (adsorptive separation and membrane-based separation) that are directly related to CO_2 capture.

1. Introduction

With the rapid increase of the global population and the industrialization of more and more countries, the consumption of energy is explosively growing. Currently over 85% of the global energy demand is being supported by the burning of fossil fuels [1]. The reasons for this skewed reliance on fossil fuels as our primary energy source is due to the inherent energy density, abundance, and the economic dependence of modern society on the acquisition and trade of these resources. Fossil fuels will continue to play an important role in the foreseeable future, mainly in power generation and industrial manufacturing. The burning of these fossil fuels releases large amounts of CO_2 into the atmosphere; this disturbs the carbon balance of our planet which has been steady over hundreds of millions of years. Although anthropogenic CO_2 emissions are relatively small compared to the natural carbon fluxes, such as photosynthetic fluxes, the increased release has had obvious influences on the global climate in a very short period of time [1,2]. Since the beginning of the industrial age in ca. 1750, the CO_2 concentration in atmosphere has increased from 280 to 390 ppm in 2010 (Fig. 1) [1]. The increase of the CO_2 concentration in atmosphere influences the balance of incoming and outgoing energy in the atmosphere system, leading to the raise of average surface temperature of earth. Thus, CO_2 has often been cited as the primary anthropogenic greenhouse gas (GHG) as well as the leading culprit in climate change. Although there are many uncertainties, it is beyond all doubt that strategies to reduce CO_2 emissions are urgently required to minimize climate change.

The ultimate goal of a green society will only be achieved when we relinquish our dependence on fossil fuels in favor of clean energy sources such as hydrogen fuel or solar energy. In the interim period to a low-carbon society, however, it is imperative to reduce anthropogenic CO_2 emission [3]. The estimation from the Intergovernmental Panel on Climate Change (IPCC) has shown that CO_2 emissions could be reduced by 80–90% for a modern power plant that is equipped with suitable carbon dioxide capture and storage (CCS) technologies [4]. The use of CCS will also complement other crucial strategies, such as switching to less carbon fuels, improving energy efficiency, and phasing in the use of renewable energy resources.
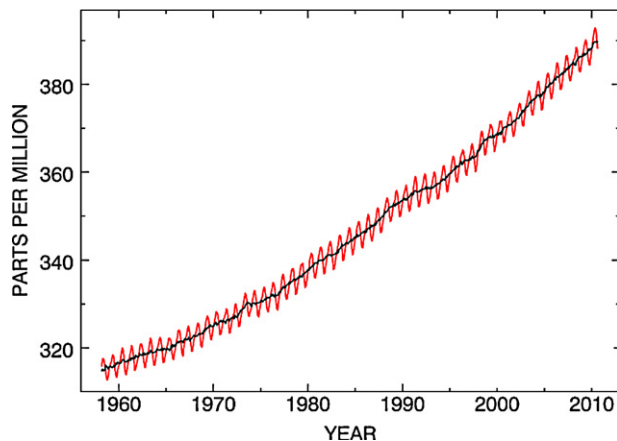

Fig. 1. Atmospheric CO_2 concentration during 1958–2010 (at Mauna Loa Observatory), showing the continuing and accelerating increase of CO_2 in atmosphere. Reproduced with permission [6].
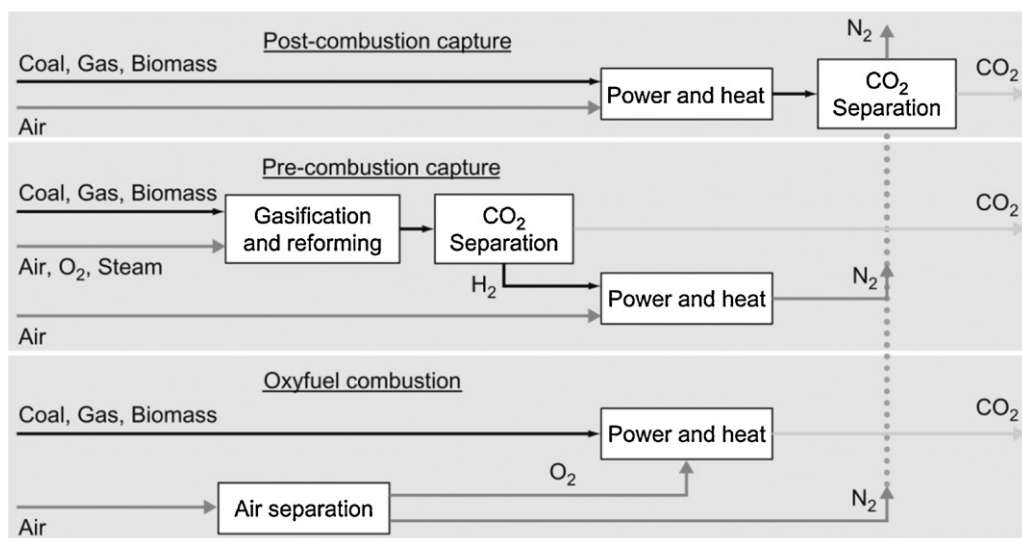
Fig. 2. Three options for CO_2 capture from power generation plants.

Reproduced with permission from Ref. [1].

CCS is a three-step process including CO_2 capture, a process consisting of separating CO_2 from other emissions before it enters the atmosphere; CO_2 transportation to a storage site; and its permanent storage. The transportation and storage of CO_2 are relatively mature technologies and a growing number of fully integrated CCS projects have reached the pilot-stage prior to commercialization [5]. However, the considerable cost of capture, approximately two thirds of the total cost for CCS (primarily separating CO_2 from other gases), is slowing down the deployment of commercial CCS projects. In the majority of the proposed technologies, one significant contributor to lower cost is the maximum separation efficiency that can be achieved by a given capture material. Thus, the discovery of new materials with high separation ability becomes one of the biggest challenges. Several monographs have been published on this topic, where basic knowledge, progress, and perspective for CCS were presented by experts in this field [1–3,5].

1.1. Technologies/methods and materials in CO_2 capture

Exploring cost-effective and scalable technologies and methods for CO_2 capture from power generation and industrial operation where CO_2 is produced on the combustion of fossil fuels is regarded as the most effective strategy in controlling anthropogenic CO_2 emission. Depending on the generation of CO_2, several capture options and tendentious technologies have been suggested and implemented. Generally, based on the fundamental chemical process involved in the combustion of fossil fuels, three basic CO_2 separation and capture options were adopted: (1) pre-combustion capture; (2) oxy-fuel combustion; and (3) post-combustion capture [1]. As an example, the three options for CO_2 capture from power generation plants are illustrated schematically in Fig. 2.

Pre-combustion capture involves the reaction of a primary fuel with oxygen or air to produce H_2. In some cases the produced gas mixture is mainly composed of CO and H_2, which is known as synthesis gas (syngas). The CO formed is further reacted with steam in a catalytic reactor, called a shift converter, to give CO_2 and more H_2. The separation of CO_2 and H_2 then can be achieved by a number of technologies. Pre-combustion has the advantage of lower energy requirements, but the temperature and efficiency associated with H_2-rich gas turbine fuel is a big problem. More challenging issues are the enormous capital cost and the public resistance for new construction. Chemical looping cycles are being investigated as an alternative method to generate syngas [7].

Oxy-fuel combustion has the stringent requirement of nearly pure oxygen, rather than air, for the combustion of fuels; the advantage here being that the gaseous product is nearly pure CO_2, which can be directly stored. The drawback of this option is the requirement of pure oxygen, which can usually be obtained by the separation of air or by other novel techniques that are available. However, the conventional cryogenic air separation to produce O_2 contributes to the high capital cost for this option.

Post-combustion capture requires removing CO_2 from flue gas, comprised mainly of N_2 and CO_2, before emission into the atmosphere. Post-combustion capture is the most feasible on a short time scale because many of the proposed technologies can be retrofitted to existing fossil fuel consuming power plants. One such new approach involves also using cooled and CO_2-rich flue gases to feed bioreactors to produce microalgal biomass that would be used as a biofuel. An additional advantage of post-combustion capture is that even if when the CO_2 capture unit is shut down for an emergency, one can still generate electricity, which is not possible with the other more integrated capture methods. Post-combustion methods have been deployed commercially, primarily for the removal of minor contaminants such as Hg and SO_x/NO_x gas, but the materials for the CO_2 separation require modification, especially those with high preparation and regeneration costs.

A further advantage of developing CO_2 separation techniques is their application in the purification of natural gas (mainly CH_4), which is typically soured with over 40% CO_2 and N_2 and is only useable at low concentrations of CO_2. One of the challenges in this separation is the special technologies and materials that are required to withstand the high pressures that are present during the mining of natural gas [8,9].

Fig. 3 schematically illustrates the technologies and method usually used in CO_2 separation; in each case, except for cryogenic separation, different materials are required as the carriers.

Absorption (i.e. solvent scrubbing) is a well-established CO_2 separation approach used in the chemical and petroleum industries today. Absorption falls into two categories: (1) physical, which is temperature and pressure dependent (absorption occurs at high pressures and low temperatures) and (2) chemical where absorption of CO_2 depends on the acid–base neutralization reaction (in this case caustic solvents are required). Some of the preferred solvents are amines (such as monoethanolamine), ammonia solutions, Selexol, Rectisol, and fluorinated solvents. The most recent addition is ionic liquids, which have exhibited great poten-
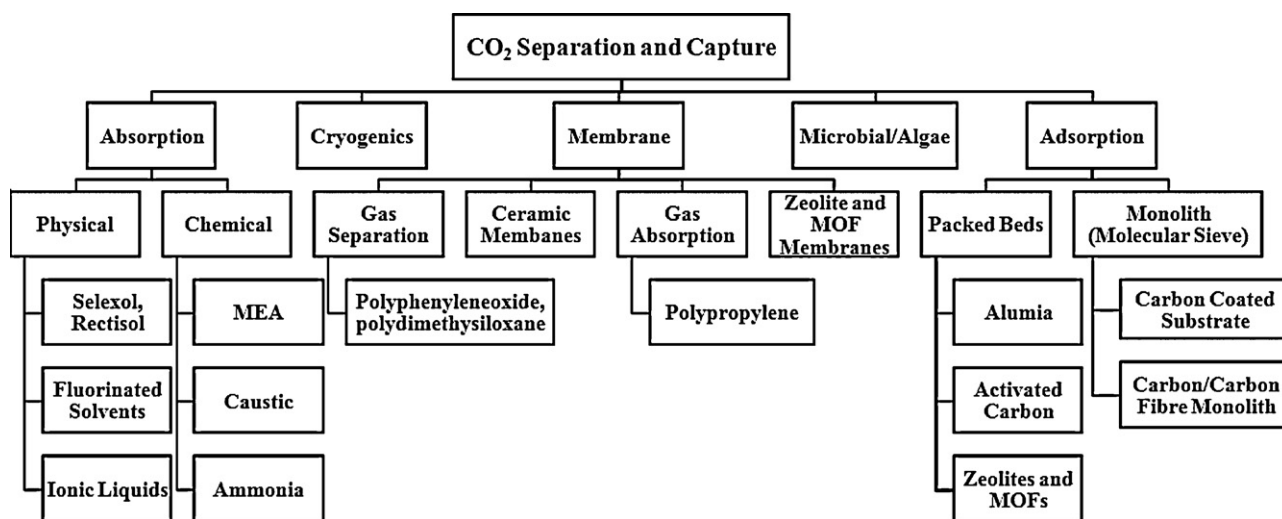
Fig. 3. Different technologies and associated materials for CO_2 separation and capture.

(modified from Ref. [10]).

tial in absorption of CO_2 and are also environmentally benign [11,12].

Cryogenic distillation uses a principle of separation based on cooling and condensation, and has been used in liquid separations for a long time. This technique is theoretically sound for CO_2 separation, however, the considerable energy demand deems it unreasonable for practical application. This method is more effective when the gas stream contains high CO_2 concentration and it can be adopted in oxygen production for oxyfuel combustion. It is presently the most widely used system for the large-scale production of O_2 from the separation of air.

Membrane-based separation is based on the differences in physical and/or chemical interactions between gases and the membrane material, which can be modified to allow some components to pass preferentially through the membrane based on size (kinetic) and/or affinity (thermodynamics). Membranes have great potential in CO_2/H_2 separation in pre-combustion capture and post-combustion CO_2/N_2 separation. A wide variety of different membrane materials and processes are available, some of which already on an industrial scale, and potentially applicable in CO_2 separation. The performance and associated cost of these membrane-based technologies in large scale CO_2 capture mainly relies on the membrane materials themselves. Inorganic ceramic membranes and organic polymeric membranes have been used in CO_2 separation from flue gas in post-combustion. However, reaching a high degree of CO_2 separation by using single-stage ceramic or polymeric membrane is difficult as of yet (although it is feasible in terms of cost). New materials are still required to achieve the desired effectiveness in CO_2 separation by membranes.

Gas separation based on adsorption has been well developed, in which the selection of a sound adsorbent is the key for specific separation. Although materials for gas adsorptive separation have been established and a diverse range of useful sorbents are available for CO_2 separation, there is still plenty of room to optimize the performance of these materials and investigate a wider range of new sorbents. These adsorbents can then be combined with a broad range of process options yielding a fertile field for the optimization of separation performance. Conventional solid adsorbents include activated carbons, silica gel, ion-exchange resins, zeolites, and meso-porous silicates, activated alumina, metal oxides, and other surface-modified porous media. In recent years, a few of new adsorbents such as carbon fibres and their composites as well as metal-organic frameworks have been developed for gas separation. A recent review has comprehensively described the adsorbent

materials for CO_2 capture from large anthropogenic point sources [13]. Depending on the regeneration methods, several adsorption processes can been adopted to achieve CO_2 separation, including (1) vacuum and pressure swing adsorption (VSA and PSA), (2) temperature swing adsorption (TSA), (3) electric swing adsorption (ESA), (4) simulated moving bed (SMB), and (5) purge displacement.

Apart from physical and chemical methods mentioned above, biological methods have also been proposed for CO_2 separation [14,15]. Algal bio-fixation of CO_2 in photo-bioreactors has, for example, recently gained great interest in CO_2 capture. In addition, attempts using chemoautotrophic microorganisms which use inorganic chemicals instead of light energy for CO_2 removal have also been investigated [16].

It is evident that the progress and achievement of almost all of these technologies relies heavily on the development of materials. The challenges that arise in the development of these materials and techniques lies in being able to transfer the technology from the lab to the harsh conditions that it will be subjected to while maximizing efficiency and minimizing costs.

1.2. Advances and challenges in CO_2 capture

CCS is a fast growing field of research and a broad range of technologies are being explored and developed on a daily basis. A few technologies have already reached the deployment stage, but most require further improvements to the technical capabilities and reduction in the associated costs. The most mature technology, post-combustion amine absorption, has been employed in industry for a long time [17]. Simultaneously, a number of materials are available for different technologies and some new materials are emerging. However, the commercialization of any one these technologies still faces substantial challenges not only in the final technological and processes aspects but also in the capabilities of the capture materials themselves.

Up to date, three options have developed to a stage commercially viable, namely post-combustion CO_2 capture using amine solvents based on chemical absorption, oxyfuel combustion, and calcium looping [18]. The membrane-based separation and adsorption of CO_2 into advanced sorbents, such as zeolites and metal-organic frameworks (MOFs), have become intense research subjects in the last ten years. Tuning the properties of traditional adsorbents can be quite challenging which is why these new, advanced sorbents have become such a hot topic. Since separation is a combination of a kinetic (diffusion selectivity) and a thermo-
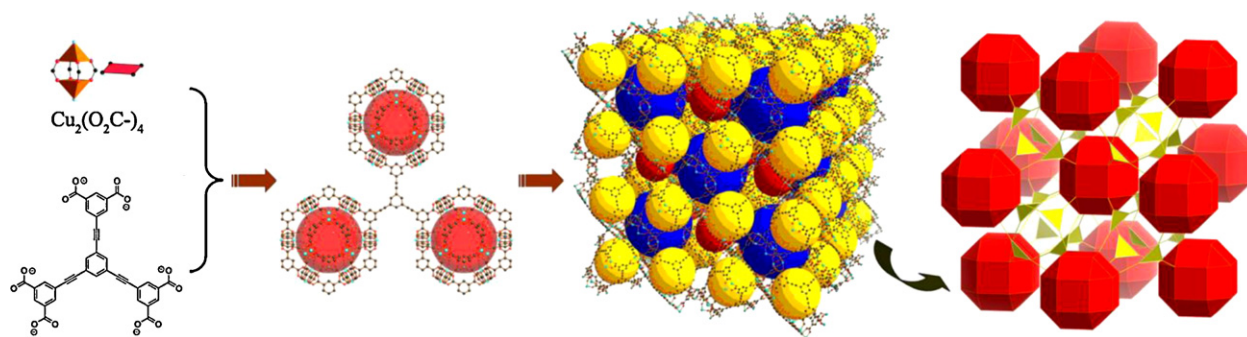
Fig. 4. Construction of a designed MOF, from metal-containing node and bridging organic ligand to supramolecular building unit and then to three-dimensional framework with pores. The last image highlights the geometrical assembly of the framework with the ligands and polyhedral cages acting as three- (yellow) and twenty-four- (red) connected nodes, respectively.

dynamic (adsorption) properties, the materials of tomorrow will have to account for both the size and electronic properties of the gas molecules. The relatively small difference in kinetic diameters between CO_2 (3.30 Å), CH_4 (3.76 Å), and N_2 (3.64 Å) makes exclusion based purely on size very challenging, but the differences in electronic properties such as quadrupolar moment and polarization can be used to accomplish the tasks at hand [19].

Challenges and shortcomings in terms of the three basic capture options for CO_2 are outlined briefly below. For pre-combustion capture: (1) poor availability and operability is the primary deficiency; (2) no single process is responsible for the overall operational performance; (3) high cost remains; and (4) systems are not mature for large-scale application. For oxy-fuel combustion capture: (1) the technology is only at a developmental stage without commercial experience; and (2) the air-separation that supplies pure oxygen consumes a lot of energy. For post-combustion capture: (1) low pressure and dilute CO_2 concentration of the flue gas requires a high volume of gas to be treated; (2) compression of the captured CO_2 requires additional energy; and (3) the regeneration of the sorbent (the amine solution) requires a high energy input. Most of these problems can be solved with the implementation of advanced materials.

The three basic technologies for CO_2 separation: absorption, adsorption, and membrane processes, have been extensively studied, using the amine-based absorption process as the current bench mark. Despite the intensive investigation, however, no single technology has been demonstrated to be capable of meeting the requirements set by the DOE/NETL: 90% CO_2 capture at less than a 35% increase in the cost of electricity (COE) [20,21]. In almost all absorption and chemical adsorption processes, the capture and separation steps consist of the formation of CO_2-based molecular complexes via chemical interactions and subsequent regeneration of CO_2 through significant increases in temperature. This regeneration accounts for the majority of the parasitic power requirement [22]. There is therefore a critical need to develop transformative CO_2 capture materials and processes that can drastically lower the operation cost by addressing the regeneration cost. In this regard, CO_2 capture by physical sorbents and membranes can provide promising energy-efficient alternatives to the current amine-based absorption systems if the following challenges can be addressed.

CO_2 capture by physical sorbents such as carbonaceous materials and inorganic porous materials such as zeolites is much more energy-efficient as compared to that by chemical sorbents. This is due to the absence of the formation of new chemical bonds between the sorbate and sorbent, thereby requiring significantly less energy for regeneration [13]. However, the traditional carbonaceous materials, such as activated carbon, are limited by low CO_2/N_2 selectivities (ca. 10), and while zeolites show significantly higher selectivities, they suffer from lower CO_2 loading and their perfor-

mance is impaired in the presence of water [13,22]. Therefore, there is an urgent need to develop advanced physical sorbents with a high CO_2 capacity and high CO_2/N_2 selectivity.

Membrane-based CO_2 separation is one of the most energy-efficient ways to capture CO_2 [22]. However, the traditional polymer membranes suffer from low CO_2/N_2 selectivity (less than 100). For the membrane-based separation to be commercially viable, the CO_2/N_2 selectivity must be in the range of 200 [23]. Despite the potential of molecular sieve membranes, conventional molecular sieves (i.e. zeolites) are limited for their use for CO_2/N_2 separation due to the similarity of the kinetic diameters of CO_2 (3.3 Å) and N_2 (3.64 Å). Therefore, it is highly desirable to develop advanced molecular sieve membranes with high CO_2/N_2 selectivity.

In summary, the stability, scalability, CO_2 affinity, and involved energy in application will be the dominant considerations in the search for capture materials that will compete with the technologies mentioned above. Engineering of gas-sorbent interactions at molecular level, such as the design of a molecular basket for CO_2 may be one of key notions to future success.

1.3. Metal-organic frameworks (MOFs), a new class of materials available for CO_2 capture

In the past two decades, a new class of crystalline porous materials, metal-organic frameworks (MOFs) has emerged and the associated research has been developed into one of the most prolific areas in chemistry and materials science [24–28]. MOFs are comprised of metal-containing nodes linked by organic ligand bridges and assembled principally through strong coordination bonds. MOFs have geometrically and crystallographically well-defined framework structures and in most cases, these structures are robust enough to allow the removal of the included guest species resulting in permanent porosity. The crystallinity of MOFs also allows precise structural characterization by diffraction methods, thus facilitating their rational design and the formulation of structure–function relationships.

MOFs can be conceptually designed and synthesized based on how building blocks come together to form a net (an example is shown in Fig. 4 [29,30]). As a result, the structures and properties of MOFs can be designed and systematically tuned by the judicious choice of building blocks. Besides the pre-design in synthesis, post-synthetic modifications have also been successfully used in tuning the pore properties of MOFs [31]. This remarkable and easy tunability is quite different from that of traditional porous materials, such as zeolites and activated carbon. It allows facile optimization of the pore structure, surface functions, and other properties for specific applications as porous material.

MOFs can be categorized into rigid and flexible/dynamic classes. Rigid MOFs usually have comparatively stable and robust porous
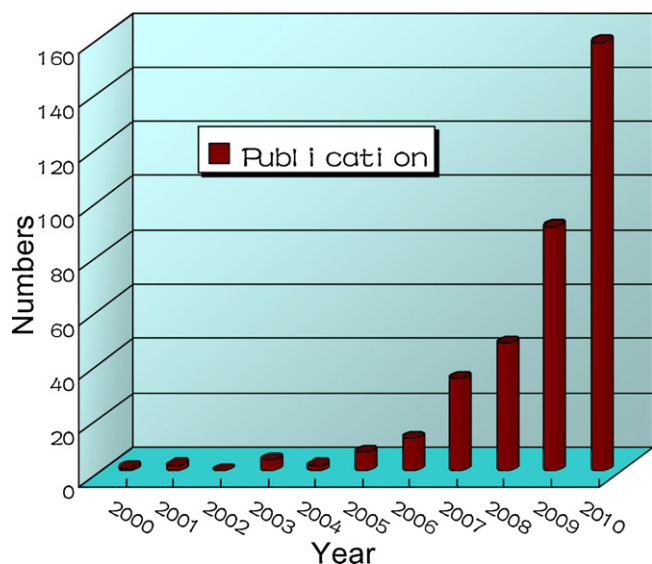
Fig. 5. Publications on "CO_2 adsorption and/or separation in MOFs" per year, showing the increasing research interest in this topic.
Data from ISI Web of Knowledge, Thomson Reuters.

frameworks with permanent porosity, similar to zeolites, whereas flexible MOFs possess dynamic, "soft" frameworks that respond to external stimuli, such as pressure, temperature, and guest molecules. This extraordinary sensitivity to external stimuli affords MOFs special properties such as pressure/temperature dependent molecular sieving, which is beyond the reach of traditional adsorbents, such as zeolites and activated carbons.

MOFs can be made with exceptionally high porosity and are typically synthesized by a self-assembly reaction between various metal ions and organic linkers under mild conditions. Different synthetic approaches have been developed including solution reaction under ambient (r.t.) conditions, solvothermal synthesis (including hydrothermal synthesis), solid state synthesis (so-called green synthesis), and microwave synthesis [32].

MOFs hold several records in porous materials including highest surface areas [33], hydrogen uptake based on physical adsorption [34], methane [35] and CO_2 storage [33]. Recently, several thematic reviews have highlighted the rapid developments in the design, synthesis, and potential applications of these materials [19,31,36–65]. As porous material, MOFs are therefore ideal adsorbents or membrane materials for gas storage and separation, including CO_2 capture due to their large surface areas, adjustable pore sizes, and controllable pore surface properties.

A number of recent qualified and comprehensive reviews were published with emphasis on different topics of the CCS field [10,13,18,66–90]; readers are directed to these papers for a more detailed understanding for CO_2 capture. Following the above general introduction of CO_2 capture, the progress in CO_2 adsorption, storage, and related gas separation research, which is directly related to CO_2 capture in MOFs is reviewed in this paper. The rapidly growing number of related primary research articles (Fig. 5) is an indication that a comprehensive review in this field is necessary in order to draw general conclusions and provide some guided perspectives for future research; despite the fact that a few reviews involving related topics of CO_2 capture with MOFs have appeared very recently [13,18,90–93].

2. Experimental exploration of CO_2 adsorption and adsorptive separation in MOFs

Experimental exploration is the most direct approach in the evaluation of any adsorbent material for separation application,

with initial attention being paid to both adsorption equilibrium and kinetics (diffusion selectivity) for adsorptive separation. These investigations can provide not only an effective way to screen suitable adsorbents for their separation capabilities but can also contribute to a better understanding of related adsorption processes. A lot of MOFs have been experimentally examined for CO_2 adsorption and related gas separation. While initial works in this area only tested general equilibrium adsorption isotherms, the more recent work has shifted its focus closer to practical application, including ultimate storage capacities and selective adsorption and separation of gases, particularly those linked to CCS. The total body of work has mimicked the traditional experimental methods for gas adsorption and separation in solid-state porous materials, including single-component equilibrium adsorption, diffusion, co-adsorption, mixed gas breakthrough experiment (fixed-bed adsorption), column chromatography separation, along with stability and porosity tests (such as surface area).

2.1. Single-component CO_2 adsorption in MOFs

Over 100 individual MOFs with single-component adsorption of CO_2 have thus far been reported; the results of these experiments have been summarized in Table S1 (see supplementary data). These adsorption data were obtained from the single-component isotherm measurements at a given temperature, with pressures ranging from very low to atmospheric pressure in most cases, to high pressures in a few cases. Measurements at room (or slightly elevated) temperature and low pressure most resemble practical CO_2 capture, because of the low CO_2 component in the gas streams that need to be separated. Adsorption isotherms at low temperature and normal pressure are, however, useful in evaluating the adsorption properties, testing the CO_2 selective adsorption capacities, and optimizing the design of MOFs. Furthermore, the adsorption under room temperature and high pressure is directed to the evaluation of the total CO_2 storage ability of a MOF; all of these fall under the CCS umbrella.

2.1.1. CO_2 adsorption in MOFs

Like most porous materials, CO_2 adsorption and uptake in MOFs are pore size/volume and surface dependent. Compared to other porous materials, such as zeolites and activated carbon, most MOFs have a higher pore volume and surface area, leading to record CO_2 uptakes as shown in Table S1. The majority of these results, are not discussed in detail, instead some unique adsorption phenomena and experimental explorations, along with typical examples, are touched upon herein.

Usually, the CO_2 adsorption isotherm in rigid porous materials, such as traditional zeolites and the majority of rigid MOFs, presents a normal type-I shape, but in a few rigid MOFs, stepwise isotherms have been observed. This can be related to the structural features of these MOFs, as per example, Zhang et al. [94] reported the two-step CO_2 adsorption at low temperature in a highly connected MOF, $Ni^{II}_2Ni^{III}(\mu_3\text{-OH})(pba)_3(2,6\text{-ndc})_{1.5}$ (MCF-19; pba = 4-(pyridin-4-yl)benzoate, 2,6-ndc = 2,6-naphthalenedicarboxylate), which has a biporous structure with cages and channels that co-exist. On the other hand, several similar stepwise CO_2 adsorption behaviors, giving sigmoidal isotherms, have been observed in some ultrahigh pore MOFs, such as $Zn_4O(bdc)_3$ (MOF-5 or IRMOF-1, bdc = 1,4-benzenedicarboxylate), $Zn_4O(btb)_2$ (MOF-177, btb = benzene-1,3,5-tribenzoate), and $Zn_4O(bte)_{14/9}(bpdc)_{6/9}$ (MOF-210, bte = 4,4′,4″-(benzene-1,3,5-triyltris(ethyne-2,1-diyl))tribenzoate, bpdc = biphenyl-4,4′-dicarboxylate) at near room temperature and high pressures [33,95] (Fig. 6a). In these cases, this phenomenon was attributed to the attractive electrostatic interactions between CO_2 molecules that lead to their bulk condensation, which has been explained by Snurr and
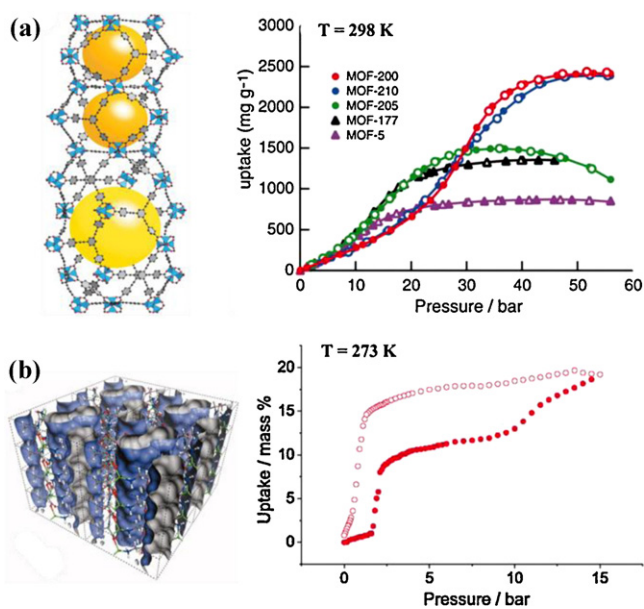
Fig. 6. Structures and *unique* CO_2 adsorption–desorption isotherms in (a) rigid MOF-5, -177, -200, 205, and 210 (only the crystal structure of MOF-210 is shown here) and (b) in a flexible MOF, Zn(Gly-Ala)$_2$.
Reproduced with permission from Refs. [33,119], respectively.

coworkers in terms of molecular simulation [96]. As a last example, hysteretic CO_2 adsorption in rigid MOF, Zn(2,7-ndc)(2,7-ndc = 2,7-naphthalenedicarboxylate) was attributed to the unique arrangement of the pore channels and their narrow passages compared to the critical dimensions of a CO_2 molecule [97].

In contrast, flexible MOFs usually result in stepwise adsorption and/or show hysteretic desorption isotherms for CO_2 and other gases. This flexibility is a unique property of some MOFs, which shows great potential in selective adsorption and separation of gases and other small molecules. The M(OH)(bdc) (MIL-53) series provides typical examples of MOFs that "breathe" during the adsorption and desorption of CO_2, which has been associated with a phase transition of these MOF structures [98–105]. For MIL-53(Cr), these phase transformations were tracked by gas-sorption-coupled X-ray diffraction. The geometric parameters switch from the almost square (8.5 Å × 8.5 Å), so-called large pore (LP), to the narrow-pore (NP) form, with trapezoidal pores (2.6 Å × 13.6 Å) upon CO_2 adsorption; simultaneously, the unit cell volume decreases by 40%. More interesting is that as the CO_2 loading increases, the structure converts back from the NP to the LP form. Similarly, CO_2 adsorption in Sc$_2$(bdc)$_3$ at 235 K and 1 bar resulted in a symmetry change of crystal structure from orthorhombic *Fddd* to monoclinic *C2/c* through the tilting of bdc linkers. CO_2 molecules take up different adsorption sites in two symmetrically different channels of framework that result from this symmetry change [106]. A post-synthetic modification strategy has also been used to modulate the breathing behavior of MOFs. Cohen and coworkers [107] reported the modification of DMOF-1-NH$_2$, Zn$_2$(NH$_2$-bdc)$_2$(dabco) (dabco = 1,4-diazabicyclo[2.2.2]octane), to DMOF-1-AM($n-1$) where 'n' denotes the chain length of the newly formed linear alkyl amide. Systematic CO_2 adsorption measurements on DMOF-1-AM($n-1$) showed that the breathing is related to the alkyl chain length of the post-added groups. The step adsorption and hysteresis of desorption at 196 K for DMOF-1-AM3 is very similar to that observed in MIL-53. Another example, Ni(bpee)Ni(CN)$_4$ (bpee = *trans*-1,2-bis(4-pyridyl)ethylene), reported by Culp and coworkers, is a three-dimensional (3D) framework constructed by a flexible organic bridging ligand, bpee, pillaring two-dimensional (2D) rigid

Ni(CN)$_4$ inorganic layers. The hysteretic CO_2 adsorption/desorption isotherm observed in this MOF, was attributed to a structural phase transition resulting from a variation in the tilt angle of the bpee pillars. A structurally similar MOF, but with a rigid organic linker, 4,4′-bipyridine gave rise to a normal type-I isotherm for CO_2, clarifying the provenance of the hysteresis [108].

Interpenetrated MOFs sometimes show flexible character due to the moving between the single frameworks with respect to each other. Dramatic steps in the adsorption and hysteresis in the desorption of CO_2 have been observed in a twofold interpenetrated MOF, Zn$_2$(bttb)(dpni) (bttb = 4,4′,4″,4‴-benzene-1,2,4,5-tetrayltetrabenzolate, dpni = N,N′-di-(4-pyridyl)-1,4,5,8-naphthalenetetracarboxydiimide) reported by Hupp and coworkers [109]. Characterization of the structure by PXRD and pair distribution function (PDF) analysis indicated that structural changes upon CO_2 sorption most likely involve the moving of the interpenetrated frameworks.

A "gate" phenomenon has been observed in several flexible MOFs [110–117]. An early example that clearly illustrates this "gate" effect is Cu(pyrdc)(bpp) (pyrdc = pyridine-2,3-dicarboxylate, bpp = 1,3-bis(4-pyridyl)propane), reported by Kitagawa and coworkers [117]. The CO_2 adsorption isotherm of this MOF shows a sudden increase at a relatively low pressure, referred to as the gate-opening pressure, and saturation at another pressure. The desorption isotherm, on the other hand, does not retrace the adsorption isotherm and shows an abrupt drop at a third pressure. To elucidate the involved mechanism, the authors have determined the crystal structure of the MOF after CO_2 inclusion. Perfectly correlating with the adsorption experiment, two CO_2 molecules in two different channels are found for each Cu(II) atom. CO_2 molecules form C–H⋯O (2.46–2.59 Å) H-bonding interactions with the channel walls, providing the driving force for the sorption with strong confinement in the framework. A similar "gate" phenomenon for CO_2 adsorption has also observed in [Cu(4,4′-bipy)(H$_2$O)$_2$(BF$_4$)$_2$](4,4′-bipy) (4,4′-bipy = 4,4′-bipyridine), after exposure to water [118]. Another very interesting example is an adaptable peptide-based MOF, Zn(Gly-Ala)$_2$, reported recently by Rosseinsky and coworkers [119]. As shown in Fig. 6b, CO_2 adsorption exhibited gating opening above a pressure of 2 bar, and further step adsorption at high pressure and desorption hysteresis. Extensive experiments and molecular simulations indicated that the torsion and displacement of the peptide linkers, combined with the changing of the pore confirmation is responsible for these unusual phenomena. This flexibility enabled pore volume to increase smoothly with an increase of CO_2 loading.

2.1.2. Tuned adsorption and the heat of adsorption of CO_2 in MOFs

The impact on CO_2 adsorption in MOFs by various other factors has also been explored. Kajiro and coworkers [120] examined the effect of metal ions on the CO_2 adsorption in two isostructural MOFs, M(4,4′-bipy)$_2$(OTf)$_2$ (M = Cu and Co). Although the difference in metal ions in these MOFs results in only slightly different structures, the gas adsorption properties, based on the expansion/shrinkage of these MOF structures, are largely dependent on the metal ions. As an alternative strategy, partial doping of MOF-5 with Co(II) by isomorphic substitution during synthesis has been investigated to explore the effect on CO_2 adsorption [121]. The adsorption result showed that the CO_2 uptake of these MOF-5-based materials systematically increases with the increase of Co(II) content at high pressure. Rosi and coworkers [122] demonstrated recently that post-synthetic exchange of extra-framework cations within an anionic MOF, [Zn$_8$(ad)$_4$(bpdc)$_6$O](cation) (bio-MOF-1, ad = adeninate, bpdc = 4,4′-biphenyldicarboxylate), can be used as a means to systematically modify its pore dimensions, thereby, tuning the CO_2 adsorption capacity. From this work, they concluded
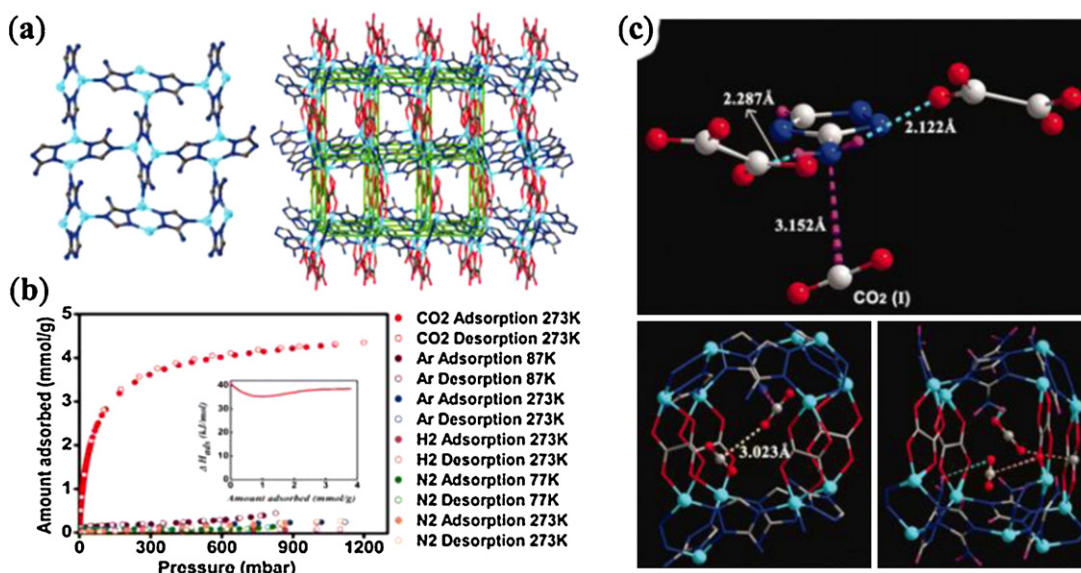
Fig. 7. Structure (a) and gas adsorption properties (b) of $Zn_2(Atz)(ox)$; (c) the CO_2 binding (directly determined by X-ray structure refinement at 173 K) within the pores of $Zn_2(Atz)(ox)$ (c).
Reproduced with permission from Ref. [128].

that smaller pores in MOFs (with large cations in this case) may be ideal for condensing CO_2 at temperatures relevant to practical application. Similarly, using cation exchange to tune CO_2 adsorption has also been reported by Kitagawa and coworkers in a flexible MOF, $[Ni(bpe)_2(N(CN)_2)](cations)$ (bpe = 1,2-bis(4-pyridyl)ethane) [123]. Furthermore, Snurr and coworkers [124] have demonstrated that CO_2 uptake in $Cu_3(btc)_2$ (HKUST-1 or Cu-BTC, btc = 1,3,5-benzenetricarboxylate) was significantly enhanced by the presence of water molecules coordinated to metal sites in the framework. A detailed analysis of simulation data revealed that the interaction between the quadrupole moment of CO_2 and the electric field created by water molecules is responsible for the increased CO_2 uptake. Hydration of flexible MIL-53(Cr) has also been demonstrated to enhance the CO_2 adsorption relative to CH_4 [103]. In addition, Cao and coworkers [125] recently showed that the incorporation of CNTs into MOFs can enhance the uptake of CO_2, which can be further improved by doping the CNT-modified MOFs with lithium.

For gas adsorption, the isosteric heat of adsorption, calculated usually from the adsorption isotherms at different temperatures, is another definitive property that is directly related to the separation and storage ability. A detailed analysis of the CO_2 adsorption heat in the examined MOFs has been done by Sholl and coworkers in their recent review [91]. The heats of adsorption for CO_2 (ref. Table S1) stretch across a large range, between 20 and 50 kJ/mol, for most MOFs, with the record of 90 kJ/mol being held by an ethylenediamine-functionalized MOF reported by Long and coworkers (*vide infra*) [126]. In most cases, the heat of adsorption decreases with increased loading, and that a high heat of adsorption is not necessarily good in terms of the CO_2 separation application, because of the large energy requirement associated with the regeneration (i.e. desorption) of the materials. Complementary to typical method mentioned above, measurements of the heats of adsorption by pulse-response experiments in an ultrahigh-vacuum reactor, referred to as a TAP reactor (temporal analysis of products), have been reported for the adsorption of CO_2 in three MOFs: IRMOF-1, $Zn_4O(NH_2\text{-}bdc)_3$ (IRMOF-3), and HKUST-1 [127].

2.1.3. Probing CO_2 adsorption sites and adsorption modes in MOFs

Probing into adsorption sites and adsorption/binding modes is critical for the design of new sorbent. Several examples on the exploration of CO_2 adsorption sites in MOFs have been mentioned above. Very recently, Shimizu and coworkers [128,129] directly observed the CO_2 bonding within an amine-functionalized MOF, $Zn_2(Atz)(ox)$ (Atz = aminotriazolato, ox = oxalate) at low pressure from the X-ray crystallographic resolution of the adsorbed CO_2 molecules (Fig. 7). From the structural refinement, two independent CO_2 binding sites were located in the pores of this MOF: one is near the free amine group and another is close to the oxalates. The $O(CO_2)\cdots H–N(NH_2)$ hydrogen bond and interactions between the N lone pair of the amine group and C atom of CO_2 and between the O atom of oxalate group and O atom of CO_2 have been confirmed. Furthermore, the $CO_2\cdots CO_2$ cooperative interaction (between C and O atoms) was also observed. Accompanied with molecular simulation studies, they concluded that the combination of appropriate pore size, strong interaction between CO_2 and functional groups on the pore surface, and cooperative binding of CO_2 molecules is responsible for the low-pressure binding of CO_2 in this MOF. Besides X-ray diffraction related investigations of adsorbed CO_2 in MOFs, IR spectroscopy coupled adsorption has proven to be a useful technique in probing CO_2 adsorption sites in MOFs. Bordiga et al. [130] investigated the CO_2 adsorption in HKUST-1 by IR spectroscopy. Their results showed that the coordinatively unsaturated Cu(II) centers in this MOF act as specific interaction sites and play an important role in the adsorption. Similarly, Blom and coworkers [131] have shown that CO_2 adopts the end-on coordination mode when interacting with the coordinatively unsaturated nickel sites of $Ni_2(dhtp)$ (H_4dhtp = 2,5-dihydroxyterephthalic acid), which gives rise to high CO_2 adsorption capacity at low pressures and ambient temperatures. Vimont et al. [102] studied the CO_2 adsorption mode at low coverage in MIL-53(Cr). The red shift of the ν_3 band and splitting of the ν_2 mode of CO_2 in addition to the shifts of the $\nu(OH)$ and the $\delta(OH)$ bands of the MIL-53(Cr) hydroxyl groups provide evidence that CO_2 interacts with the O atoms of framework –OH groups as an electron-acceptor via its carbon atom.

2.1.4. Cyclic CO_2 adsorption and its impact on stability of MOFs

The cyclic and thermal stability of MOFs during adsorption/desorption is very important when connected to practical application. The cyclic CO_2 adsorption of MOF-5 prepared by microwave synthesis showed that the uptake capacity is invariably near 3.6 wt% when cycled between 30 and 300 °C at atmospheric
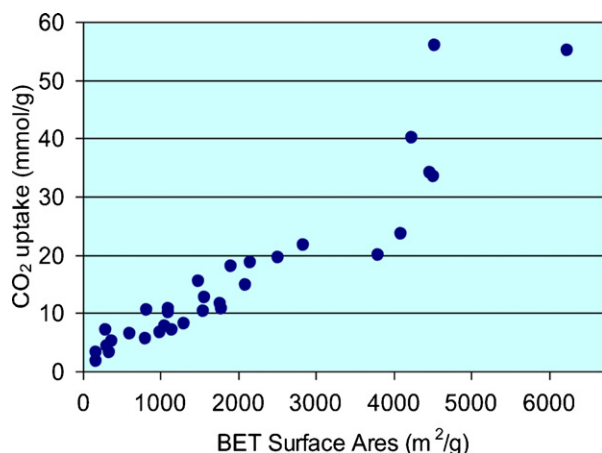
Fig. 8. CO_2 uptake vs surface area in selected MOFs (at ambient temperature and high pressure, at which the uptake approaches saturation in most cases).

pressure through 10 separate adsorption/desorption cycles. Above 400 °C, however, MOF-5 underwent thermal decomposition and was no longer capable of adsorbing CO_2 [132]. Most of MOFs have good thermal stability, but in terms of hydrothermal sensitivity, a large number of MOFs, especially those constructed by Zn_4O cluster nodes, decompose upon contact with humid air [133,134]. One subclass of MOFs, zeolitic imidazolate frameworks (ZIFs), have however been tested to be water and even acid stable, thereby showing great potential in practical applications for CO_2 capture [84]. It should be pointed out that the synthesis of stable MOFs, especially those being water stable, is still one of biggest challenges in the research field of MOFs for their practical applications.

2.1.5. CO_2 storage in MOFs

The saturated adsorption measurements of CO_2 at (or near) room temperature and high pressure are directly related to the ultimate storage capacity of MOFs for CO_2, which is another significant issue in CCS. Table S2 lists selected MOFs with high CO_2 storage capacities at near room temperature and high pressure. As has been found with other gases, for CO_2 storage, the total pore volume of MOFs is essentially proportional to the amount of CO_2 that can be adsorbed at high pressure; from Fig. 8, we can conclude that surface area is also strongly correlated with the CO_2 storage ability.

Yaghi and coworkers [95] were the first to report MOFs for CO_2 storage at ambient conditions: nine MOFs were selected in order to examine a range of structural and pore attributes. Since then, several MOFs with high porosity and surface area have been examined for CO_2 storage, with the initial record capacity changing from MOF-177 to MIL-101 [135]. MOF-210, synthesized again by Yaghi's group currently holds the CO_2 storage record with the saturated CO_2 uptake of 2400 mg/g at room temperature and ca. 50 bar [33]. This MOF has an estimated bulk density of 0.25 g/cm³, a measured pore volume of 3.60 cm³/g and a BET surface area of 6240 m²/g, the highest reported for any crystalline material.

2.2. Co-adsorption, adsorption dynamics, and diffusion of CO_2 in MOFs

For the practical separation application of MOFs in CO_2 capture, the evaluation from co-adsorption and diffusion (dynamics) experiments are essential, unfortunately, however, only very limited data have been reported to date.

2.2.1. CO_2 co-adsorption in MOFs

The co-adsorption of CO_2 and CH_4 in flexible MIL-53(Cr) has been studied by Llewellyn and coworkers [136] using a combina-

tion of several techniques. The results showed that CO_2-rich and equimolar CO_2–CH_4 mixtures lead to the structural transition, or breathing, from the LP to the NP form and then back to the LP form as the pressure was increased. CH_4-rich mixtures, on the other hand, always maintain the LP framework. The closing and opening of the structure is thus entirely controlled by the partial pressure of CO_2, only a mild influence on the extent of the transition being attributed to CH_4. Experimental results also suggested that CH_4 is probably not adsorbed at all in the NP-form (when it is filled with CO_2).

Multi-component fixed-bed adsorption of CO_2, N_2, and CH_4 (together with the adsorption kinetics) was conducted on crystals of $Zn_2(bdc)(4,4'-bipy)_{0.5}$ (MOF-508b) [137]. Chen and coworkers showed that MOF-508b is very selective for CO_2, and that the loadings of CH_4 and N_2 are temperature independent. A dynamic model based on the linear driving force (LDF) approximation for mass transfer was used to describe the adsorption kinetics of single, binary, and ternary breakthrough curves. The intra-crystalline diffusivity for CO_2 is one order of magnitude faster than that for CH_4 and N_2.

2.2.2. Adsorption dynamics and diffusion of CO_2 in MOFs

Adsorption dynamics of CO_2 in $Ni_2(4,4'-bipy)_3(NO_3)_4$ has been explored by Thomas and coworkers [138]. The stepwise isotherm that was observed from the CO_2 adsorption at 10–20% occupancy of the total pore volume of this MOF, was ascribed to discrete structural changes in the host framework that are induced by adsorption on different sites. Detailed studies showed that the adsorption kinetics obey a LDF mass transfer model for the adsorption at low surface coverage. The rates of adsorption in the region of the CO_2 isotherm steps are slower than those observed either before or after each step. Salles et al. [139] examined the transport diffusivity of CO_2 in MIL-53(Cr) by using a combination of quasi-elastic neutron scattering measurements and molecular dynamics simulations. The results indicated that CO_2 follows a one-dimensional (1D) diffusion mechanism in both the NP and LP structures of MIL-53(Cr). They also used similar methods to characterize the self and transport diffusivities of CO_2 in V(O)(bdc) (MIL-47(V)) [140]. As shown in Fig. 9, D_s and D_0 monotonously decrease with an increase in loading, whereas D_t exhibits a slight decrease at low loading followed by a sharp increase at higher loading. In both MOFs, the magnitude of the transport diffusivities was ∼10 m²/s. Garcia-Ricard and Hernandez-Maldonado [141] evaluated the kinetics of CO_2 adsorption on three forms of $Cu_2(pzdc)_2(4,4'-bipy)$ (pzdc = pyrazine-2,3-dicarboxylate) pretreated at 373, 398, and 423 K. They used the adsorption uptake to estimate the diffusion constant and elucidate the kinetics involved during the transport of CO_2 through the micropores of the material. Based on the determination of particle morphology from scanning electron microscopy, the transport phenomenological model was used to fit the adsorption data. Such as, for the sample pretreated at 373 K, the analysis revealed an average diffusion time constant of ca. $0.5 s^{-1}$ at 298 K. Lin and coworkers [142] examined the CO_2 diffusion in cubic MOF-5 crystals, measuring about 40–60 μm in size. Their results showed that CO_2 diffusion in MOF-5 crystals is an activated process with the diffusion coefficient being in the range of 8.1–11.5×10^{-9} cm²/s at 295–331 K and that the CO_2 loading has almost no effect on the rate of the diffusion. Further studies into the adsorption kinetics of CO_2 in MOF-5 (and MOF-177), performed by Deng and coworkers [143], indicated that at 298 K, MOF-5 and MOF-177 reached the adsorption saturation level in an interval of time of about 5–10 s. The average diffusivities of the gas onto MOF-5 and MOF-177 are 1.17×10^{-9} and 2.3×10^{-9} m²/s at 298 K and pressures up to 800 Torr, with a marked slowing as pressure increased. The diffusion related to MOF-based membranes will be discussed in Section 3 of this paper.
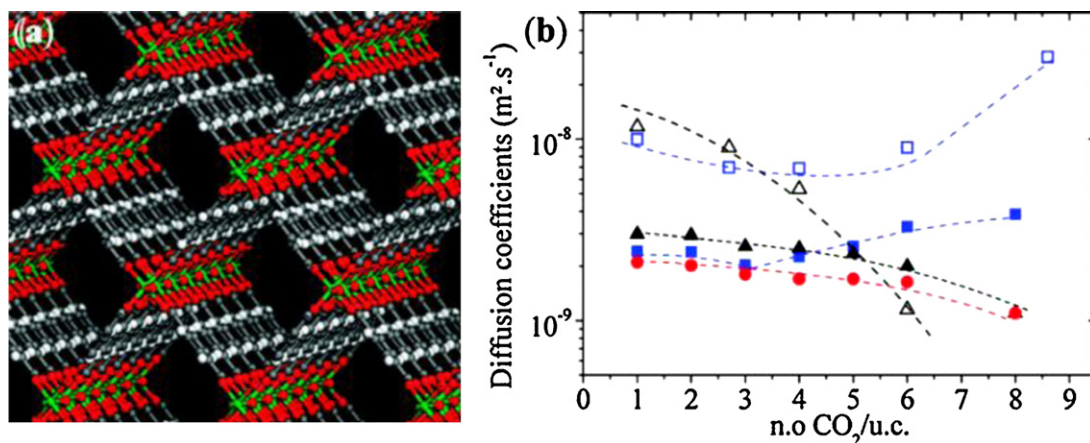
Fig. 9. Structure (a) and the experimental D_o (black $\triangle$) and D_t (blue $\square$) and the simulated D_s (red $\bullet$), D_o (black $\blacktriangle$), and D_t (blue $\blacksquare$) as a function of CO_2 concentration (b) of MIL-47(V).
Reproduced with permission from Ref. [140].

2.3. Selective adsorption of CO_2 in MOFs

As mentioned above, CCS related gas separation primarily includes CO_2/N_2 separation in post-combustion capture, CO_2/H_2 separation in pre-combustion capture, air (O_2/N_2) and CO_2/CO separation in oxy-combustion, and CO_2/CH_4 separation in the purification of natural gas. In the majority of reported literature, selective adsorption is the primary tool used give the reader a guided view of a particular MOF's potential for separation. In selective adsorption, both the adsorption capacity and the selectivity are the central concerns. Selective adsorption, in most cases, uses single-component isotherms and the Ideal Adsorbed Solution Theory (IAST) [144] to calculate a material's selectivity factor. However, as the name indicates, the calculation does not always account for all experimental variables, and should be viewed as a reference; gas mixture adsorption experiments should thus be conducted, to complete the picture. The selective adsorption of CO_2 over CH_4 and N_2 on single-component (in most cases) and mixed-gas experiments, of the reported MOFs has been summarized in Tables 1 and 2, respectively.

2.3.1. Direction observation of CO_2 selective adsorption in MOFs

From the single-component adsorption isotherm the CO_2 selective adsorption over other gases has been observed in some MOFs. Generally speaking, the selective adsorption of CO_2 over N_2 or CH_4 in rigid MOFs can be attributed to either size exclusion or a favorable gas–pore surface interaction. These factors are determined by the sizes and properties of both the gas adsorbates and the pores in a given MOF. Compared to N_2 and CH_4 the kinetic diameter of CO_2 is smaller and its quadrupole moment is higher, which, in many cases, results in strong interactions with the pore surface of the adsorbents. Based on the size exclusion, several MOFs including $Er_2(pda)_3$ (pda = 1,4-phenylendiacetate) [200], $Mn(HCOO)_2$ [183], $Cd_3(OH)_2(apta)_4$ [196], $Cu(fma)(bpee)_{0.5}$ [175], $Co[Fe(Tp)(CN)_3]_2$ [191], $[Cu_5(Tz)_9](NO_3)$ [192], and $Zn(dtp)$ (Fig. 10) [171] have shown selective adsorption of CO_2 over N_2 at low temperature and atmospheric pressure; additionally, size-selective adsorption of CO_2 over CH_4 has also been observed in $Mn(HCO_2)_2$ [183]. Besides these, a number of rigid MOFs have the capability to selectively adsorb CO_2 over N_2 and CH_4 because of the strong interaction between CO_2 and their pore surface [94,106,126,135,141,146,148,151,153–157,159,162–166,168–172, ,179,181,182,184,186,188–191,193,194,196–198,201–204]. Based on the collected data, all examined MOFs adsorbed very low quantities of N_2 at room temperature, implying that increasing the CO_2 adsorption capacity is a straightforward strategy for enhancing the selectivity of CO_2 over N_2 (at this condition).

Flexible MOFs have a different story in the selective adsorption of CO_2 over CH_4 or N_2. A typical example is $Cu(dhbc)_2(4,4'-bipy)$, which has a different "gate" opening pressures for CO_2, N_2, and CH_4 (Fig. 11) [114]. At different pressure ranges these gases can be selectively adsorbed by this MOF, which shows the potential for playing a role as a multi-functional adsorbent of this material. A similar "gate" phenomenon for the selective adsorption of these gases has also been observed in $Zn(pydc)(dma)$ [158]. Another interesting MOF with a high CO_2 adsorption selectivity that has been associated with framework flexibility is $(Ni_2)(dpce)(bptc)$ (SNU-M10, dpce = 1,2-di(1,3,5,8,12-pentaazacyclotetradecan-3-yl)ethane, bptc = 1,1'-biphenyl-3,3',5,5'-tetracarboxylate) [205]. Choi and Suh showed that the adsorption selectivity of SNU-M10 for CO_2 over N_2 at room temperature is pressure-dependent, having a selectivity of 24:1 (v/v) at 0.61 atm and 98:1 (v/v) at 1.0 atm. They attributed this phenomenon to CO_2-induced "gate" opening and closing of pores.

2.3.2. Evaluation of CO_2 adsorption selectivity in MOFs

Besides the direct observation on differences in uptakes between separated gases under given measurement conditions to give the qualitative evaluation, the single-component adsorption isotherms can also be used to quantitatively estimate the adsorption selectivity. Two methods are usually used to assess the adsorption selectivity, in terms of the single-component adsorption data. If adsorption species are presented at low loadings, namely within the Henry's regime, the adsorption selectivity for an equimolar mixture is close to the ratio of the Henry's constants for each species as if it were adsorbed as a pure component [206]. At non-dilute loadings, however, more information is required to estimate multi-component adsorption. One common approach is to use well-developed Ideal Adsorbed Solution Theory (IAST) [144] to predict multi-component adsorption isotherms and selectivity based on single-component adsorption isotherms. This approximate theory is known to work accurately in many porous materials, including MOFs [207,208]. However, most of the reports on CO_2 selective adsorption in MOFs are based on simulated adsorption isotherms, which will be discussed in another part of this paper.

Limited adsorption selectivities of CO_2 over other gases in MOFs evaluated from experiments were reported recently. Deng and coworkers [143] reported the adsorption equilibrium selectivity of CO_2 over N_2 and CH_4 in MOF-5 and MOF-177, which were calculated from the ratio of Henry's constants. The results

Table 1
Selective adsorption of CO_2 over CH_4 in selected MOFs.

MOF	Uptake CO_2 vs CH_4 (conditions)	Selectivity (conditions)	Ref.
Cu(Hoxonic)(4,4′-bipy)$_{0.5}$	2.5 vs 0.5 mmol/g (273 K, 2500 kPa)		[145]
Cu(bdc-OH)	52 vs 13 cm^3/g (296 K, 1 atm)	6.7 (296 K)[a]	[146]
Zn$_2$(tcom), 'Adamantanoid' type structure	7.3 vs ~0 wt% (298 K, 1 atm)		[147]
Zn$_2$(tcom), 'Lonsdaleite' type structure	5.5 vs ~0 wt% (298 K, 1 atm)		[147]
Zn$_4$O(bdc)(btb)$_{4/3}$ [UMCM-1]	23.8 vs 8.0 mmol/g (298 K, 24.2 bar)		[148]
Zn$_8$(bhfp)$_{33}$ [FMOF-2]	5.1 vs 1.3 mmol/g (298 K, 30 bar)		[149]
Zn$_2$(BPnDC)$_2$(4,4′-bipy) [SNU-9]	219 vs 30 cm^3/g (195 K, 1 atm); 29.9 vs 3.2 wt% (298 K, 30 bar)		[150]
Zn(mIm)$_2$ [ZIF-8]	35 vs 6.5 wt% (298 K, 30 bar)		[151]
Cu(1,4-ndc)	74.3 vs 31.3 cm^3/g (298 K, 20 bar)		[152]
Cu$_2$(ebtc)$_3$	178 vs 31 cm^3/g (273 K, 1 bar)		[153]
Cu$_2$(Hbtb)$_2$	7.5 vs 3.5 mmol/g (298 K, 25 bar)	12.4 (1 bar)[b] 5 (20 bar)[b]	[154]
Ni$_2$(dhtp)	1.5 vs 0.6 mol/mol (298 K, 500 kPa)		[155]
Cu-BTC (HKUST)	12.7 vs 4.6 mmol/g (298 K, 15 bar)		[156]
Zn(bIm)(nIm) [ZIF-68]	38 vs 10 cm^3/g (298 K, 1 atm)	5.5[c]	[157]
Zn(cbIm)(nIm) [ZIF-69]	41 vs 12 cm^3/g (298 K, 1 atm)	5.6[c]	[157]
Zn(Im)$_{1.13}$(nIm)$_{0.87}$ [ZIF-70]	32 vs 10 cm^3/g (298 K, 1 atm)	5.6[c]	[157]
Zn(nbIm)(nIm) [ZIF-78]	51 vs 14.5 cm^3/g (298 K, 1 atm)	10.5[c]	[157]
Zn(mbIm)(nIm) [ZIF-79]	34 vs 11 cm^3/g (298 K, 1 atm)	6[c]	[157]
Zn(bbIm)(nIm) [ZIF-81]	39 vs 11 cm^3/g (298 K, 1 atm)	6.3[c]	[157]
Zn(cnIm)(nIm) [ZIF-82]	54 vs 11.5 cm^3/g (298 K, 1 atm)	9.8[c]	[157]
Zn(pydc)(dma)	140 vs 19 cm^3/g (195 K, 100 kPa)		[158]
Cu$_3$(btc)$_2$(H$_2$O)$_x$ [Hydrated HKUST-1]	500 vs n/a mg/g (298 K, 4.8 bar)	7.5 (298 K)[b]	[124]
Zn$_2$(bttb)(dma)$_2$	3.2 vs 1.8 mmol/g (298 K, 17.5 bar)	5.8 (298 K)[b]	[159]
Zn$_2$(bttb)	5.0 vs 3.4 mmol/g (298 K, 17.5 bar)	4.8 (298 K)[b]	[159]
Zn$_2$(bttb)(py-CF$_3$)$_2$	2.2 vs 1.1 mmol/g (298 K, 17.5 bar)	6.5 (298 K)[b]	[159]
Ni$^{II}_2$Ni^{III}(μ_3-OH)(pba)$_3$(2,6-ndc)$_{1.5}$	480 vs 100 cm^3/g (195 K, 1 atm)		[94]
Al(OH)(2,6-ndc)	9 vs 0.04 g/g (303 K, 10 bar)		[160]
Zn$_4$O(fma)$_3$	65 vs 8 wt% (300 K, 25 bar)		[161]
[H$_3$O][Zn$_7$(μ_3-OH)$_3$(bbs)$_6$]	2 vs 0.57 mmol/g (273 K, 1 atm)	15.7 (273 K)[a]	[162]
Al$_4$(OH)$_8$[btec] [MIL-120]	4.8 vs 1.8 mmol/g (303 K, 1MPa)		[163]
Mg(tcpbda) [SNU-25]	134 vs 68.1 cm^3/g (195 K, 1 atm); 46.38 vs 15.1 cm^3/g (273 K, 1 atm); 33.43 vs 10.22 cm^3/g (298 K, 1 atm)		[164]
Sc$_2$(bdc)$_3$	4.0 vs 2.0 mmol/g (304 K, 30 bar)		[106]
Zn(bdc)(4,4′-bipy)$_{0.5}$ [MOF-508b]	26.0 vs 2.0 wt% (303 K, 4.5 bar)	3–6 (303 K)[a]	[165]
Zn$_3$(OH)(p-cdc)$_{2.5}$	0.586 vs 0.0754 mmol/g (298 K, 0.5 bar)	7–31 (298 K)[b]	[166]
Zn$_3$(OH)(p-cdc)$_{2.5}$(DMF)$_4$	0.277 vs 0.0682 mmol/g (298 K, 0.5 bar)	4.5–10 (298 K)[b]	[166]
Cr$_3$F(H$_2$O)$_3$O(btc)$_2$ [MIL-100]	18 vs 7.5 mmol/g (304 K, 5.0 MPa)		[167]
Cr$_3$F(H$_2$O)$_2$O(bdc)$_3$ [MIL-101]	40 vs 12 mmol/g (304 K, 5.0 MPa)		[167]
Cu-BTC, extrudates	6.6 vs 1.8 mmol/g (303 K, 2.5 bar)	4–6 (0.1–3 bar, 303 K)[b]	[168]
β-Zn(F-pymo)$_2$	8.5 vs 1.0 mmol/g (273 K, 2800 kPa)		[169]
β-Co(F-pymo)$_2$	7.0 vs 1.5 mmol/g (273 K, 2800 kPa)		[169]
Cu(H-pymo)$_2$	5.5 vs 3.5 mmol/g (273 K, 2800 kPa)		[169]
Zn$_2$(cnc)$_2$(dpt)	145 vs 80 cm^3/g (195 K, 1 atm)		[170]
Zn(dtp)	99 vs ~0 cm^3/g (195 K, 1 atm)		[171]
Zn$_2$(2,6-ndc)$_2$(dpni), microwave sample	4.5 vs 2.5 mmol/g (298 K, 1750 kPa)	~30 (298 K)[b]	[172]
Zn$_2$(2,6-ndc)$_2$(dpni), solution sample	3.5 vs 2.0 mmol/g (298 K, 1750 kPa)	4.8 (298 K)[b]	[172]
Ni$_2$(pbmp) [Ni-STA-12]	2.65 vs 0.25 mmol/g (304 K, 1 bar)		[173]
Zn(abdc)(bpee)$_{0.5}$	130 vs 60 cm^3/g (195 K, 1 bar)		[174]
Cu(fma)(bpee)$_{0.5}$	100 vs 36 cm^3/g (195 K, 1 bar)		[175]
Co$_3$(2,4-pdc)$_2$(μ_3-OH)$_2$ (CUK-1)	90 vs 8 cm^3/g (298 K, 1 atm)		[176]
H$_2$[Ni$_3$O(H$_2$O)$_3$(tatb)$_2$] [PCN-5]	210 vs 30 mg/g (195 K, 760 Torr)		[177]
Zn$_3$(ntb)$_2$	151 vs 74.9 cm^3/g (195 K, 1 atm)		[178]
Zn(Pur)$_2$ (ZIF-20)	70 vs 17 cm^3/g (273 K, 760 Torr)		[179]
Cr(OH)(bdc) [MIL-53(Cr)]	8.8 vs 4.6 mmol/g (304 K, 20 bar)		[180]
Cr(OH)(bdc)(H$_2$O) [Hydrated MIL-53(Cr)]	7.8 vs 0.2 mmol/g (304 K, 20 bar)		[180]
Mn(2,6-ndc)	3.0 vs 1.7 mmol/g (195 K, 1 atm); 1.5 vs 0.8 mmol/g (273 K, 1 atm)		[181]
Cr$_3$O(H$_2$O)$_2$F(ntc)$_{1.5}$ [MIL-102(Cr)]	3.4 vs 1.4 mmol/g (304 K, 3 MPa)		[182]
Mn(HCOO)$_2$	105 vs ~0 cm^3/g (195 K, 1 atm)		[183]
Cu(dhbc)$_2$(4,4′-bipy)	Different pressures have different selective adsorption properties at 298 K		[114]
Cu(tip)	21.8 vs 1.64 wt% (298 K, 1 atm)		[184]
Zn$_5$(bta)$_6$(tda)$_2$	37 vs 10 cm^3/g (295 K, 1 atm)	9.2 (1:1, 295 K, 1 atm)[b]	[185]
Zn$_4$(OH)$_2$(1,2,4-btc)$_2$	42 vs 10 cm^3/g (295 K, 1 atm)	4.5 (295 K)[a]	[186]
Cu(pmc)$_2$	41 vs <5 cm^3/g (273 K, atm)		[187]

showed that the selectivity of CO_2 over N_2 is 17.48 for MOF-5 and 17.73 and MOF-177, both of which are lower than that of Zeolite 5A, and the selectivities for CO_2 over CH_4 are 15.53 and 4.43, respectively. Similarly, the calculated CO_2/CH_4 selectivity in [H$_3$O][Zn$_7$(μ_3-OH)$_3$(bbs)$_6$] (UoC-1′), from the corresponding Henry's law constants is 15.7 at 273 K and 21.5 at 263 K [162]. In addition, Yaghi and coworkers [209] reported the CO_2 adsorption

selectivities over CO based on the ratio of Henry's constants as 19.2, 20.9, and 37.8 for ZIF-68, -69, and -70, respectively. They used the same method to calculate the CO_2 adsorption selectivities of ZIF-100 and ZIF-95, resulting in values of 6, 4, and 17 and 11, 25, and 18 over CH_4, CO, and N_2, respectively [210]. Furthermore, this method has also been used in Cu(bdc-OH) [146] and Zn$_4$(OH)$_2$(1,2,4-btc)$_2$ [186], for evaluating the respective CO_2/CH_4 adsorption selectivity.

Table 2
Selective adsorption of CO_2 over N_2 in selected MOFs.

MOF	Uptake CO_2 vs N_2 (conditions)	Selectivity (conditions)		Ref.
Zn(1,4-ndc)(bpe)	79.6 vs ~0 cm³/g (195 K, ~1 atm)			[188]
Cu$_2$(pzdc)$_2$(4,4′-bipy)	1.6 vs 0.06 mmol/g (298 K, 1 atm)			[141]
Zn(dabco)(3,3′-tpdc)	69 vs ~0 cm³/g (196 K, ~1 atm)			[189]
Zn$_2$(tcom), 'Adamantanoid' type structure	7.3 vs 0.1 wt% (298 K, 1 atm)			[147]
Zn$_2$(tcom), 'Lonsdaleite' type structure	5.5 vs 0.1 wt% (298 K, 1 atm)			[147]
Zn$_8$(bhfp)$_{33}$ [FMOF-2]	23 vs ~2 cm³/g (298 K, 1 bar)			[149]
Co$_2$(ad)$_2$(OAc)$_2$ [bio-MOF-11]	6.0 vs 0.43 mmol/g (273 K, 1 bar); 4.1 vs 0.13 mmol/g (298 K, 1 bar)	81:1 (273 K)[c]	75:1 (298 K)[c]	[190]
Co[Fe(Tp)(CN)$_3$]$_2$	15.9 vs ~0 cm³/g (298 K, 100 kPa)			[191]
[Cu$_5$(Tz)$_9$](NO$_3$)	49.7 vs ~0 cm³/g (195 K, 1 atm)			[192]
Zn(H$_2$O)(BenzTB) [DUT-10(Zn)]	160 vs ~0 cm³/g (195 K, 0.95 bar)			[193]
Ni$_2$(dhtp)	1.5 vs 0.5 mol/mol (298 K, 500 kPa)			[155]
Zn(bIm)(nIm) [ZIF-68]	38 vs 2.9 cm³/g (298 K, 1 atm)	19.5[c]		[157]
Zn(cbIm)(nIm) [ZIF-69]	41 vs 3.4 cm³/g (298 K, 1 atm)	20[c]		[157]
Zn(Im)$_{1.13}$(nIm)$_{0.87}$ [ZIF-70]	32 vs 3.3 cm³/g (298 K, 1 atm)	18[c]		[157]
Zn(nbIm)(nIm) [ZIF-78]	51 vs 4.2 cm³/g (298 K, 1 atm)	50[c]		[157]
Zn(mbIm)(nIm) [ZIF-79]	34 vs 2.9 cm³/g (298 K, 1 atm)	22.5[c]		[157]
Zn(bbIm)(nIm) [ZIF-81]	39 vs 2.9 cm³/g (298 K, 1 atm)	23[c]		[157]
Zn(cnIm)(nIm) [ZIF-82]	54 vs 3.9 cm³/g (298 K, 1 atm)	35.5[c]		[157]
Zn(pydc)(dma)	140 vs ~0 cm³/g (195 K, 100 kPa)			[158]
Fe(pz)Ni(CN)$_4$	0.9 vs 0.13 mol/mol (298 K, 2.5 bar)			[194]
Cu(btc)H$_2$O$_{(0.5/Cu)}$ [hydrated 4 wt%]	500 vs n/a mg/g (298 K, 4.8 bar)	28 (298 K)[b]		[124]
Zn$_2$(bttb)(dmf)$_2$	3.2 vs 1.1 mmol/g (298 K, 17.5 bar)	21.5 (298 K)[b]		[159]
Zn$_2$(bttb)	5.0 vs 2.1 mmol/g (298 K, 17.5 bar)	22 (298 K)[b]		[159]
Zn$_2$(bttb)(py-CF$_3$)$_2$	2.2 vs 0.6 mmol/g (298 K, 17.5 bar)	41 (298 K)[b]		[159]
Sc$_2$(bdc)$_3$	4.5 vs 1.0 mmol/g (304 K, 50 bar)			[106]
H$_3$[(Cu$_4$Cl)$_3$(BTTri$_8$]	0.277 vs ~0 mmol/g (298 K, 0.06 bar); 3.24 vs <0.1 mmol/g (298 K, 1 bar)	10:1 (0.09 bar) 20:1 (1 bar)		[126]
H$_3$[(Cu$_4$Cl)$_3$(BTTri)$_8$](en)$_{1.25}$	0.336 vs ~0 mmol/g (298 K, 0.06 bar); 1.27 vs < 0.1 mmol/g (298 K, 1 bar)	13:1 (0.1 bar) 25:1 (1 bar)		[126]
Zn(bdc)(4,4′-bipy)$_{0.5}$ [MOF-508b]	26.0 vs 1.9 wt% (303 K, 4.5 bar)	3–6 (303 K)[a]		[165]
Zn$_2$(tcom)(4,4′-bipy)	23 vs ~0 cm³/g (298 K, 1 atm)			[195]
Cu(fma)(bpee)$_{0.5}$	100 vs 10 cm³/g (195 K, 1 bar)			[175]
Cd$_3$(OH)$_2$(apta)$_4$	65 vs ~0 mL/g (195 K, 1 atm)			[196]
Cr$_3$O(H$_2$O)$_2$F(ntc)$_{1.5}$ [MIL-102(Cr)]	3.4 vs 0.9 mmol/g (304 K, 3 MPa)			[182]
Mn(HCOO)$_2$	~105 vs ~0 cm³/g (195 K, 1 atm)			[183]
Zn$_2$(Atz)(ox)	4.5 vs ~0.2 mmol/g (273 K, 110 mbar)			[128]
[Ni(bpe)$_2$(N(CN)$_2$)](N(NC)$_2$)	35 vs ~0 cm³/g (195 K for CO_2, 77 K for N_2 at 1 atm)			[123]
Al(OH)(bpydc) (MOF-253)	~6.2 vs ~0.48 wt% (298 K, 1 bar)	2.8 (298 K)		[197]
Al(OH)(bpydc)·0.97Cu(BF$_4$)$_2$	~11.8 vs ~0.5 wt% (298 K, 1 bar)	12 (298 K)		[197]
Cu$_3$(btei) [PCN-61]	21.4 vs ~3.8 mmol/g (298 K, 20 bar)	15 at 1 bar and 22 at 20 bar (298 K)[b]		[198]
Cu$_3$(tpbtm)	23.5 vs ~4 mmol/g (298 K, 20 bar)	22 at 1 bar and 33 at 20 bar (298 K)[b]		[198]
Mg(3,5-pdc)	0.7 vs 0.1 mmol/g (298 K, 1 bar)			[199]

Ligand abbreviations for MOFs in Tables 1 and 2. H$_2$bhfp = 2,2′-bis(4-carboxyphenyl)hexafluoropropane; F-pymo = 5-fluoropyrimidin-2-olate; H-pymo = pyrimidin-2-olate; pbmp = N,N′-piperazinebismethylenephosphonate; Pur = Purinate; H$_3$oxonic = 4,6-dihydroxy-1,3,5-triazine-2-carboxylic acid; H$_2$bdc-OH = 2-hydroxybenzene-1,4-dicarboxylic acid; H$_4$tcom = tetrakis[4-(carboxyphenyl)oxamethyl]methane; BPnDC = benzophenone 4,4′-dicarboxylicacid; 1,4-ndc = 1,4-naphthalenedicarboxylate; ebtc = 1,10-ethynebenzene-3,3′,5,5′-tetracarboxylate; Im = imidazolate; mIm = 2-methylimidazolate; nIm = 2-nitroimidazolate; bIm = benzimidazolate; cbIm = 5-chlorobenzimidazolate; nbIm = 5-nitrobenzimidazolate; mbIm = 5-methylbenzimidazolate; bbIm = 5-bromobenzimidazolate; cnIm = 4-cyanoimidazolate; pydc = 3,5-pyridinedicarboxylate; dma = N,N′-dimethylacetamide; fma = fumarate; H$_2$bbs = 4,4′-bibenzoic acid-2,2′-sulfone; btec = 1,2,4,5-benzenetetracarboxylate; H$_2$tcpbda = N,N,N′,N′-tetrakis(4-carboxyphenyl)-biphenyl-4,4′-diamine; p-cdc = deprotonated form of 1,12-dihydroxydicarbonyl-1,12-dicarba-closo-dode-caborane; cnc = 4-carboxycinnamic; dpt = 3,6-di-4-pyridyl-1,2,4,5-tetrazine; dtp = 2,3-di(tetrazolate-5-yl)pyrazine; abdc = 4,4′-azobenzenedicarboxylate; 2,4-pdc = pyridine-2,4-dicarboxylate; tatb = represents-4,4′,4′′-s-triazine-2,4,6-triyl-tribenzoate; ntb = 4,4′,4′′-nitrilotrisbenzoate; ntc = naphthalene-1,4,5,8-tetracarboxylate; dhbc = 2,5-dihydroxybenzolate; 3,3′-tpdc = terphenyl-3,3′-dicarboxylate; Tp = hydrotris(pyrazolyl)borate; Tz = tetrazolate; BenzTB = N,N,N′,N′-benzidinetetrabenzoate; pz = pyrazine; apta = 4-aminophenyltetrazolate; bpydc = 2,2′-bipyridine-5,5′-dicarboxylate; btei = 5,5′,5′′-benzene-1,3,5-triyltris(1-ethynyl-2-isophthalate); tpbtm = N,N′,N′′-tris(isophthalate)-1,3,5-benzenetricarboxamide; tip = 5-(1H-tetrazol-1-yl)isophthalate; Hbta = 1,2,3-benzenetriazole; tda = thiophene-2,5-dicarboxylate; 1,2,4-btc = benzene-1,2,4-tricarboxylate; pmc = pyrimidine-5-carboxylate; 3,5-pdc = pyridine-3,5-dicarboxylate. Also see text. For the calculation of selectivity: a, from Henry's Law; b, from IAST; c, from slopes of adsorption isotherms at low pressure.

Using experimental single-component adsorption isotherms to calculate the adsorption selectivity of a multi-component mixture by IAST has been pioneered by Snurr and Hupp in the MOF field. They studied the selective adsorption of CO_2 over N_2 in several modified MOFs based on the Zn$_2$(bttb)(X)$_2$ (X = pyridine substitutes) parent framework [159]. For Zn$_2$(bttb)(CF$_3$-py)$_2$ (py = pyridine), the best one in terms of selectivity, their results showed that the selectivity increases with decreasing pressure of CO_2, and in fact surpasses the selectivities reported for zeolite and carbon adsorbents under similar conditions. They also found that, the selectivity increases as N_2 content, $y(N_2)$ approaches unity, but does not depend on the gas composition at zero coverage. In the case of $y(N_2) = 0.85$, conditions resembling flue gas, the selectivity was in the range of 25–45; fairly high selectivities of

17–41 were found even at equimolar mixtures of CO_2 and N_2. Several other MOFs have also been evaluated for the selective adsorption and separation of CO_2 over CH_4 [166,211,109,172] by them. For Zn$_2$(2,6-ndc)$_2$(dpni) (the microwave-synthesized sample), a selectivity of ~30 of CO_2 over CH_4 was found, with rapidly increasing values as the gas-phase mole fraction of CH_4, $y(CH_4)$ approaches unity [172]. At $y(CH_4) = 0.95$, extremely high selectivities of 8–67 were obtained. Even at $y(CH_4) = 0.5$, the selectivity was in the range of 4–30. Similarly, for Zn$_3$(OH)(p-cdc)$_{2.5}$, the selectivity was in the range of 7–31 at a mole fraction of 0.95 of CH_4 [166]. The same approach has also been used by Walton and coworkers [154] to evaluate the adsorption selectivity of an equimolar CO_2/CH_4 mixture in Cu$_2$(Hbtb)$_2$ over a range of pressures, giving higher values of 12.4 at 1 bar and decreasing with
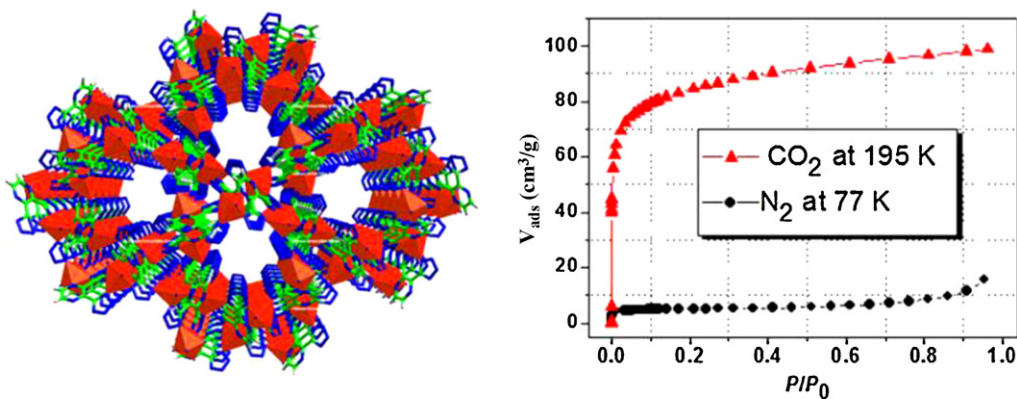
Fig. 10. Structure (left) and the selective adsorption of CO_2 over N_2 (right) of Zn(dtp).
Reproduced with permission from Ref. [171].

increasing bulk pressure to 5 at 20 bar. Recently, Bai and coworkers [198] reported the CO_2/N_2 selectivities of 33 and 22 at 298 K and 20 bar for $Zn_5(bta)_6(tda)_2$ and $Cu_3(btei)$ [PCN-61], respectively (calculated using the same method).

Some reports have approximated the adsorption selectivity factors by comparing the adsorption capacity of single-component adsorption isotherms. Chaffee and coworkers [156] calculated the adsorption selectivities of CO_2/N_2 and CO_2/CH_4 in HKUST-1 from the single gas isotherms by dividing the CO_2 adsorption capacity by that of N_2 or CH_4 at each pressure point. Their results showed that the selectivity towards CO_2 at 25 °C decreases slowly as pressure is increased. Long and coworkers [126] evaluated the adsorption selectivity of CO_2 over N_2 in Fe-BTT, resulting in a separation factor of approximately 5.5:1 at room temperature. Rosi and coworkers [190] reported the CO_2/N_2 adsorption selectivity of 81:1 at 273 K and 75:1 at 298 K for $Co_2(ad)_2(OAc)_2$ (bio-MOF-11) as the ratios of the initial slopes of the CO_2 and N_2 single-component adsorption isotherms. The similar method has also been used by Yaghi and coworker [157] in series of ZIFs for their CO_2/CH_4, CO_2/N_2, and CO_2/O_2 adsorption selectivities. Furthermore, Grande and coworkers [168] reported the selectivity of CO_2/CH_4 in HKUST-1 ranging from 4 to 6 at a pressure range of 0.1–3 bar. These estimations for adsorption selectivity have the same theoretical base as those using the ratio of the Henry's constants mentioned above; all are based on single-component adsorption isotherms.

2.3.3. Other related gas selective adsorption in MOFs

The selective adsorption of O_2 over N_2 was reported in several MOFs, including UMCM-1 [148] and $Sc_2(bdc)_3$ [106] at ambient temperature, $Co_3(2,4-pdc)_2(\mu_3-OH)_2$ (CUK-1) [176], Mg(tcpbda) [164], Zn(dtp) [171], and $Zn_4O(adc)_3(H_2O)_3$ (adc = 9,10-anthracenedicarboxylate) [212] at low temperature; all results are based on the direct observation of adsorption isotherms. One MOF of particular interest, $Cr_3(btc)_2$, reported recently by Long and coworkers [213], displayed both a high O_2 loading capacity and strong selective binding of O_2 over N_2 at 298 K. This can be attributed to the chemical adsorption of O_2 by coordination to open Cr(II) sites.

Experimental selective adsorption of CO_2 over H_2 has been reported for $Zn_2(Atz)(ox)$ [128,129], $Zn(3,3'-tpdc)(dabco)$ [189], $Zn(Me-Im)_2$ (ZIF-8, Im = Imidazolate) [151], HKUST-1 [156], and $Sc_2(bdc)_3$ [106]. Due to the weak interactions between H_2 and most pore surfaces, MOFs in general have the ability to selectively adsorb CO_2 over H_2 if the pore size is large enough for CO_2 pass.

Selective adsorption of CO_2 over CO was reported in several ZIFs and functionalized MOF-5. The details of these results can be found in a recent review contributed by Yaghi and coworkers [84] and also in the breakthrough experiments discussed below. Recently, they also examined multi-functional MOF-5, MTV-MOF-5-EI and MTV-MOF-5-EHI for the selective adsorption of CO_2 over CO [214]. The former has an adsorption capacity of 22 vs 2.7 and the latter has a capacity of 37 vs 3 cm^3/cm^3 for CO_2 and CO at 298 K and 800 Torr. Compared with MOF-5, which has an uptake ratio of 11.5:2.5 cm^3/cm^3 for CO_2 to CO under similar conditions, the selective uptake capacity of the two functional MOFs increases significantly (400% better in the case of MTV-MOF-5-EHI).

2.4. Adsorptive separation of CO_2 in MOFs

Experimental results on the adsorptive separation of gas mixture containing CO_2 in MOFs are limited in the literature. Among various separation methods the breakthrough experiment and gas chromatographic separation are simple and straightforward in the evaluation of the separation. The process of breakthrough exper-
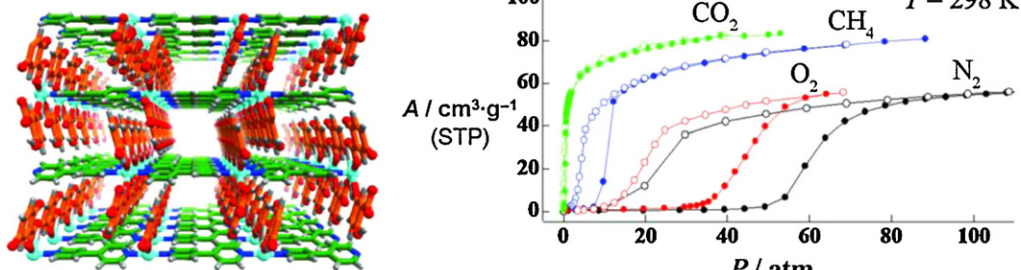

Fig. 11. Structure (left) and gas adsorption/desorption isotherms (right) of $Cu(dhbc)_2(4,4'-bipy)$.
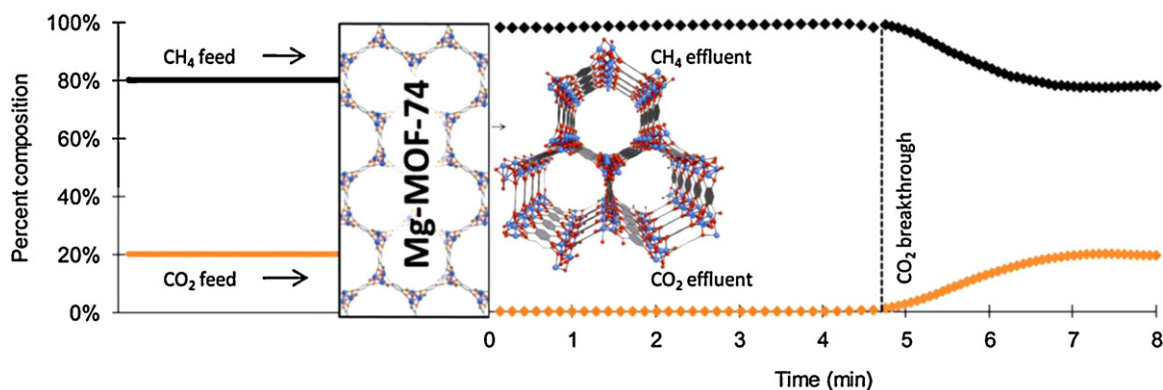Reproduced with permission from Ref. [19].

Fig. 12. Breakthrough experiment of Mg-MOF-74 using a 20% mixture of CO_2 in CH_4 (inset highlights the structure of the MOF). Reproduced with permission from Ref. [215].

iment consists of exposing a "bed" packed with the adsorbent to a mixed-gas stream, typically two components and then detecting the 'breakthrough' of the components from the adsorbent bed. The difference in breakthrough times of two gases is representative of the adsorbent's selectivity. The adsorbed amounts of each gas can be estimated by integration of the breakthrough curves. An average selectivity is then defined as the ratio of the adsorbed amounts normalized by the initial composition of the gas mixture [91].

2.4.1. Breakthrough experiments on CO_2 separation in MOFs

Some breakthrough experiments on CO_2 separation in MOFs have been performed and gave qualitative evaluations in most cases. Yaghi and coworkers examined several ZIFs for CO_2 separation by breakthrough experiments. It was determined that for ZIF-68, -69, and -70 using binary mixtures of CO_2/CO at room temperature [209], for ZIF-78 and -82 using CO_2/CH_4 [157], and for ZIF-95 and -100 using streams containing CO_2/CH_4, CO_2/CO, or CO_2/N_2 [210] these MOFs are feasible for the separation of CO_2 from other gases and have longer retention times for CO_2 than BPL Carbon under the same conditions. Besides these ZIFs, several other MOFs have also been tested by breakthrough experiments for their performance in CO_2 separation. Yaghi's group performed the tests using a 20% mixture of CO_2 in CH_4 on $Mg_2(dhtp)$ (Mg-MOF-74) [215]. As shown in Fig. 12, the adsorption for CO_2 in this MOF is highly preferred over CH_4 a dynamic capacity of 8.9 wt% CO_2 uptake, higher than that of zeolite NaX under similar conditions. To test the effect of the metal ion on CO_2 adsorption, they also performed CO_2 breakthrough in isostructural Zn-MOF-74, which took up just 0.35 wt% CO_2, a reduction of 96% compared to Mg-MOF-74. In the same time period, Dietzel et al. studied CPO-27-M (M = Ni, Mg), i.e. Ni-MOF-74 and Mg-MOF-74, for the separation of CO_2/N_2 and CO_2/CH_4 mixtures by breakthrough experiments, giving similar results of preferential adsorption of CO_2 [155].

Breakthrough experiments have also been performed on the MIL-53 series. This class of materials has a bistable structure, as described above, with a narrow pores at low CO_2 pressures and a larger pores at higher CO_2 pressures [104,216]. Denayer and coworkers [217] studied the separation of CO_2/CH_4 mixtures using a fixed-bed packed with MIL-53(Al). Because the adsorption of CO_2 in MIL-53(Al) at higher pressures leads to expansion of the framework and an increase in the adsorbed amount of both gases, the CO_2 selectivity decreased from ca. 7 to ca. 4 at pressures above 5 bar. They also examined amine-functionalized MIL-53(Al) [98], concluding that CH_4 travels rapidly through the column, while only weakly adsorbing to the pore walls and without causing framework contraction, whereas CO_2 adsorbs and can replaces pre-adsorbed CH_4 molecules. A mass-balance calculation showed that essentially no CH_4 was adsorbed while 0.83 mmol/g of CO_2 was adsorbed at

1 bar. In addition, the pulse chromatography experiment generated a retention time of 5.7 min for CO_2 but less than 5 s for CH_4 at 30 °C and a very low degree of pore filling. Similarly, Llewellyn and coworkers tested MIL-53(Cr) for separation of a mixture containing CO_2 and CH_4 resulting in selectivities ranging from 2 to 16, depending on the fraction of CO_2 [136].

Chen and coworkers [137,165] examined MOF-508b for its performance in the separation and removal of CO_2 from binary CO_2/N_2 and CO_2/CH_4 and ternary $CO_2/CH_4/N_2$ mixtures by fixed-bed adsorption. The separation efficiency was rationalized and compared in terms of the sorption selectivity, S ($S = q1/q2$, where component 1 is more adsorbed). The results indicated that S_{CO_2/CH_4} and S_{CO_2/N_2} of this MOF are moderate (3–6) at 303 K, which is lower than the selectivity of activated carbon, and decreases with increasing temperature.

2.4.2. Gas chromatographic separation of CO_2 in MOFs

Gas chromatography is an alternative experimental method used for the evaluation of gas separation in an adsorbent. Chang and coworkers [176] reported the gas chromatographic separation of a gas mixture composed of $H_2/O_2/N_2/CH_4/CO_2$ (0.6:2:28:10:27, mol%) by passing it through a column packed with CUK-1. The clear separation demonstrated that this material is potent in the separation of a complex mixture such as here containing five gases. A second example was reported recently by Navarro and coworkers [218], in which the possible utility of an ionic MOF, $A[Cu_3(\mu_3\text{-OH})(\mu_3\text{-4-carboxypyrazolato})_3]$ (A = NH_4^+ or Et_3NH^+) for gas separation was examined (Fig. 13). In their work, variable-temperature pulse gas chromatography experiments were carried out in the temperature range of 273–363 K with a gas mixture containing N_2, CH_4, CO_2, and C_2H_2. The results revealed that these materials have strong interactions with CO_2 and C_2H_2, whereas the interactions with N_2 and CH_4 are negligible, thus solidifying the effectiveness of ionic MOFs as a viable option for gas separation of CO_2 from N_2 and CH_4.

3. MOF-based membranes for CO_2 separation

As mentioned in a previous section, absorption and adsorptive separation processes for CO_2 capture, such as amine absorption and PSA or TSA separate gases usually based on differences in thermodynamic solubility [5,22,219]. Membrane-based gas separation is an attractive alternative to both of processes for a number of reasons [220–222]. Firstly, membrane separation is a passive separation and involves no moving parts, making it a far less energy consumptive process comparatively. Secondly, membrane separation is a continuous process, making membrane modules a more attractive option for plant retrofitting. Thirdly and perhaps most importantly, membrane separation takes advantage not only of
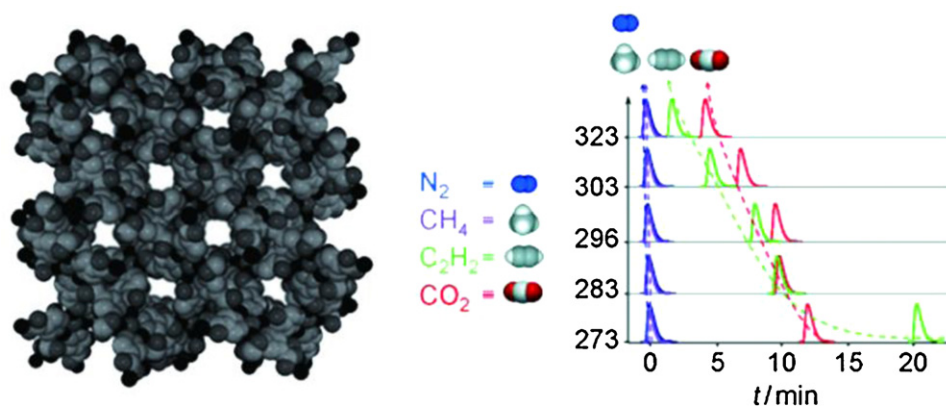
Fig. 13. Structure of $NH_4[Cu_3(\mu_3\text{-}OH)(\mu_3\text{-}4\text{-carboxypyrazolato})_3]$ (left) and the results of variable-temperature pulse gas chromatography experiments based on an equimolecular $N_2/CH_4/CO_2/C_2H_2$ gas mixture passing through a chromatographic column packed with this material (right).
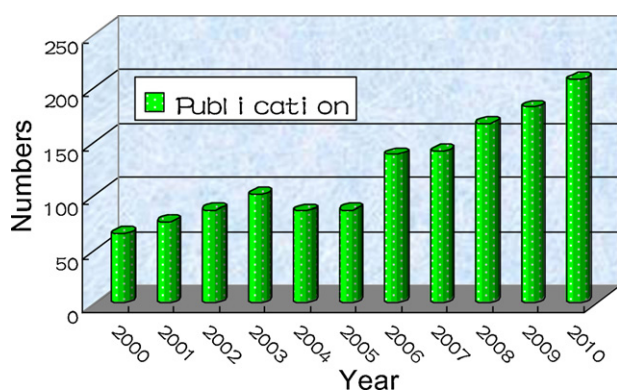Reproduced with permission from Ref. [218].

Fig. 14. Publications per year for CO_2 separation membranes, showing the increasing research interest in this topic.
Data from ISI Web of Knowledge, Thomson Reuters.

differences in solubility of the chemicals to be separated but also of differences in diffusivity, thereby potentially achieving higher selectivity for a given separation [91]. Many investigators have turned their attention to membranes for CO_2 capture and, as indicated by the number of recent publications, interest is still growing (see Fig. 14).

3.1. Current CO_2 separation membranes

Efforts to study membranes for CO_2 separation have generally focused on a few different classes of materials such as polymers, zeolites, and their derivatives (e.g. silicoaluminophosphates), and facilitated transport (often immobilized liquid) membranes. Pure polymer membranes for CO_2 separation have a few distinct advantages over other materials, such as very low production cost and generally high gas fluxes. However, traditional polymer membranes suffer from low CO_2/N_2 selectivity (less than 100). For membrane-based separation to be economically viable, the CO_2/N_2 selectivity has to be in the range of 200 [23]. Plasticization (depression of the glass transition temperature usually accompanied by drastic changes in membrane properties) in the presence of CO_2 is also a serious issue for polymeric materials. A number of reviews of polymeric membranes are available and the interested reader should turn their attention there [77,220,222–224].

Another class of materials that have been studied for membranes for CO_2 separation are zeolites and their derivatives. Zeolites are well known for their high chemical and thermal stability. Their rigid pore structure generally affords very high selectivities as has been demonstrated for many zeolite membranes [225,226]. Despite

the potential of these materials for molecular sieve membranes, zeolites are limited for use in CO_2/N_2 separation due to the similarity of the kinetic diameters of CO_2 (3.3 Å) and N_2 (3.6 Å) and the limited pore sizes available for zeolites. The interested reader should direct their attention to several excellent zeolite membrane-related reviews [227–229].

Facilitated transport membranes have also been reported for CO_2 separation [230–234]. These membranes rely on a carrier molecule (metallic ions or liquid amines for example) with a special CO_2 affinity to achieve selective CO_2 transport. Many of these membranes are immobilized liquids supported by polymeric or ceramic porous supports. The highest CO_2/N_2 selectivities observed to date have been reported for these kinds of membranes [234]. Immobilized liquid membranes are promising because of the high selectivities reported, but could face challenges with long-term stability.

Mixed matrix membranes (MMMs) consist of a continuous phase (polymer) and a homogeneously distributed discrete phase (typically inorganic particles). The purpose of including inorganic particles is to enhance the properties of the polymer phase. MMMs are promising materials for CO_2 capture because of their potential to marry the strengths of two different materials (e.g. the flexibility and low cost of the polymer phase with the high selectivity of the filler phase). However, MMMs face similar challenges to pure polymeric membranes for CO_2 capture such as plasticization in the presence of CO_2 in addition to the difficulties specific to MMMs such as preventing non-selective void spaces around filler particles. Several reports discussing these materials, their challenges and strategies for overcoming those challenges are available [77,235–238].

Despite the progress made with traditional materials as membranes for CO_2 capture, challenges such as insufficient CO_2/N_2 selectivity and low CO_2 permeability remain. Consequently there is a great need for new materials to help answer some of these challenges. As mentioned in previous sections, MOFs have been noted for their chemical functionalizeability and pore size tailorability [24,239,240]. These properties along with their regular pore structure make MOFs exciting candidates for CO_2 capture as membrane materials.

3.2. MOF-based membranes

MOF-based membrane for gas separation is an emerging field with only a few reports that include gas permeation data available to date [241–253], only one of which specifically discusses the membrane's potential for CO_2 capture [248]. Challenges associated with MOF membrane fabrication such as poor substrate–MOF interaction [244], moisture instability [254], and easy microscopic and

Table 3
Reported MOF membranes with CO_2 and N_2 permeabilities and CO_2/N_2 ideal selectivities. Note that permeabilities are estimated using membrane thickness data given in the report. Values marked with an asterisk (*) were estimated from a graph.

MOFs, Ref.	Permeability (10^{-15} mol m m^{-2} s^{-1} Pa^{-1})		Selectivity (conditions) Ideal
	CO_2	N_2	CO_2/N_2
MOF-5 [242]	~10,000	~12,000	0.8 (ΔP 100–200 kPa, 25 °C)
MOF-5 [241]	~17,000	~20,000	0.8 (ΔP 101.3 kPa, 25 °C)
MOF-5 [241]	~28,000	~34,000	0.8 (ΔP 101.3 kPa, 25 °C)
ZIF-7 [247]	16.5	16.5	1.0 (ΔP 100 kPa, 200 °C)
ZIF-7 [251]	7	4.4	1.6 (ΔP 100 kPa, 220 °C)
ZIF-8 [245]	532	208	2.6 (ΔP 100 kPa, 25 °C)
ZIF-8 [249]	890	298	3.0 (ΔP 101.3 kPa, 25 °C)
ZIF-22 [250]	952	1136	0.8 (ΔP 100 kPa, 50 °C)
ZIF-69 [248]	1225*		
ZIF-90 [252]	696	396	1.8 (ΔP 100 kPa, 200 °C)
MMOF [244]	70*	70*	1.0 (ΔP 101.3 kPa, 25 °C)
MMOF [244]	7.0*	1.8*	3.9 (ΔP 100-200 kPa, 25 °C)
HKUST-1 [243]	~17,000	~16,000	1.0 (ΔP 100 kPa, 25 °C)
HKUST-1 [246]	~12,500*	~12,500*	1.0 (ΔP 101.3 kPa, 25 °C)
HKUST-1 [246]	~5,500*	~3,750*	1.5 (ΔP 101.3 kPa, 190 °C)
MIL-53 [257]	~960*	~1120*	0.86 (ΔP 800 kPa, 25 °C)

macroscopic crack formation [246] present hurdles to the investigation of these materials as membranes for CO_2 capture. These challenges can mainly be attributed to the coordination bond in the MOF structure. In general, metal–ligand coordination bonds are not as kinetically strong as covalent bonds, resulting in moisture instability (water replacing carboxylates) and crack formation. Zeolite membranes, for example, do not require any kind of slow cooling steps or careful drying during fabrication to prevent crack formation due to the strong Si–O covalent bonds in the zeolite structure.

A number of synthesis techniques for MOF membranes have been reported and can be broken down into two broad categories: (1) *in situ* synthesis (synthesis on supports without seed crystals) [241,243,245,248–250,252] and (2) seeded (secondary) growth [242,246,247,251,255]. *In situ* growth is simple and involves only one synthesis step to produce membranes, but does not have the same microstructure control and substrate independence that secondary growth affords. MOF membranes have been reported using conventional [241,248] and microwave induced [245] *in situ* growth of bare supports, solvothermal growth on a supporting copper net [243], solvothermal growth on supports modified with organic linkers [249], and supports modified with amino-propyltriethoxysilane [250,252]. For secondary growth methods, the most important step is seed crystal attachment to the support prior to solvothermal membrane synthesis. Some reported seed crystal attachment methods include microwave induced thermal deposition [242], seed attachment with polymer binders [244,247,251,255], and seed attachment using thermal deposition (thermal seeding) [246].

MOFs, in general, are not known for their detailed thermal and chemical stability. A notable exception to this is ZIFs [248,256]. ZIF-8 and ZIF-69 are particularly interesting for CO_2 capture in industrial settings as they have been demonstrated to maintain their crystal structure in harsh environments such as boiling water, boiling benzene, and supercritical CO_2 [248,256].

3.3. MOF membranes for CO_2 separation

Due to the newness of this field of research, there are currently no MOF membranes specifically studied for CO_2/N_2 separation. However, many of these initial MOF membrane reports have included single gas permeation data for common gases including CO_2 and N_2. This data is summarized in Table 3.

3.3.1. Pure MOF-based membranes for CO_2 separation

The first metal-organic framework membranes were reported as recently as early 2009 [241,242]. These membranes are well-intergrown and randomly oriented polycrystalline MOF films consisting of IRMOF-1 crystals (see Fig. 15). They exhibited Knudsen diffusion for small gas molecules due to the large pore size of IRMOF-1 (~14.5 Å) [241,242]. Also in 2009, Zhu and coworkers [243] demonstrated an essentially freestanding membrane of HKUST-1, grown on oxidized copper nets. The copper mesh acted both as physical supports and as an extra copper source for the MOF crystallization. The membrane exhibited good separation selectivity for H_2/N_2 (~7.04) and better permeation flux than conventional zeolite membranes, but due to its freestanding nature it may face long-term mechanical stability problem. Jeong and coworkers [246] recently reported HKUST-1 membranes fabricated on porous α-alumina supports using secondary growth of deposited HKUST-1 nanocrsytals. These HKUST-1 membranes exhibited comparable gas separation properties to that previously reported by Zhu and coworkers [243].

Ranjan and Tsapatsis [244] demonstrated a gas separating membrane of Cu(hfipbb)(H_2hfipbb)$_{0.5}$ (H_2hfipbb = 4,4′-(hexafluoroisopropylidene)-bis(benzoic acid)) [258], a microporous MOF (MMOF) in 2009. As seen in Fig. 16, this membrane exhibited moderate to high ideal selectivity for H_2/N_2 (~4 at room temperature and ~23 at 190 °C) but with relatively poor permeation flux. The poor flux can be attributed to pore blocking from randomly oriented seed crystals. The first ZIF membrane was also reported in 2009 [245]. This membrane exhibited good H_2/CH_4 selectivity (11.2 for a 1:1 mixture) at room temperature, indicating the molecular sieving effect (preferential permeation of small molecules).

Jeong and coworkers [249] recently reported the first MOF membranes (ZIF-8) with controlled microstructures. These membranes have well-intergrown or poorly intergrown structures depending on the presence or absence of a common base (sodium formate) and the choice of metal salt in growth (see Fig. 17). ZIF-7 membranes were also reported recently [247,251]. These membranes exhibited negligible ideal selectivity for CO_2/N_2 which is unsurprising as the pore size of ZIF-7 (~3 Å) is smaller than the kinetic diameter of both CO_2 and N_2. ZIF-22 membranes were reported which exhibit similar CO_2/N_2 separation properties to ZIF-7 [250]. In addition, *c*-oriented ZIF-69 membrane fabricated on a porous α-alumina was reported by Lai and coworkers [248]. This report tested the chemical stability of ZIF-69 membrane by immersing it in various boiling solvents for 7 days and then checking the membrane crystallinity. The membrane maintained their crystal structure in boiling benzene, boiling methanol, boiling water, and supercritical CO_2 indicating their potential suitability for CO_2 capture in real environments. Despite the large pore size of ZIF-
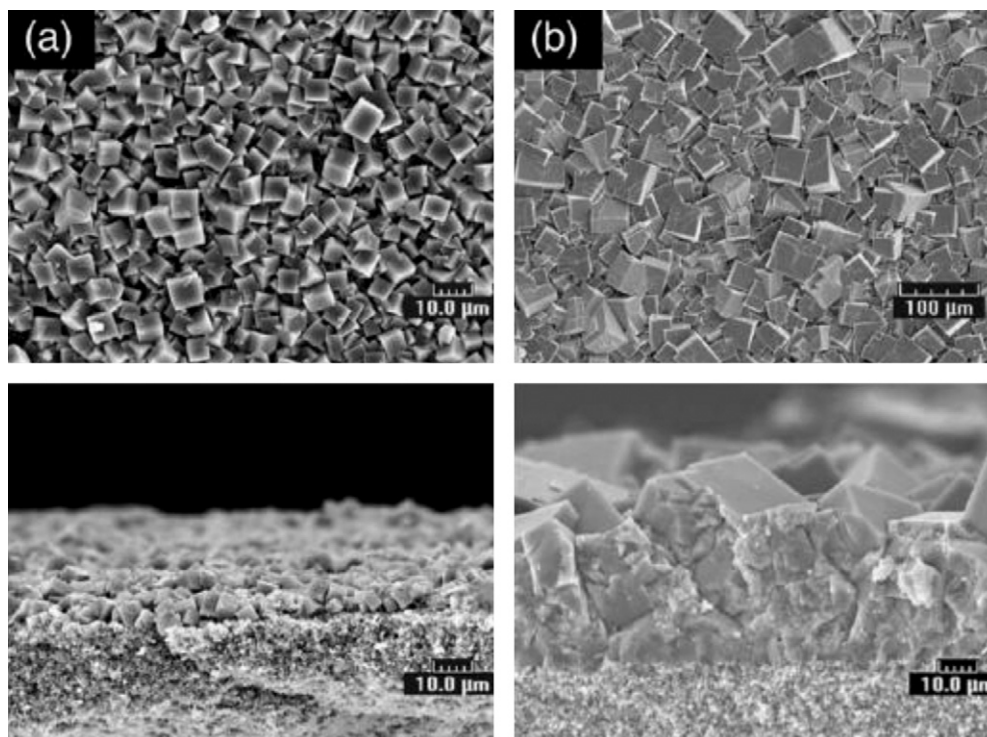
Fig. 15. SEM images of one of the first MOF membranes. (a) IRMOF-1 seed layers on porous α-alumina supports and (b) randomly oriented IRMOF-1 membrane after secondary growth of seeded support.
Reproduced with permission from Ref. [242].

69 (~7.8 Å), this membrane exhibited CO_2 permeance better than expected for Knudsen diffusion. The CO_2/CO mixture permselectivity of this membrane was 3.5 at room temperature. The CO_2 permeability when measured as a single component is equivalent to that of a zeolite membrane with similar pore size (zeolite Y) [259]. However, when CO_2 permeability was measured in binary mixture it was about 5 times higher for the ZIF-69 membrane. This indicates that this membrane exhibits preferential adsorption of CO_2 and may be useful for CO_2 capture. A ZIF-90 membrane was also reported which has selectivity properties similar to ZIF-7 [252]. Most recently a membrane of MIL-53 was reported which exhibits Knudsen diffusion for small gases [257].

3.3.2. Mixed matrix membranes using MOFs as the discrete phase for CO_2 separation

Mixed matrix membrane (MMM) using MOFs as the filler material is also a new area of research and there are also only a

very few reports available [260–265]. Koros and coworkers [262] reported an MMM comprised of poly(vinyl acetate) (PVAc) and a MOF composed of copper and terephthalic acid (Cu–TPA). This membrane exhibited increased selectivity for many gases, including CO_2 upon inclusion of the MOF compared to the pure PVAc membrane. The ideal selectivity of pure PVAc for CO_2/N_2 is ~32 and for 15% CuTPA–PVAc is ~35. All gases were tested at 65 psia (~4 atm) except for CO_2 which was tested at 1.35 psia (~0.09 atm) to prevent plasticization. Musselman and coworkers [263] reported the first ZIF-based polymer MMM using ZIF-8 as the filler phase and Matrimid® as the polymer phase. Inclusion of the ZIF phase had substantial impact on the membrane selectivity. Pure Matrimid® exhibited an ideal selectivity for CO_2/CH_4 of ~43, and at 50% loading of ZIF crystals the ideal selectivity increased to ~124. Binary gas measurements of 10:90 CO_2/CH_4 also showed selectivity enhancement; pure Matrimid® gave selectivity of ~42, and at 50% loading the selectivity increased to ~89.
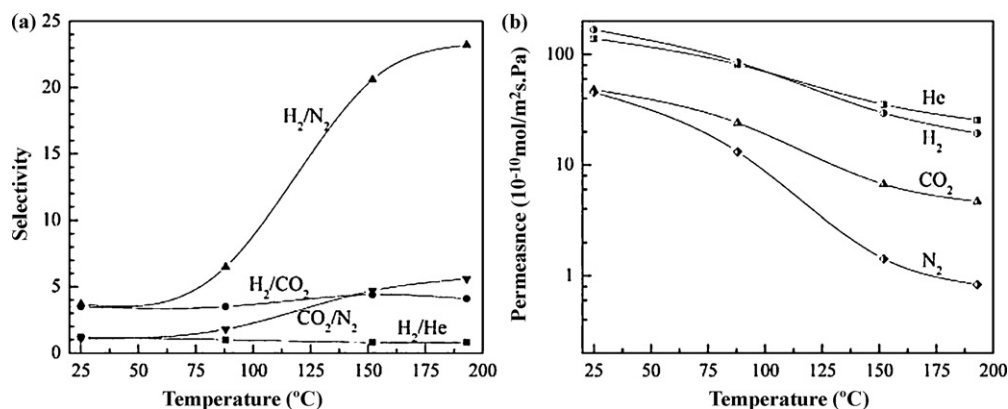

Fig. 16. Gas permeation results on Cu(hfipbb)(H₂hfipbb)$_{0.5}$ membrane: (a) ideal selectivity for various gases and (b) permeance values for different gases.
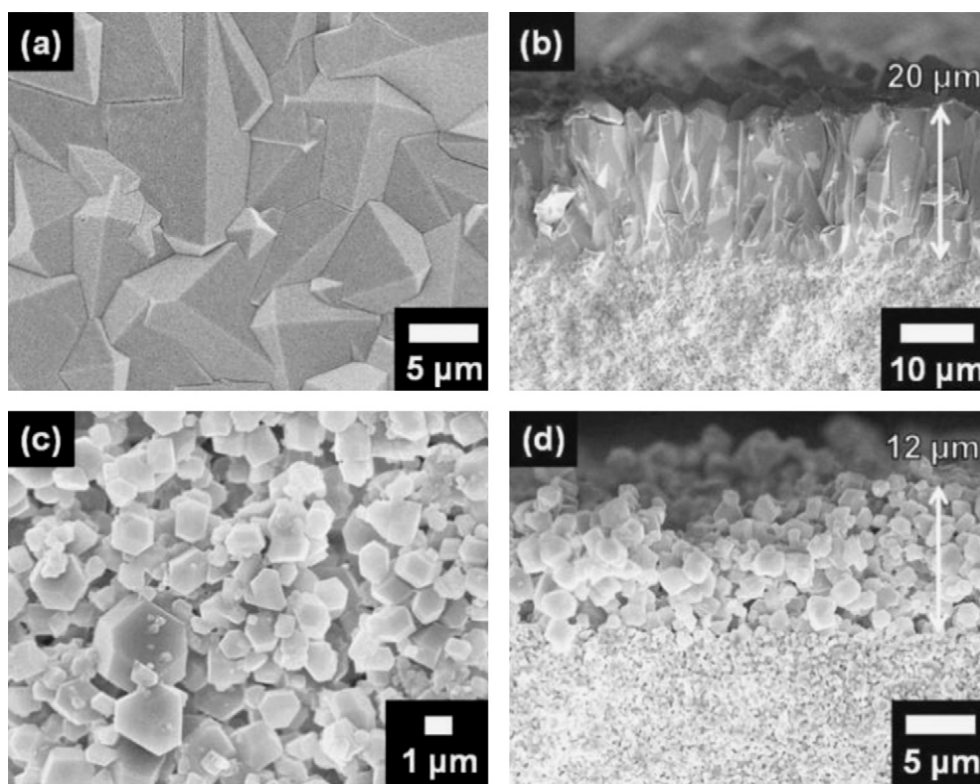Reproduced with permission from Ref. [244].

Fig. 17. (a) Top-down and (b) cross section FE-SEM images of ZIF-8 membrane with larger, well intergrown crystals grown from organic linker modified supports. (c) Top-down and (d) cross section FE-SEM images of a ZIF-8 film with poorly intergrown crystals also grown on modified supports.
Reproduced with permission from Ref. [249].

3.4. Potential MOF structures for membrane-based CO_2 separation

When contemplating potential MOFs to investigate for CO_2 capture membranes, many properties in addition to CO_2 adsorption affinity must be considered, such as pore size, pore structure, stability in humid environments, and thermal stability. Choosing a MOF with the appropriate pore size to differentiate gases is not as straightforward as it may seem since the framework structure of MOFs used in MOF membranes has been observed to be rather flexible [245,247]. This is particularly noticeable in a recent report of a ZIF-90 membrane [252]. According to crystallographic data, the pore size of ZIF-90 is 3.5 Å, which should be a good size to differentiate CO_2 and N_2. However, at least according to single gas measurements, this membrane's selectivity for these gases is negligible likely due to framework flexibility. However the poor CO_2/N_2 ideal selectivity of this membrane may also be attributed in part to non-selective inter-crystalline diffusion through grain boundaries as observed in zeolite membranes [226].

Based on their unusual stability and the range of pore sizes available [209,256], ZIFs seem to have good potential for CO_2 capture membranes. Recent results for ZIF membranes with pore aperture size of 3.0 Å (ZIF-7 [247,251] and ZIF-22 [250]) indicated that even relatively large molecules, such as CH_4 (3.8 Å) can still appreciably permeate through the membrane, implying that it may be worthwhile to pursue those ZIFs with smaller aperture. For examples, ZIF-64 has aperture size of 2.5 Å [209] and ZIF-74 and -75 have even smaller aperture sizes of 1.2 Å. ZIF-74 and ZIF-75 have the added advantage of using asymmetric ligands, a property recently noted for increasing CO_2 affinity [266].

Another potential strategy to follow would be incorporating bulkier, less flexible organic ligands into the MOF matrix. One would expect that this would dramatically enhance the molecular sieving effect in membranes of such MOFs.

Apart from the potential MOFs mentioned above, there are stimuli-responsive MOFs whose structures, thereby properties, change reversibly upon external stimuli such as temperature [115,116] and gas adsorption [105]. This offers unique opportunities for membrane-based gas separation including CO_2 capture by controlling gas diffusion/adsorption properties. One such material is mesh adjustable molecular sieves (MAMS), which are a class of MOFs that proposed to (probably) exhibit temperature tunable molecular gates within their pores [115,116]. These gates afford control over the gases absorbed into the material by discriminating based on molecular size; a property that is of particular interest for membrane-based CO_2 separation. A membrane capable of continuously adjusting its pore size would be useful not only for high resolution separation of similar gases such as CO_2/N_2 but for its market flexibility (a single membrane could be used to achieve separation of many different gas mixtures). Another important feature of MAMS is that although the molecular gates within the structure open and close with temperature change, the lattice constants do not. This means that, unlike previously reported titanosilicate molecular sieves [267], the MAMS unit cell is unaffected by the molecular gating effect [115]. Recent reports [115,116] described MAMS in powder or crystalline form, however no reports exist describing MAMS films or membranes. Development of MAMS membranes could open the way for transformative separation technology, such as membrane units for gas separation made up of consecutive MAMS membrane modules at increasing temperatures as illustrated in Fig. 18.

4. Computational approaches of CO_2 adsorption and separation in MOFs

In addition to enormous experimental efforts, advances in computational power have allowed molecular simulation to play
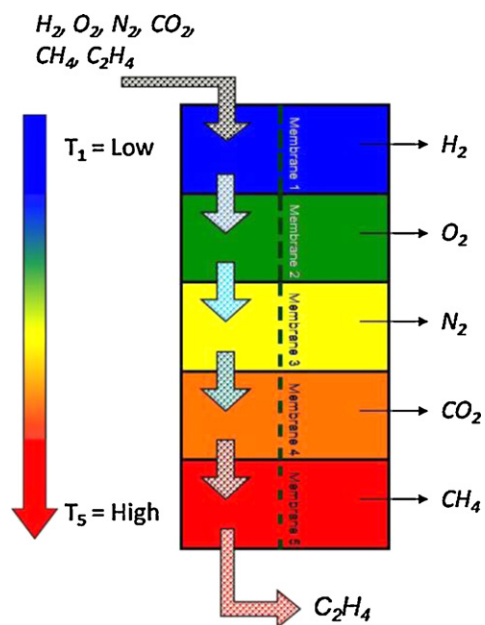
Fig. 18. Concept of a distillation tower-type unit for gas separation based on consecutive modules of MAMS membranes at increasing temperatures.

a significant role in the investigation and prediction of MOF's properties and potential applications. By providing microscopic information that sometimes is not accessible or difficult to obtain with experiment, simulations complement the experiment. In addition, simulations are extremely useful to evaluate adsorption performance not only of real materials but also of hypothetical materials based on the atomistic model of their structures. In conjunction with experiments, simulations also play an important role on the rational design of new materials (MOFs) for specific applications. Based on these advantages, computer simulations have been used to study MOFs applications, such as in CO_2 adsorption and separation.

4.1. Simulation methods

The main molecular simulation techniques used for the investigation of CO_2 adsorption and separation in MOFs are *ab initio* and density functional theory (DFT) calculations, Grand Canonical Monte Carlo (GCMC) simulations, and molecular dynamics (MD) simulations.

4.1.1. Ab initio and density functional theory (DFT)

Ab initio and density functional theory (DFT) methods are normally implemented when detailed information regarding chemical and physical interactions is required. During the past years, *ab initio* and DFT calculations have been employed extensively to study, for example, specific adsorption sites, interaction mechanisms, and interaction energies between MOFs and small gas molecules, including H_2 [268–271], CH_4 [272,273], and CO_2 [100,274–277]. In contrast to H_2 and CH_4, CO_2 has a significant quadrupole moment, which induces its specific interactions with MOFs, such as much higher binding energy with open metal sites in MOFs, hydrogen bonding, and so on. In quantum-based simulations, the DFT method has been widely used from small clusters to large systems because it includes electron correlation effects and shows exceptional computational efficiency. Among different DFT methods, the widely used B3LYP can normally give a good approximation of binding geometries, which is comparable with high level *ab initio* methods. However, DFT has some deficiencies when applied to systems with weak interactions, such as dispersion interactions.

In comparison with DFT, high level *ab initio* methods, such as second order Moller–Plesset (MP2) [278] show superiority in treating dispersion interaction in weakly bonded systems and give more accurate results [273]. However, MP2 is computational expensive and only affordable for small systems. Considering both calculation time and accuracy, the combinations of high level *ab initio* and DFT or low level *ab initio* was the optimal choice for investigations of these "big" MOF systems [273]. In addition to MP2, some newly developed techniques including GGA-DFT [279] and MP2-DFT [280] are also available to treat systems with long-range dispersion interactions and provide good results for binding geometries and energies [281,282]. To get reliable binding energy results, basis set superposition error (BSSE) [283] should be corrected to avoid overestimating the interaction energies between MOFs and CO_2 [273,276,282]. It has been found that BSSE shows strong effects on adsorption energy obtained from the MP2 method [284]. However, DFT only shows relatively small dependences on BSSE [285].

Another important role of DFT calculations in CO_2 adsorption and separation in MOFs is to provide force constants and atomic charges for molecular simulations. For example, calculated atomic point charges can be used to develop force fields (FFs) for classical simulations. B3LYP is frequently applied in MOFs since it provides better descriptions of transition metals. Regarding the selection of basis sets, to balance simulation accuracy and computation time, 6-31+G(d) or 6-31G(d) is normally used for light atoms [286,287], while the effective core potential (ECP) basis sets are often chosen for heavy atoms. LANL2DZ is one of the most common ECP basis sets for complexes involving transition metal elements [288]. There are a couple of approaches available to evaluate atomic charges, such as Mulliken population analysis [289], the electrostatic potential (ESP) [290], the restrained electrostatic potential (RESP) [291], the charges from electrostatic potentials using a grid (CHELPG) [292], and the recently developed REPEAT method [293].

4.1.2. Grand Canonical Monte Carlo (GCMC)

Grand Canonical Monte Carlo (GCMC) has been recognized as one of the most extensively used techniques to study gas adsorption properties of MOFs, such as gas uptake and the heats of adsorption. In GCMC, simulations are conducted at fixed chemical potential of the molecules, temperature, and volume [294,295]. GCMC is suitable to study guest molecule adsorption because it models a system at equilibrium, where the chemical potentials of the adsorbate in adsorbed and bulk phases are equal. Each Monte Carlo simulation involves four types of movement of adsorbates: insertions, deletions, displacements, and rotations to achieve equilibrium of the system. The results are then averaged over the run of simulations. With a series of simulations at different pressures, the adsorption isotherms can be obtained by relating the chemical potential and gas phase pressure through an equation of state. This technique, however, often suffers convergent problems when the probability of particle creation in a dense phase is low.

The input of GCMC simulation includes separation of models for adsorbate and adsorbent, and force field to describe the interactions between them. In most simulations, it is assumed that the frameworks are rigid and the periodic boundary conditions are normally applied to mimic the crystalline periodicity thus avoiding boundary or finite size effects [296]. To date, only few simulation studies have been performed in the adsorption of flexible MOFs [216,297]. To model the adsorbate–adsorbate interactions, Lennard–Jones (LJ) potential is generally used in first-approximation. The force field parameters can be obtained by fitting the LJ potential to experimental vapor–liquid equilibrium data. The early investigation normally uses a sphere model to describe small molecules, such as CO_2 [298]. However, more accurate potential models are more commonly used today, where both the van der Waals (normally modeled by

LJ potential) and the Coulombic interactions are considered. The new model of CO_2 generally consists of three LJ sites (two O and one C atom sites) with charges located on each site to describe its intrinsic quadrupole moment [299–301]. In a more complex model to describe $CO_2 \cdots CO_2$ interactions, the angle of O–C–O in CO_2 is not fixed and allowed to vary to mimic bond bending of CO_2 [299,302]. Similarly, adsorbate–adsorbent interactions are also modeled as a combination of LJ and Coulombic potentials. To date, many GCMC simulations of gas adsorption on MOFs have employed general-purpose force fields, including the universal force field (UFF) [303], DREIDING [304], and optimized potential for liquid simulations-all atom (OPLS-AA) [305] models, which include the force field parameters for the atoms in most of the periodic table. These empirical force fields were mainly developed for covalent bonds between atoms so it gives only approximate predictions of interaction energy for non-bonded interactions, such as the interaction between gas molecules and MOF's pore surface. As a result, inaccurate gas adsorption properties are often generated with the empirical force fields [306]. In addition, because a wide range of possible inorganic (inorganic-organic) fragments are involved in MOFs, the force field parameters for these new fragments are not available in some cases. It limits the investigations in the screening and design of MOFs for specific applications. Therefore, more accurate force field parameters are required for describing these frameworks precisely. Recently, first-principle-based force fields are proposed to describe interactions between atoms in adsorbate and adsorbent. The approach combines first-principles calculations and GCMC simulations [268,307,308]. In the new developed force fields, as discussed also in Section 4.1.1, the interaction energies between the gas molecules and MOFs are obtained using *ab initio* or DFT methods, which can be later fitted to an appropriate potential functions, and then force field parameters can be obtained. In comparison with empirical force fields, first-principle-based force fields can precisely describe the non-bonded interactions between gas molecules and MOFs and therefore lead to more accurate prediction for the adsorption properties of MOFs.

GCMC simulations can be used not only to evaluate the adsorption properties of simple gas on MOFs; in the case of gas mixtures, but also to predict the selectivity. Since the selectivity is not easily accessible from experiments, GCMC simulations show a clear advantage to predict gas mixture separations. The separation factor of a binary mixture is usually quantified by the adsorption selectivity S_{12}, which is defined as: $S_{12} = (x_1/x_2)(y_2/y_1)$, x_i is the mole fraction of species i in the adsorbed phase and y_i is the mole fraction in the bulk phase, respectively.

4.1.3. Molecular dynamics

Molecular dynamics (MD) has been employed to investigate the kinetic properties of gas molecules in various MOFs, including CO_2 diffusion inside MOFs [140,286]. The kinetic properties, together with adsorption equilibrium properties, are crucial to evaluate the overall performance of MOFs. In characterizing the diffusion of a single adsorbate, two most common quantities are the self-diffusion coefficient and transport diffusion coefficient. The self-diffusion coefficient describes the displacement of individual gas molecules, while the transport diffusion coefficient quantifies the mass transport induced by a concentration gradient in the adsorbed species [309,310]. Both coefficients depend on the concentration of adsorbate loading, which can be remarkably different [311,312] and only equal each other in the region of dilute pore loading [313]. In MD simulations, MOFs are normally assumed to be rigid. The force fields described in GCMC can usually be used in MD simulations.

One of the challenges in understanding the diffusion behavior of CO_2 in MOFs is the little experimental information available in regard with molecular transport. So far, MD is the main technique to

estimate the diffusion properties of CO_2 in MOFs. Moreover, experimental measurement of mixture diffusion in MOFs is extremely challenging, so the MD simulation can provide some precious information about transport properties of gas mixtures, which is very helpful in screening and designing MOF materials for CO_2 separation [314,315].

4.2. Simulation in selected MOF systems for CO_2 adsorption and separation

Despite more than 100 MOFs have been explored experimentally to date in CO_2 adsorption and separation, only several typical (or representative) MOFs were widely studied by theoretical calculations based on molecular simulations.

4.2.1. IRMOFs and Cu-BTC

In 2005, Skoulidas and Sholl first studied CO_2 diffusion in MOF-5 (IRMOF-1) [316] using equilibrium molecular dynamics (EMD). In their simulation, the EP2 model [299] was employed for description of CO_2's quadrupole moment and charges were added for all the atoms in MOF-5 for evaluating the charge–charge interactions. The calculation showed that CO_2 adsorption is considerably stronger compared to other gases such as Ar, CH_4, N_2 and H_2. The calculated self-diffusivity and transport diffusivity have the order of $H_2 > N_2 \approx CH_4 \approx Ar > CO_2$ at room temperature. Notably, the computed transport diffusivity of CO_2 is a non-monotonic function of pore loading.

The first computational study of CO_2 separation in MOFs was carried out by Zhong and coworkers [317]. The separation behaviors of gas mixtures (CO_2, CH_4, and C_2H_6) in Cu-BTC were investigated with GCMC simulations. Two microdomains with different electrostatic field strengths, tetrahedron-shaped pockets and square-shape pores, were identified. The different adsorption properties of the microdomains lead to significant enhancement of gas separation. They also examined $CO_2/CH_4/H_2$ adsorption in two MOFs, MOF-5 and Cu-BTC [318]. Their simulation showed that gas separation was influenced by the geometry and pore size. MOF-5 possesses a simple channel structure and consequently exhibits simple selectivity properties; whereas Cu-BTC has a more complicated channel/pocket structure, leading to complex selectivity. More importantly, the strength of electrostatic interactions can tremendously alter the gas separation performance, particularly for the components with different dipoles/quadrupoles. The CO_2/CH_4 and CO_2/H_2 selectivities in Cu-BTC are significantly enhanced compared to those in MOF-5, because the open metal sites of Cu-BTC have strong electrostatic interactions with CO_2 molecules. Furthermore, Zhong and coworkers [319] also conducted a computational study of adsorption and separation of CO_2/CO and C_2H_4/CO_2 mixtures in Cu-BTC. They noted that the selective adsorption can be mostly attributed to topology structure of the side pockets. Most gas molecules occupy the side pocket at low pressures; and more molecules enter into the channel pores at higher pressures, primarily due to saturation of the pockets. The simulated selectivity of equimolar CO_2/CO is 10–25 (298 K, 0–5 MPa) in Cu-BTC. Cu-BTC also shows good selectivity of CO_2 from flue gases ($CO_2/N_2/O_2$) mixtures, according to the simulation results by Zhong and coworkers [320]. The high selectivity is mainly benefited from the different quadrupole moments of the gas components: CO_2 possesses the largest quadrupole in the mixtures and thus the strongest electrostatic interactions with the framework; while N_2 and O_2 have smaller quadrupole moments and relatively weaker interaction. GCMC simulations demonstrated that difference of electrostatic interactions enhanced the separation of gases. Remarkably, they found the gas selectivity also depended on temperature and gas composition: the selectivity decreases sharply with increasing temperature, and also changes significantly with the ratio of the

components. These factors are important and need to be considered in gas separation.

In 2007, Snurr and coworkers studied the adsorption sites of light gases in MOF-5 by using Monte Carlo (MC) simulations [277]. They reported that the positions and occupations of the binding sites can be correctly predicted when an appropriate force field was applied. For CO_2, the primary adsorption site is located near the Zn_4O cluster with a planar orientation pointing towards the zinc atom. Snurr and coworkers examined the experimental adsorption isotherms of CO_2 in MOF-5 at various temperatures. Dramatic steps of the isotherms were found with decreasing temperature [96]. They further conducted GCMC simulations, aiming at reproducing the adsorption isotherms. Their research indicated that the sorbate–sorbate electrostatic interactions must be included for predicting the inflections and steps. The unusual shape of isotherms is subsequently ascribed to the electrostatic interaction between CO_2 molecules.

Pianwanit et al. [273] investigated the optimal binding sites of CO_2 in MOF-5 by ONIOM (MP2/6-31G(d,p): HF/6-31G(d,p)) calculations. Three model clusters are respectively composed of one, two, and three $(Zn_4O)_2(OAc)_{10}(COO)_2C_6H_4$ molecule(s), and CO_2 is located at linker and corner domains of the clusters with parallel and perpendicular orientations. The study revealed the cluster size only affects the binding energy slightly for the configurations at the linker part but has a significant effect on the configurations at the corner part. To evaluate the binding energy of CO_2 in MOF-5, the model cluster needs at least a $(Zn_4O)(CO)_6$ unit at the corner and three $(Zn_4O)(CO)_6C_6H_4$ fragments at the edges. The perpendicular configuration at the MOF corner was determined as the optimal one with the lowest binding energy of -9.27 kJ/mol.

Heats of adsorption are thought to be directly related to gas adsorption and separation in MOFs. Farrusseng et al. [127] made a systematic study of the heats of adsorption for 7 gases in three MOFs (IRMOF-1, IRMOF-3 and Cu-BTC). In general, the experimental and simulated heats of adsorption matched very well each other for IRMOF-1 and IRMOF-3. For Cu-BTC, the GCMC simulations gave larger adsorption energies. A plausible explanation is that the gas molecules were permitted to access the small pockets of Cu-BTC in the simulations but these pockets are inaccessible for the molecules in experiments. Further simulations in which the pockets were blocked led to much better agreement with the experimental results. The calculated adsorption heat of CO_2 is 21.8 kJ/mol in Cu-BTC, and the value decreases to 14.9 kJ/mol when the small pockets are blocked, which is very close to the experimental value (14.6 ± 0.5 kJ/mol, measured by TAP-2). Zhong and coworkers [321] also studied the effect of small pockets on gas separation in Cu-BTC. Blocking of the side pockets results in big differences in their simulated selectivity curves at low-pressure range. The pocket-blocked Cu-BTC was shown always to exhibit lower selectivity than the non-blocked Cu-BTC for six binary gas mixtures. Since the selectivity in the small side pockets is larger than other regions, it would generate unrealistic results if the pockets are inaccessible for gas molecules and not blocked in the simulations. The phenomenon was also noticed by Krishna and van Baten [322]. They pointed out that the experimentally inaccessible pockets of MOFs should be blocked appropriately in GCMC simulations. A relatively simple approach is to make a spherical space from the center of the pockets, where any molecule movement or molecule generation into the space is prohibited in each MC step.

4.2.2. Charged MOFs

Some MOFs carry charges in their frameworks. The charges are usually balanced by extraframework ions. Jiang [323] first investigated the structural and adsorption properties of charged *soc*-MOF using atomistic and molecular simulations. The extraframework ions, NO_3^-, encage in the capsule structures. For each capsule, four

NO_3^- ions are statistically located in near eight trimer building blocks. The ionic framework shows much higher affinity for CO_2 because of the enhanced charge–quadrupole interactions. The predicted CO_2/H_2 selectivity in *soc*-MOF is up to 600, among the most efficient nanoporous materials for gas separation. The presence of trace H_2O in the mixtures considerably affects the selectivity. At low pressures, the selectivity slightly increases because the H_2O binding around trimers provides additional adsorption site for CO_2. At high pressures, however, the selectivity drops due to the competitive adsorption between CO_2 and H_2O.

Another charged MOF investigated by Babarao and Jiang [287] is *rho* zeolite-like MOF (*rho*-ZMOF), which contains an anionic framework and extraframework Na^+ ions. Analogous to *soc*-MOF, *rho*-ZMOF also shows extraordinary CO_2 separation selectivities in CO_2/H_2, CO_2/N_2 and CO_2/CH_4: for the CO_2/H_2 mixture (15:85), the predicted selectivity in *rho*-ZMOF is 165,000 at infinite dilution and 1800 under ambient conditions; For the CO_2/CH_4 mixture (50:50), the selectivity is 3800 at infinite dilution and 80 at 1 atm; for the CO_2/N_2 mixture (15:85), the selectivity reaches to 19,000 at infinite dilution and drops 500 under ambient conditions. All of these selectivities are the highest predicted to our knowledge. In *rho*-ZMOF, Na^+ ions are distributed around two types of binding sites, the single eight-membered ring and the α-cage. Compared to NO_3^- in *soc*-MOF [323], Na^+ ions have larger mobility in the framework and can be acted as additional binding centers. This gives stronger charge–quadrupole interactions and accordingly, higher adsorption selectivity. They further conducted computational studies to examine to effect of water in *rho*-ZMOF [324]. In general, the presence of water significantly influences the adsorption of CO_2/CH_4 mixtures. Their simulations showed that CO_2 adsorption drops sharply with only 0.1% of H_2O and CH_4 adsorption roughly remains same. H_2O significantly reduced the selectivity of CO_2/CH_4 mixtures by around one order of magnitude. This is because the water molecules surrounding the Na^+ ions weaken the interactions between CO_2 and Na^+.

Very recently, Babarao and Jiang [325] studied the storage and separation of CO_2 in a highly porous ionic *rht*-MOF using molecular simulations. The MOF has a cationic framework and the charges are balanced by NO_3^- ions, which show low mobility and reside near the small windows connecting the tetrahedral and cuboctahedral cages. The MOF has three different types of cages and is suitable for gas storage. The calculations indicated the selectivity of CO_2/H_2 in *rht*-MOF is not as high as *rho*-ZMOF and *soc*-MOF. This can be attributed to the highly porous structure and relatively low charge density of *rht*-MOF. Similar to *rho*-ZMOF, the selectivity of CO_2/H_2 in substantially reduces in *rht*-MOF in the presence of H_2O, as the interactions between CO_2 and NO_3^- is shielded by the water molecules around the NO_3^- ions.

Introducing ions into MOF systems generally leads to enhanced adsorption and selectivity for CO_2. The structure and separation properties of Li^+ exchanged MOFs (Li^+-MOFs) were examined by Babarao and Jiang [325]. The structures of the hydrated and dehydrated Li^+-MOFs were optimized from DFT calculations. The preferential adsorption sites are near the cations and metal clusters. The predicted selectivity of CO_2 over H_2 and N_2 is 550 and 60 at room temperature and 1 atm. Li^+-MOFs possess higher selectivity than non-ionic MOFs and most other porous materials. According to GCMC simulations, the high selectivity is originated from the charges of cations and frameworks. The hydrated Li^+-MOFs displays slightly less adsorption and selectivity due to the reduced free volume.

Xu and Zhong [326] modified MOF-5 by introducing O–Li groups into the organic linkers and tested the separation selectivity of CO_2/CH_4 for 3 Li-modified MOFs. The results from GCMC simulations showed significant changes of the framework charges, the isosteric heats of adsorption and the preferential adsorption

sites in the modified MOFs. These changes result in huge enhancement of the CO_2 selectivity from the gas mixtures. For example, the selectivity reaches as high as 190 at a pressure of 0.1 MPa (298 K, CO_2:CH_4 = 1:9). Their research confirmed that incorporation of ionic or ionic-like groups into MOF systems is an effective approach to improve the selectivity of gas mixtures.

4.2.3. ZIFs

Zeolitic imidazolate frameworks (ZIFs) generally have high thermal and moister stability compared to other types of MOFs. Zhong and coworkers [327] studied the adsorption and diffusion behaviors of CO_2 in two typical ZIFs, ZIF-68 and ZIF-69 using combined GCMC and MD techniques. CO_2 molecules preferentially adsorb in the small pores encompassed by the nIM (nitroimidazole) linkers. With the increasing pressure, the molecules can also be adsorbed in the corners formed by the phenyl ring in the large pores and further occupy the pores. For ZIF-69, the chlorine atoms in cbIM linkers play an important role in the enhancement of CO_2 binding energy. Similar to many other MOF systems, the contribution of framework charges cannot be ignored at low pressures. Their MD calculations indicated that the diffusion of CO_2 in ZIF-69 is slower than ZIF-68 due to the pore size and steric hindrance. Moreover, the study suggested a slower CO_2 diffusion in ZIFs than that in other MOFs.

Johnson and coworkers [281] also reported their computational results of adsorption and diffusion of CO_2, H_2, N_2 and CH_4 in ZIF-68 and ZIF-70. They found the X-ray diffraction structure of ZIF-70 had a wrong ratio of IM to nIM and thus failed to predict experimental adsorption isotherms for N_2. The error was corrected after ratio adjustment and DFT geometry optimization. The simulated N_2 adsorption data was in good agreement with experimental results when taking framework charges into account. However, incorporation of charges failed to generate reliable CO_2 isotherms at low pressures for both ZIF-68 and ZIF-70. The discrepancy has not been understood, though it perhaps arises from an unrealistic framework-CO_2 attraction in the models. Notably, the results are not consistent with previous computational studies [327]. They claimed that Liu and coworkers model underestimated adsorbent–adsorbent attractions and the good agreement between experiments and the simulations by Liu and coworkers may be caused by a fortuitous cancellation of errors. Furthermore, the inclusion/exclusion of charges significantly influences the calculated diffusivities, particularly, at low loading.

Recently, Nieto-Draghi and coworkers [328] investigated the adsorption of CH_4, N_2, and CO_2 on three ZIFs, ZIF-8 and ZIF-76 and ZIF-69. Their GCMC simulations showed that standard force fields were not reliable and failed to reproduce experimental data. A modified force field optimized by experimental data was adopted to examine the adsorption behavior. The simulated adsorption isotherms predicted the CO_2 uptake order (ZIF-69 < ZIF-8 < ZIF-76) at high pressures, which is partially verified by experiments. The simulations also indicated preferential adsorption sites of ZIF-8, located at the organic linkers. Furthermore, the charge–quadrupole contribution prevails in the interactions between the metal atoms and CO_2; whereas the vdW contribution is only <10% in the overall binding energy. According to the calculated Henry constant and isosteric heats of adsorption, vdW interactions dominate the adsorption of CH_4 and N_2, while vdW and electrostatic interactions co-govern the adsorption of CO_2 in the ZIFs. Remarkably, the study indicated ZIFs possess some properties similar to zeolites. Woo and coworkers [329] carried out GCMC and MD studies of CO and CO_2 adsorption in ZIF-68 and ZIF-69. The GCMC simulation was performed at low pressures (0–1 atm) at 273 K. In the low-pressure range, the uptake of gas molecules is not determined by the geometric structure, but controlled by the properties of binding sites in the framework. The aromatic functional groups were identified as

the adsorption sites. CO/CO_2 was observed in both pores and channels in the ZIFs. In particular, CO_2 molecules are rarely distributed in the central region of the pores because of the loss of entropy in the confined space at low pressures. Two groups of binding sites, respectively lying in the equatorial and polar region of the pores, were found in the pores of the ZIFs. In addition, the channel structures can also hold 2–6 gas molecules. MD simulations revealed CO/CO_2 molecules rarely inter-diffuse between pores and channels in the ZIFs. The diffusion rates of CO/CO_2 are not equal in the pores and channels due to the different aperture sizes.

4.2.4. MIL-53 series

MIL-53 has already triggered a lot of interest due to its unusual microscopic adsorption behavior. Two interchanging configurations of MIL-53(Al) structure upon CO_2 adsorption, named the large pore (MIL-53lp(Al)) and narrow pore (MIL-53np(Al)) forms, were identified [104]. The two forms share the same chemical composition but differ in the pore width. Maurin and coworkers calculated the Mulliken and electrostatic potential (ESP) charges using DFT for GCMC simulations [297]. The predicted enthalpies of adsorption at low CO_2 coverage match the experimental values very well for both forms. The results suggested that a structural transition occurs during the CO_2 adsorption process. Their GCMC simulation further provided evidence for the breathing effect (structural transition upon CO_2 adsorption) [216]: the simulated isotherms for each MIL-53(Al) form are in good agreement with the corresponding region of the experimental isotherm. Furthermore, the calculated enthalpies of adsorption for MIL-53np(Al) and MIL-53lp(Al) correspond to the experimental data at low pressures (<6 bar) and at high pressures, respectively. The structural analysis showed that the breathing effect may be induced by the quadrupole moment of CO_2. The breathing mechanism can only be induced by molecules with big dipole or quadrupole moments such as CO_2 and H_2O. Non-polar molecules such as CH_4 have no such effect [330].

To further understand the breathing effect in MIL-53, Maurin and coworkers [331] compared adsorption of CO_2 in MIL-53(Al) and MIL-47(V). The breathing was found in MIL-53(Al) but not in MIL-47(V). They proposed a mechanism to describe the structural transition between the large pore (NP) and narrow pore (LP) forms: the μ_2-OH groups in MIL-53(Al) are the preferential CO_2 adsorption sites, and the adsorption geometries are controlled by the interactions between CO_2 and the μ_2-OH groups. Before the adsorption sites are not fully occupied, the NP form prevails due to the strong double interaction of CO_2 and two μ_2-OH groups. When the adsorption sites are fully occupied with the increasing CO_2 loading, the geometry is not energetically favorable and thus switches to LP, of which the larger free volume counterbalances the packing effect. Maurin and coworkers [100] examined the plausible CO_2 adsorption sites in MIL-53(Al or Cr) and MIL-47(V) using DFT and further revealed the key role of the μ_2-OH group of MIL-53 in the adsorption process. In MIL-47(V), there are no preferential adsorption sites like μ_2-OH, and therefore the breathing mechanism is not applicable. Maurin and coworkers [99] conducted MD simulations to study CO_2-induced structural transition of MIL-53 aiming to capture the structural switching directly. They successfully reproduced the breathing in the process of CO_2 adsorption for MIL-53(Cr) using a bonded force field. Furthermore, their study on the transport diffusivity of CO_2 in MIL-53(Cr) showed that the diffusion follows a 1D mechanism (along the channel) and the diffusivity of LP is two orders of magnitude larger than that in NP [139].

The adsorption and separation of CO_2/CH_4 in the highly flexible MIL-53(Cr) MOF was investigated using various experimental and computational techniques [136]. The breathing of MIL-53(Cr) was only observed for CO_2-rich and equimolar mixtures. CH_4 is unable to adsorb in the narrow pore form. This can lead to an extremely high CO_2/CH_4 selectivity if the narrow-pore form dominates. How-

ever, this was not confirmed by experiments, possibly due to the high energy barrier of LP/NP transition. The selectivity drops when the pressure increases. Notably, since the narrow form and the large form of MIL-53(Cr) can coexist in a large range of pressure and CO_2/CH_4 composition, the selectivity is very difficult to predict.

Coudert et al. [110] proposed an osmotic framework adsorbed solution theory (OFAST) to predict the structural transformation upon adsorption of gas mixture in flexible MOFs. The theory was used to predict the adsorption of CO_2/CH_4 in MIL-53(Al) and led to some insights into the structural transition: (1) MIL-53NP(Al)/MIL-53LP(Al) mixtures are only formed above the critical composition ($CO_2:CH_4 = 0.12:0.88$); (2) breathing only occurs below ~7.8 bar at 304 K; (3) the transition from narrow pore from to large pore form varies non-monotonically with the mixture composition. Ghoufi and Maurin [332] also developed a hybrid osmotic Monte Carlo (HOMC) approach integrating both MD and GCMC techniques. The structural transitions of MIL-53(Cr) upon CO_2 adsorption were simulated using the HOMC approach. The microscopic transition from MIL-53LP (Cr) to MIL-53NP (Cr) was captured at low pressures; whereas the second transition from MIL-53NP (Cr) to MIL-53LP (Cr) was absent at high pressures. Moreover, it was found that a "phase mixture" model must be combined with the approach for producing the experimental adsorption isotherms.

4.2.5. Other MOFs

A carborane-based MOF, $[Zn_3(OH)(p\text{-cdc})_{2.5}(DEF)_4]_n$ was synthesized by Snurr and coworkers [202]. This was the first MOF built based on boron-rich components. The coordinated solvent molecules in the MOF can be removed and this leads to unsaturated metal sites, which may exhibit enhanced selectivity for the quadrupolar CO_2/non-quadrupolar CH_4 mixtures. Snurr and coworkers [166] examined the separation of CO_2/CH_4 mixtures in the MOF by GCMC techniques and verified the hypothesis. The MOF with open metal sites shows considerably larger selectivity and adsorption capacities than the one without open sites. The Ideal Adsorbed Solution Theory (IAST) calculations predicted a superior CO_2/CH_4 selectivity of the MOF. $Zn_2(2,6\text{-ndc})_2(dpni)$ is a mixed-ligand MOF synthesized by Hupp and coworkers [172] with two different methods. According to the IAST calculations based on the experimental single-component isotherms, the evacuated sample from microwave-assistant methods (**1-M′**) shows much higher CO_2/CH_4 selectivity than the one from conventional method (**1-C′**). However, as the IAST analysis may fail at high pressures, GCMC simulations were used to verify the reliability of the IAST model. The simulated isotherms fully agreed with the IAST results. The GCMC calculations further confirmed that **1-M′** is a promising material for CO_2/CH_4 separation.

Recently, a combined experimental and computational study on the adsorption of CO, N_2 and CO_2 on a new MOF, Mg-MOF-74, was conducted by Palomino and coworkers [282]. The geometry and adsorption enthalpy (ΔH^0) were calculated using periodic DFT-D method [279], in which the long-distance dispersion interactions are taken into account with an empirical scheme. The results showed that CO and N_2 form roughly linear 1:1 complexes with Mg^{2+} while CO_2 forms an angular complex. Remarkably, dispersion interactions contribute ~1/2 gas-framework interaction energies in all the adsorption complexes and should be included in the calculations. The calculated ΔH^0 indicated that CO_2 has the strongest adsorption on Mg-MOF-74 among the 3 gases, in good agreement with the experimental values. The difference of ΔH^0 is 18 kJ/mol for CO_2/CO and 26 kJ/mol for CO_2/N_2, which is big enough for the corresponding gas separation.

The presence of water substantially influences the adsorption and selectivity of gas mixtures in most MOFs. Chen et al. studied a highly hydrophobic MOF, $Zn(bdc)(ted)_{0.5}$ (ted = triethylenediamine) [333], H_2O adsorption is not applicable

due to the hydrophobic structure of the pores. In the presence of water, the adsorption and selectivity of CO_2/CH_4 mixtures remain essentially unchanged.

4.3. Exploring and optimizing performances of CO_2 storage, selectivity adsorption, and separation in MOFs

Compared with experiments, molecular simulations are much easier to be used to explore some MOF systems for their optimized performances, such as in CO_2 uptake, selective adsorption, and separation. Besides real MOFs, some conceptually modified and hypothetical MOFs have also been studied by the molecular simulations in this topic.

4.3.1. CO_2 storage in MOFs

MOFs are promising materials for gas storage owing to their porous structures. Zhong and coworkers systematically investigated nine typical MOFs with various pore sizes, topologies, organic linkers and electrostatic properties using molecular simulations [286]. The results indicated that a suitable pore size for CO_2 storage is around 10–20 Å. CO_2 uptake is governed by the strength of the CO_2–MOF interactions at low pressures. Other factors, such as accessible surface area and free volume, are also crucial to CO_2 adsorption capacity at high pressures. The electrostatic interactions between CO_2 and MOFs contribute up to 30% of the total adsorption capacity at low pressures, however, the contribution decreases rapidly with the increase of pressure and the value drops to a few percent at high pressures. In general, MOFs have higher capacities for CO_2 storage and comparable self-diffusivity in comparison to most zeolites and carbon materials. To further understand the influence of framework charges on CO_2 uptake, Zhong and coworkers [334] examined 20 different MOFs. The contribution of framework charges was estimated by switching on and switching off the electrostatic interactions between MOFs and CO_2 in their GCMC simulations. The results are consistent with their previous work [286]: at low pressures, CO_2 molecules preferentially adsorb around the polar centers in the framework and the electrostatic contribution is therefore large. The adsorption sites are saturated at high pressures and most CO_2 molecules are located far from the charge centers. The effect is more pronounced in big pores. Consequently, the electrostatic interaction decreases and can be neglected in many cases. Babarao and Jiang [302] systematically evaluated the performance of various MOFs using Gibbs ensemble Monte Carlo (GEMC) (Fig. 19). Their work revealed that MOFs exhibit remarkably higher adsorption capacity than zeolites and single-wall nanotubes. The capacity is primarily determined by the strength of CO_2 adsorption at low pressures, while it is mainly dependent on the free volume and accessible surface area at high pressures.

4.3.2. CO_2 selective adsorption and adsorptive separation in MOFs

Jiang and coworkers [335] computationally investigated the adsorptive separation of CO_2/CH_4 in seven different MOFs, including IRMOF-5, metal exposed Cu-BTC, PCN-6′ and PCN-6, catenated IRMOF-13 and non-catenated IRMOF-14, and charged *soc*-MOF. Catenation leads to constricted small pores and additional adsorption sites in IRMOF-13 and PCN-6, and accordingly, adsorption enhancement at low pressures compared to non-catenated IRMOF-14 and PCN-6′; whereas the trend is reversed at high pressures. Although the adsorption behaviors change with different pressures, catenated MOFs show higher CO_2/CH_4 selectivity than their non-catenated counterparts because the catenation enhances the interaction with CO_2. The uncoordinated open metal sites, small pockets and narrow pores can enhance electrostatic interactions and therefore increase the selectivity. In particular, the presence of extraframework ions in charged *soc*-MOF can greatly boost the
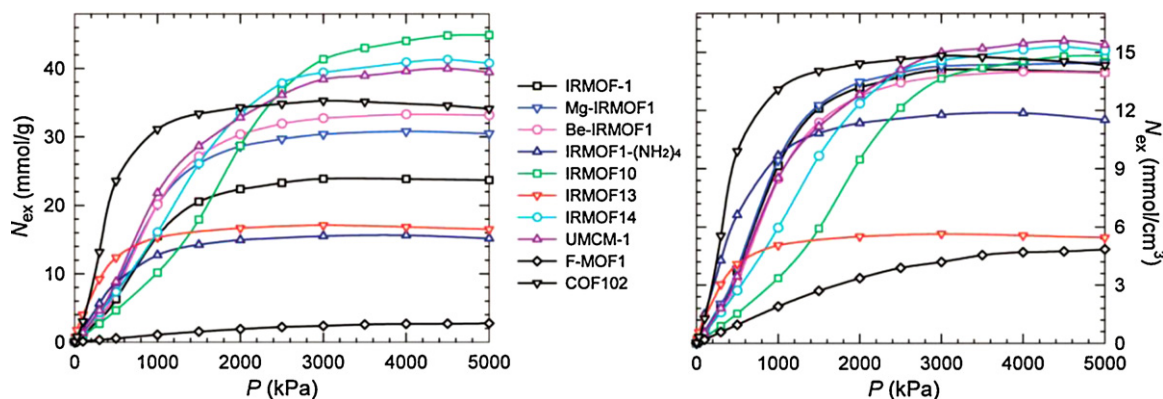
Fig. 19. Gravimetric (left) and volumetric (right) isotherms of CO_2 adsorption in IRMOF1, Mg-IRMOF1, Be-IRMOF1, IRMOF1-(NH_2)4, IRMOF10, IRMOF13, IRMOF14, UMCM-1, F-MOF1, and COF-102, obtained by GEMC simulations. Reproduced with permission from Ref. [302].

strength of interactions with adsorbates and results in the highest CO_2/CH_4 selectivity.

Zhong and coworkers [336] compared CO_2/H_2 adsorption of three pairs of MOFs, including three catenated MOFs (IRMOFs-9, -11, and -13) and their non-catenated counterparts (IRMOFs-10, -12, and -14). The simulation results showed that the catenated IRMOFs have much higher CO_2/H_2 selectivity than the non-catenated ones. The enhanced CO_2 selectivity of catenated IRMOFs can be mainly attributed to the electrostatic interactions. The strength of interactions is correlated to the pore size. The electrostatic interactions between CO_2 and MOFs dominate the selectivity at low pressures and the electrostatic interactions of CO_2–CO_2 become evident and eventually dominant at high pressures. Zhong and coworkers also evaluated the performance of COFs and MOFs for $CH_4/CO_2/H_2$ mixtures [337] and found similar adsorption selectivities of COFs and MOFs.

Liu and Smit compared the separation and storage efficiency of CO_2/N_2 mixture in three zeolites and seven MOFs using GCMC simulations [338]. Not surprisingly, CO_2 adsorption is more preferable for all the materials. Although the gas storage capacity of all the MOFs is substantially higher than that of zeolites at higher pressures, comparable separation selectivity of the two classes of materials was obtained. Cu-BTC possesses the best performance and MOFs with large pores display relatively low selectivity. In the simulation, switching off the electrostatic interactions between gases and adsorbents resulted in lower selectivity, indicating the framework charges play a more significant role for CO_2 adsorption than for N_2 adsorption. Accordingly, the difference in quadrupole of gas molecules must be considered in order to achieve high separation selectivity. Moreover, pore size was found an important factor for separation efficiency. The pore size of 5.0–10.0 Å is suitable for CO_2/N_2 separation.

Snurr and coworkers [201] compared the performance of 14 MOFs for CO_2 capture at low pressures using a combined experimental and computational approach. Their study aimed to develop a model for fast screening of MOFs for gas capture, leading to substantial savings in the experimental time and cost. CO_2 uptake correlates with the heat of adsorption at low pressures. The proposed model gave some successful predictions. For instance, MOFs with a high density of open metal sites has the highest efficiency for CO_2 uptake. It is a big challenge to identify MOFs with useful properties for targeted applications due to the large numbers of MOF structures. Recently, Sholl and coworkers [315] proposed an efficient method to characterize the features which control gas diffusion in the MOFs. The method is based on the information from X-ray crystal structures and able to rapidly predict the Henry's constant for adsorption and diffusion activation energy for simple gases. The approach was used to screen more than 500 MOFs and was demonstrated an effective one in identifying suitable materials for kinetic separation of adsorbates. However, there are some limits which need to be overcome in the method: (1) the method is unable to examine non-spherical molecules; (2) the calculated Henry's constant for adsorption and diffusion activation energy are only applicable for non-polar adsorbates. (3) The method may lead to big deviations at high pressures.

4.3.3. Modeling MOF membranes for CO_2 separation

Sholl et al. [339] carried out computational studies to evaluate the performance of MOF membranes for gas mixture separation. They first tested the performance of MOF-5 membranes for the separation of CO_2/CH_4 mixtures. Although their single-component results predicted strong selectivities for CH_4 in the mixtures, the mixture adsorption and diffusion showed that MOF-5 membranes only possess weak selectivity for CO_2. Their results revealed that the performance of MOF membranes cannot be correctly predicted only using the properties of single-component gases, and mixture effects are crucial in determining the membrane properties. Keskin and Sholl [340] further predicted the selectivities of MOF-5 membranes for more binary gas mixtures such as CO_2/H_2, CO_2/N_2, and N_2/CH_4 (Fig. 20). The studies led to the same conclusion. They developed a method to predict mixture adsorption and diffusion based on the mixing theories using the results of single-component adsorption and transport simulation. The accuracy of the approach was assessed and the results are reliable. Sholl and coworkers [314] used the method to predict the performance of Cu-BTC membranes for separation of CO_2/H_2, CO_2/CH_4 and H_2/CH_4. It was found that Cu-BTC membranes possess much high selectivities for the binary gas mixtures than MOF-5 membranes; i.e. 20:1 for CO_2/H_2. Consequently, the structure of a MOF governs the performance of a MOF-based membrane. Moreover, although the performance is co-determined by the diffusion selectivity and adsorption selectivity for gas mixtures, the selectivity of adsorption dominates the overall performance of the MOF membranes.

Sholl and coworkers [341] examined a microporous MOF membrane, Cu(hfipbb)(H_2hfipbb)$_{0.5}$ using MD, GCMC and DFT calculations. Their investigations focused on the adsorption and diffusion of CO_2 and CH_4 in the MOF. Not surprisingly, CO_2 is much more strongly adsorbed than CH_4 in the MOF. The MD simulations showed that CO_2 diffusion is much more rapid and the calculated diffusivity of CO_2 is orders of magnitude larger than that of CH_4, indicating that an effective kinetic separation is applicable. In addition, DFT calculations also showed the diffusion activation energy for CO_2 (16 kJ/mol) is much smaller than for CH_4 (45 kJ/mol). According these results, they predicted that the CO_2 selectivity of
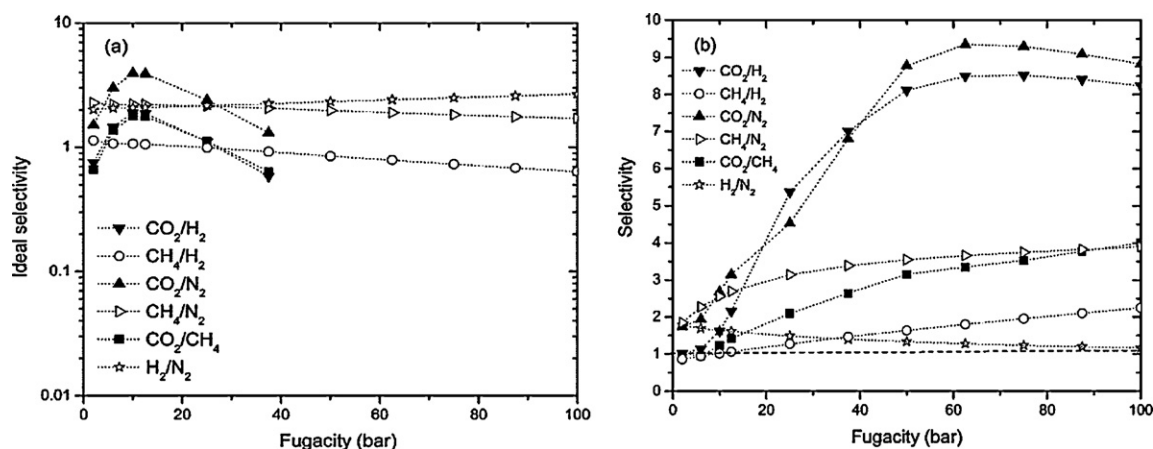
Fig. 20. Predicted (a) ideal and (b) mixture permeation selectivities for a 10 μm thick MOF-5 membrane. The transmembrane pressure drop is 80% of feed pressure. Mixture selectivities are based on an equimolar feed. The first species listed in the labels indicates that permeation of the species that is favored. Reproduced with permission from Ref. [340].

the MOF membrane is ~10^4–10^5, higher than any other polymeric membranes for CO_2/CH_4 separation.

4.3.4. Ligand effect for CO_2 adsorption

Organic linkers in many MOFs play an important role in gas adsorption. Modification the structures of the linker part can effectively enhance the adsorption. Torrisi et al. [275,276] examined the intermolecular interactions between CO_2 and a series of functionalized aromatic molecules using DFT at PW91/DNP level. Their research indicated that the strength of CO_2-atomic ring interactions can be tuned by introducing some functional groups to the ring structure. Halogen substituents exhibit a relatively strong destabilization effect, whereas methyl groups are able to slightly improve the stability, primarily due to the strengthened π-quadrupole interaction arising from the inductive effect. Other polar groups, such as –NH_2, –SO_3H, and –COOH improve the CO_2 affinity significantly, increasing the binding energy of ~5–11 kJ/mol. On the basis of the study, Torrisi et al. [342] further proposed a modified MOF-53LP(Al) structure, in which four functional groups (–OH, –COOH, –NH_2, and –CH_3) were introduced to the benzene diacarboxyle (BDC) ligands. Periodic DFT, DFT on model complexes, and GCMC calculations unanimously indicated the enhancement of CO_2 binding energy with the ligand substitution. Among the substituents, $(OH)_2$-MIL-53(LP) and $(COOH)_2$-MIL-53(LP) were found the best candidates for CO_2 capture and CO_2/CH_4 selectivity. Zhong and coworkers [343] decorated the aromatic ring of the organic linker with four different functional groups (–OH, –F, –NH_2, and –CH_3) in MOF-5. They found that introducing electron-donating groups into the organic linkers largely improves the selectivity of CO_2/CH_4 mixtures due to the strengthened electrostatic field distributions in the pores. The incorporation of electron-withdrawing groups, however, only has slight influence on the selectivity.

MIL-101 is known as one of the most porous materials to date. Jiang and coworkers [333] examined the adsorption of CO_2 and CH_4 in MOF-101 using DFT and GCMC, aiming to understand the role of terminal water molecules coordinated to metal sites. At low pressures, the hydrated MIL-101 exhibits enhanced adsorption for CO_2 compared to the dehydrated counterpart, as the water molecules act as additional adsorption sites, whereas the reverse was observed at high pressures because the water molecules reduce the total free volume. Likewise, the adsorption selectivity of CO_2/CH_4 is slightly higher in hydrated MIL-101. Removal of coordinated solvent molecules from metal sites usually boost the selectivity for some MOFs [166]; however, the opposite effect

also can be present in some cases. Snurr and coworkers [124] predicted that water bound to open-metal sites of Cu-BTC substantially improved the adsorption capacities and CO_2 selectivity over CH_4 and N_2. GCMC simulations showed a 4–11% increase of the non-Coulombic interaction and a ~210–400% increase of the Coulombic interaction with water molecules coordinated to the open Cu sites in Cu-BTC. Consequently, the enhancement of CO_2 adsorption was mostly ascribed to the Coulombic interactions between water and CO_2. This was verified by experimental adsorption measurements: CO_2 uptake increases by 71% in the 4 wt% hydrated Cu-BTC at 0.1 bar and by 45% at 1 bar. Following the idea, they found that CO_2/N_2 selectivity can also be improved by replacing coordinated solvent molecules with highly polar ligands in MOF systems, in a new synthesized 3D non-catenated Zn-paddlewheel MOF, Zn(bttb)(dmf)$_2$ [159]. A polar group, CF_3-py, was employed to replace DMF molecules coordinated with the Zn(II)$_2$ sites. Enhanced selectivities of CO_2/N_2 and CO_2/CH_4 selectivity with the CF_3-py coordinated MOF arising from the strong dipole–quadrupole interactions were predicted by their IAST calculations.

4.3.5. Clustering effect

Guest molecules usually present in a metastable state in micropores due to the reduced effect of capillary condensation, leading to a possible clustering of the molecules. Krishna and van Baten [344] investigated the cluster formation upon CO_2 adsorption at subcritical temperatures in several MOFs and zeolites. They found clustering of CO_2 occurs when the fraction vacancy $1/\Gamma_I > 1$ and the clustering is enhanced at low temperature. Furthermore, MOFs with larger pores, such as IRMOF-1 and Cu-BTC, are more favorable for clustering. A more recent study showed that the adsorption and diffusion properties in MOFs are strongly affected by molecular clustering [345]: the Fick diffusivity can be lower than self diffusivity in the conditions of severe clustering and $1/\Gamma_I \gg 1$. The adsorption selectivity in mixtures is significantly enhanced for the component with a higher degree of clustering. Moreover, the diffusion selectivity is also enhanced by increased degree of clustering. Therefore, the improvement of permeation selectivity of mixtures in membrane separation can be reached at an optimum temperature.

4.4. New computational methodologies for MOFs

Although some existing methods developed originally based on other porous materials for gas adsorption and separation, such
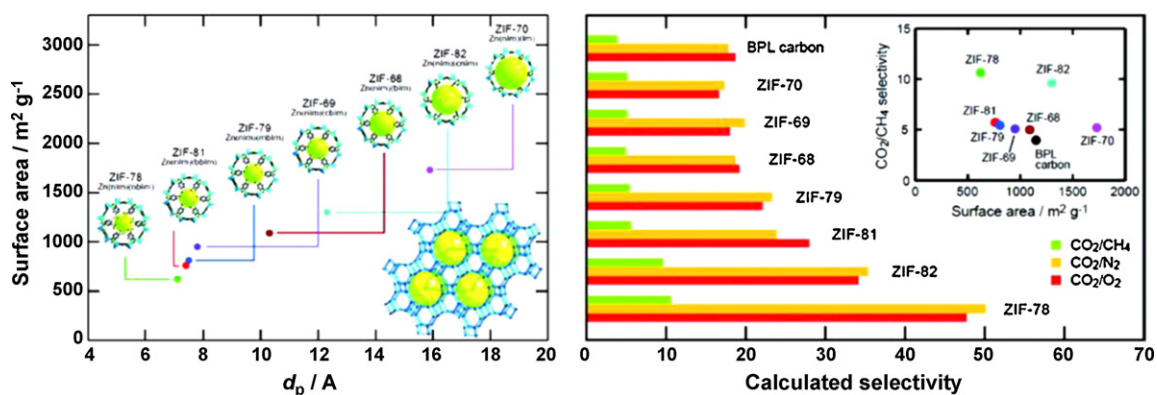
Fig. 21. Plot of pore diameter (dp) vs surface area for different GME ZIFs (left) and the evaluated CO_2/CH_4, CO_2/N_2, and CO_2/O_2 selectivities in these ZIFs (right). Reproduced with permission from Ref. [157].

as zeolites, can be used in MOFs, due to the special composition and pore properties of MOFs, new or modified simulation (theory) methods should be developed.

Framework charges are essential for an accurate description of adsorption in molecular simulations. They are usually obtained from *ab initio*/DFT calculations, which is very time-consuming. Xu and Zhong [326] proposed an empirical approach for framework charge estimation. Their method, called "connectivity-based atom contribution" (CBAC), is built on an assumption that the atomic charge of an atom in a MOF is fully determined by its bonding environment. Consequently, any atoms with the same bonding connection have identical charges. 35 most extensively used atom connection types were extracted from a set of 30 MOFs. Simulated CO_2 adsorption isotherms in 13 additional MOFs using both QM and CBAC charges were compared: the results are in excellent agreement with each other. The approach can successfully reproduce experimental isotherms and greatly saves computational time for large-scale screening of MOFs.

Like MIL-53, many MOFs exhibit unusual flexibility. Snurr and coworkers [346] developed a new computational method to efficiently calculate the unit cell shape and size for the flexible structures loaded with adsorbates. The method, based on the model-following technique for rigid bodies, is suitable to treat rigid molecules in a flexible system. Two sample studies showed that the approach can successfully minimize the structure of IRMOF-1 at 0 K and predict the structure change of MIL-53 in the presence of water. The method is expected to be very useful to evaluate gas adsorption in flexible materials.

Jiang and coworkers [347] used a classical molecular "density functional theory" for the adsorption of gas mixtures. In the classical DFT, weighted density approximations with different weighting functions are applied to the attractive and repulsive parts of excess free energy, and the excess free energy of the uniform fluid can be derived from the equations of state for hard-sphere and Lennard–Jones mixtures. Variations of this theory have been widely employed in the analysis of adsorption for fluids confined in simple geometries [348]. The theory was employed to examine the adsorption of CO_2/CH_4 and CO_2/N_2 mixtures in two MOFs, ZIF-8 and $Zn_2(bdc)_2(ted)$. Good agreement between the DFT estimated adsorption and selectivity and the molecular simulation results verified the validity of the theory.

5. Strategies for enhancing the CO_2 separation ability of MOFs

In terms of inherent characteristics in design, synthesis, structure, and porous properties of MOFs, as well as the properties of gases involved in CO_2 separation several strategies can be deduced or proposed to increase the separation ability of CO_2 in MOFs. The strategies for separation are also intimately connected to the methods and processes, which implies that adsorptive separation and membrane-based separation have different emphases when considering the materials that will be used. For adsorptive separation, high CO_2 uptake capacity and selectivity from other gases are equally important for an adsorbent material; but, for membrane-based separation, the high penetrability and selectivity are primary concerns. There are, however, some common themes that must be considered in all aspects. Considering that practical application is the ultimate goal of any of these projects, it is imperative that (1) efficacious separation can be done at room temperature or higher and at low pressure; (2) stability of the materials can survive the harsh real-world conditions; and (3) low cost in the material preparation and regeneration is considered.

5.1. Fixing pore size and shape in MOFs

The pore size and shape is always the first consideration in selecting a porous material for special separation. The molecular sieve effect has been widely used in zeolites and other porous materials for gas separation. Alternately, the performance of a porous material in kinetic separation is also directly related to the pore size and shape of adsorbent, not only in adsorptive separation but also in membrane-based separation. A balance must also be struck between small enough to separate the desired gas mixture and too small as to trap the molecules and stop gas flow all together. MOFs, due to their easily controllable synthesis and modification, have great potential and advantages compared to traditional zeolites and other inorganic molecular sieves in controlling pore size and shape for the appointed separation.

A prominent example in the control of pore size is the exploration of isoreticular ZIFs for their CO_2 selective capture properties reported by Yaghi and coworkers (Fig. 21) [157]. In this work, the authors described a new construction method for achieving precisely controlled metrics and functionality in an isoreticular series of eight ZIFs with the desirable GME topology. Within this series of ZIFs, the pore diameter was varied incrementally from 7.1 to 15.9 Å. The results showed that these ZIFs have pore size and surface functionality dependent selectivity for CO_2 capture from its binary mixtures with CH_4 and N_2.

Cation exchange has also been adopted to tune the pore size in bio-MOF-1 reported by Rosi and coworkers [122], as mentioned above. Experimental results showed that the pore size of bio-MOF-1 can be modified post-synthetically via straightforward cation-exchange and that such modifications can be used to systematically tune the CO_2 adsorption capacity of the materials.
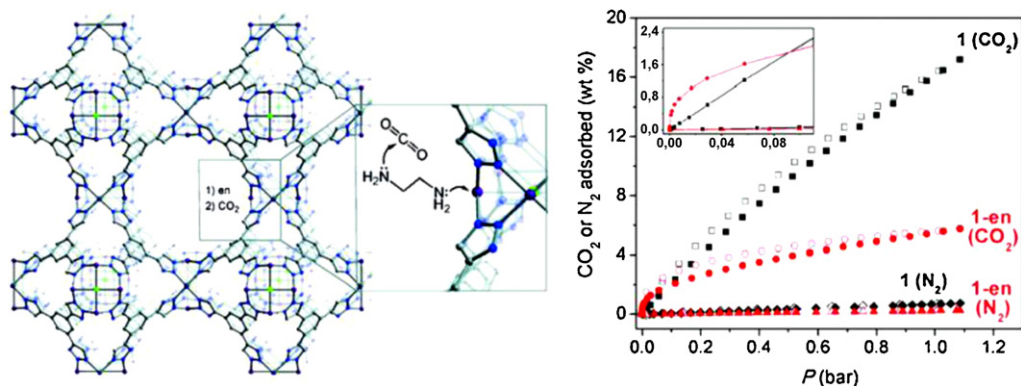
Fig. 22. Structure of Cu-BTTri showing surface functionalization of a coordinatively unsaturated Cu(II) site with ethylenediamine (en), followed by attack of an amino group on CO_2 (left) and adsorption–desorption isotherms of CO_2 and N_2 at 298 K in Cu-BTTri and Cu-BTTri-en (the inset shows the higher uptake of CO_2 for Cu-BTTri-en compared with Cu-BTTri at low pressures).
Reproduced with permission from Ref. [126].

Controlling interpenetration of the framework in MOFs is another strategy for tuning the pore size. One example, Cu(fma)(bpee)$_{0.5}$, reported by Chen et al. [175] was rationally designed from a primitive cubic net and its pores are tuned by double framework interpenetration. With pore cavities of about 3.6 Å, which are interconnected by pore windows of 2.0 Å × 3.2 Å, this MOF presented highly selective sorption behaviors of CO_2 over N_2. Similar interpenetrated MOFs with CO_2 selective adsorption ability include Zn(abdc)(bpee)$_{0.5}$ [174] and Ni(cyclam)$_2$(mtb) (cyclam = 1,4,8,11-tetraazacyclotetradecane, mtb = methanetetrabenzoate) [349]. As discussed above, MOF-508b with an interpenetrated structure and one-dimensional micropores of 4.0 Å × 4.0 Å showed preferential adsorption of CO_2 over N_2 and CH_4, partly due to the pore size [165].

5.2. Functionalizing the pore surface of MOFs

As mentioned above, CO_2 is a highly quadrupolar gas, whereas competitive sorbates in commonly concerned CO_2 capture separation, including N_2, CH_4, and H_2 are non-polar or weakly polar. This means that there are profound differences in the interaction between these gas molecules and the pore surface of porous material, which can be taken advantage of when modifying the surface properties of MOFs to greatly enhance the adsorption and separation ability. The surface properties of MOFs can be tuned not only by pre-design of ligands, metal-containing nodes, and MOF construction but also by post-modification of existing MOFs.

Open active metal sites located on the pore walls of a MOF provide an approach for the enhanced separation of (quadru)polar/non-polar gas pairs, such as CO_2/CH_4. These active adsorption centers are usually created by post treatment of MOFs, because they are always occupied by a coordinated species, such as a solvent molecule, during the synthesis. The open metal sites in paddlewheel Cu$_2$(COO)$_4$ units of many MOFs are among the most extensively studied. MOFs, such as HKUST-1 have demonstrated preferential adsorption of CO_2 over CH_4 and N_2 [156]. The adsorption mechanism has been described as coordination of the CO_2 molecule to the Cu center in an end-on fashion [130]. This preferred adsorption directly on an open metal site has also been confirmed in MIL-100 and MIL-101 [135], and the series of isostructural frameworks, M$_2$(dhtp) (CPO-27 or MOF-74, M = Ni, Co, Zn, Mg, and Mn) [155]. To back up these findings and calculate the energies involved, molecular simulation on related systems have also demonstrated that open metal sites in MOFs are very useful in CO_2 selective adsorption and separation [92].

The introduction of functional groups with a high affinity for CO_2 into pores of MOFs has been employed as another strategy to enhance the adsorption capacity and selectivity of CO_2 adsorption. Hupp and coworkers grafted the highly polar py-CF$_3$ groups onto a MOF containing open metal sites to get Zn$_2$(bttb)(CF$_3$-py)$_2$ [159]. This functionalization has led to a remarkable enhancement in the CO_2 uptake compared with N_2 at low pressure. In contrast to most of the reported frameworks where the unsaturated metal centers act as Lewis acid sites, Lewis base functionalization can also enhance CO_2 adsorption due to acid–base interactions between CO_2 (acid) and the basic active centers. This has been realized in a sulfone-functionalized MOF, UoC-1′ which exhibited selective CO_2 adsorption over CH_4, N_2, and H_2 [162]. Considering the affinity of amines towards CO_2, amine functionalized ligands have been combined into several MOFs for enhancing the adsorption and selectivity of CO_2. As discussed above, amino-MIL-53(Al) presented enhanced CO_2 uptake relative to CH_4 compared with the parent MIL-53(Al) [98]. Similar enhancements have been observed in Ni$_2$(NH$_2$-bdc)$_2$(dabco) relative to their non-functionalized analogues [350]. Furthermore, Long and coworkers [126] have demonstrated that alkylamine-functionalization of frameworks can enhance the selectivity for CO_2 adsorption, especially at the low pressures. In their report, the exposed metal sites in HCu[(Cu$_4$Cl)$_3$(BTTri)$_8$] (Cu-BTTri) were coordinated by ethylenediamine (en) by post-synthetically treating to get the en-functionalized MOF as shown in Fig. 22. Despite reduction in surface area compared with the parent framework, the en-functionalized MOF presented a higher CO_2 uptake at low pressures compared with its parent framework, as well as the highest initial heat of adsorption (90 kJ/mol) for any MOF. Similarly, acylamide groups have also been confirmed to be effective in enhancing CO_2 binding affinity, as realized in MOF Cu$_3$(tpbtm), thereby increasing the adsorption selectivity for CO_2 over N_2 [198].

Similar to most zeolites, MOFs with framework charge have been confirmed as having enhanced CO_2 adsorption and selectivity. Babarao and Jiang [287] reported a molecular simulation study for the separation of gas mixture of CO_2/H_2, CO_2/CH_4, and CO_2/N_2 in a zeolite-like metal-organic framework (rho-ZMOF), which is composed of an open anionic framework and charge-balanced by extra-framework Na$^+$ ions. The simulation results revealed that CO_2 is adsorbed predominantly over other gases because of its strong electrostatic interactions with the charged framework and the presence of Na$^+$ ions acting as additional adsorption sites. At ambient temperature and pressure, the CO_2 selectivity is 1800 for the CO_2/H_2, 80 for the CO_2/CH_4, and 500 for the CO_2/N_2 mixture. Compared with other MOFs and porous materials, this ionic MOF
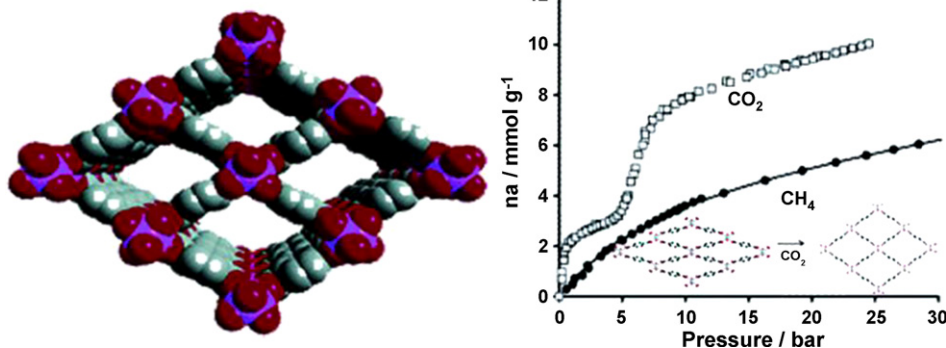
Fig. 23. Structure of MIL-53(Cr) (left) and its CO_2 and CH_4 adsorption isotherms at 304 K (right).
Reproduced with permission from Refs. [19,104].

presents unprecedentedly high selective adsorption for CO_2 over other gases.

In addition, the insertion of metal salts within the pores of MOFs has been demonstrated to be a useful approach in enhancing CO_2 binding. Recently, Long and coworkers [197] have showed that the selectivity factor for binding CO_2 over N_2 under typical flue gas conditions increase from 2.8 in Al(OH)(bpydc) (MOF-253) to 12 in Al(OH)(bpydc)·0.97Cu(BF$_4$)$_2$. The latter MOF material was obtained by the post-synthetic insertion of Cu(BF$_4$)$_2$ into the former. The insertion of metal salts is hypothesized to create electric dipoles on the surface of the MOF, which can give strong interaction with CO_2. Indeed, the heat of adsorption for CO_2 increases from 23 to 30 kJ/mol upon the insertion of Cu(BF$_4$)$_2$ into Al(OH)(bpydc).

5.3. Taking advantage of the flexibility of MOFs

Compared to rigid MOFs, flexible or stimuli-responsive MOFs have shown additional advantages for selective adsorption and separation. A number of unpredicted phenomena involved in the gas adsorption by flexible MOFs have been observed, which are not observed in traditional porous materials. These new properties can be used in the selective adsorption and separation of CO_2.

The MIL-53 series is representative of flexible MOFs and has been extensively investigated for CO_2 and CH_4 adsorption, as well as the separation of related mixtures [48]. As mentioned above, MIL-53(Cr) exhibits a small CO_2 uptake at low pressure, however, a distinct step is observed when increasing the pressure as the structure opens (breathing effect), leading to a higher gas uptake; this step is absent in the corresponding isotherm for CH_4 (Fig. 23) [104]. The adsorption of binary CO_2/CH_4 mixtures in MIL-53(Cr) showed that the breathing effect is mainly controlled by the partial pressure of CO_2 and breakthrough experiments revealed that the CO_2/CH_4 selectivity decreases as the CO_2 partial pressure increases [136].

External stimuli such as pressure and temperature can be used to induce gating effects, which are desired for selective adsorption and separation in some cases. This phenomenon has been observed in several flexible MOFs. For example, M(4,4′-bipy)$_2$(BF$_4$)$_2$ (M = Cu and Ni) and M(4,4′-bipy)$_2$(CF$_3$SO$_3$)$_2$ (M = Co and Cu) [120,351] showed a pressure induced "gate" effect in CO_2 adsorption. In the case of Cu(4,4′-bipy)$_2$(BF$_4$)$_2$, negligible CO_2 adsorption occurs up to a pressure of 0.7 bar at 298 K, at which point the interlayer spacing increases to accommodate the gas molecules at higher pressure. CH_4, on the other hand, requires a higher pressure of 4.5 bar to open the gate. Mesh-adjustable molecular sieves (MAMS) are another class of flexible MOFs with temperature dependent selective adsorption [115,116]. Structural tailoring from modifiable ligands is expected to get materials with higher selective adsorp-

tion abilities for CO_2 at near room temperature. This MAMS idea has produced a fruitful research avenue in MOFs for gas separation, carried into execution in the authors' groups.

5.4. Optimizing technical procedure

Apart from the design and modification of MOFs, especially at the molecular level as discussed above, the technical procedures and methods should also be developed or optimized for enhancing the CO_2 separation ability in MOFs. Connected to the work performance of MOF material, these procedures can include (1) the preparation of MOF material for separation, such as the particle size of MOF crystals when acting as a sorbent in adsorptive separation, and decreasing "cracking" in MOF thin film; (2) the activation of MOF material that is related directly to the separation performance of the material not only in adsorptive separation but in membrane separation; (3) the selection of separation methods that should be dependent on the properties of the MOF that is used; (4) the manipulation of MOF materials to decrease environmental factors, such as water, which can cause framework collapse; (5) the hybridization of MOFs with other materials, such as traditional carbon-based sorbents and polymers. For carbon capture technologies, there are a lot of considerations for enhancing the capture efficiency [1], which are beyond the scope of this paper.

6. Conclusion and outlook

CO_2 capture is attracting the broad attention of both science and technology. In this review article, the CO_2 capture related gas adsorption, CO_2 storage, selective adsorption, and gas separation in MOFs have been discussed. Clearly, the selection of capture materials is essential for any technology in CO_2 capture. Metal-organic frameworks (MOFs) represent a new class of crystalline porous materials with advantages such as ease of design and synthesis, high porosity, and tailored pore properties. MOFs are promising candidates as separation materials for CO_2 capture. However, further explorations are needed in several critical issues that will hamper the development of real-world applications if they are not addressed [91].

In the last decade, thousands of MOFs have been synthesized and characterized structurally, however only a small part have been checked for CO_2 adsorption, storage, and related gas separation. Because it is unreasonable to measure all of these new materials further development of scanning techniques are recommended. This can be used not only for finding useful materials but also for evaluating structure–function relationships and thereby directing the design and optimization of new MOF materials. Molecular simulation is, in fact, playing a key role in scanning MOFs for CO_2

capture, by confirming experimental results and providing further insight into key aspects of CO_2 adsorption.

The gas streams treated in practical CO_2 separations always contain water and it is not economically feasible that an additional process is added to dry the flue gas before separation; separation materials thus require a high tolerance to water. There have, however, only been a very limited number of evaluations of the effect of water on the separation performances of MOFs. Addressing this issue should include studies into both the physical co-adsorption of water in the pores of MOFs and the chemisorption of water to sites such as open metal centers, when applicable.

Besides the co-adsorption of CO_2 and water, only limited data on the co-adsorption of CO_2 and other gases in MOFs has been reported. There is no doubt that measurements of adsorption for multi-component system are more challenging than for single-component ones. However, for future application it is critical that these kinds of tests are completed directly or that calculations using the simple mixing theories, such as IAST, are used to get this data. Experimental data with mixed gas systems would also aid in the evaluation of kinetic separation, especially in advancing the developments of MOF-based membranes for CO_2 separation. When considering MOFs for industrial separations of CO_2 from other gases, information on the reproducibility of separation performance after long-term exposure to gas streams and the response of the materials to repetitive circulation are also needed. Continued work in all of these areas as well as establishing standards by which sorbents can be compared are necessary.

The sheer number of MOF structures available implies that the field of MOF-based membranes for CO_2 capture has high potential for rapid growth. Many of the properties that make MOFs exciting materials have not yet been demonstrated for gas separating MOF membranes, such as MOFs with post-synthetically functionalized pores or inherently tunable pore sizes either of which could have a significant impact on MOF membrane CO_2 capture performance. Chemically decorating pores with amines or other ligands is one example of a possible strategy for increasing CO_2 affinity in a MOF.

Despite the bright outlook, MOF membranes for CO_2 capture still face significant challenges. In most cases, the organic ligands used in synthesizing the MOFs of interest are prohibitively expensive. New, low cost ligands are necessary to realize these materials' potential as membranes for CO_2 capture in an industrial setting. This is also a concern for adsorptive separation. It is also essential that new MOF membrane fabrication methods be developed to overcome some of the unique challenges these materials face such as ease of crack formation during cooling and drying and poor support adhesion. Also, more post-synthetic functionalization methods need to be developed to tune existing MOF membranes, increasing CO_2 permeability and CO_2/N_2 selectivity to realize the potential of these materials for CO_2 capture.

Paralleling experimental studies, molecular simulation in this field must be further developed. It is clear that classical and quantum-mechanical based molecular simulations are playing a significant role in the elucidation of adsorption and separation mechanisms, evaluation of existent materials, and the design of promising materials. In this sense, these techniques are a great complement to experiments and they can save money and time otherwise invested in a much larger set of costly and difficult experiments especially in the screening stages.

In particular, for example, the simulation results have shown the role of electrostatic interactions, resulting in the identification of ionic MOFs as promising materials for CO_2 capture. Molecular simulations have also helped to elucidate other factors such as the effect of impurities in the adsorption and separation of mixtures, the existence of structural changes giving rise to breathing phenomena in flexible frameworks, the elucidation of transport mechanisms, and the roles of geometry, pore size, and nature of

the molecular interactions on preferential adsorption. With respect to selectivity properties, simulations are crucial to understand the effects of overall composition, pressure, loading, and temperature, and to characterize the influence of complex fluid phenomena such as phase transitions and clustering.

In recent decades, tremendous advances in computational hardware have given a great impulse to the recognition of simulations as the "theoretical microscope". In adsorption theory, going beyond the IAST is important as we deal with more complex molecular interactions. To accomplish this goal, accurate parameterization of effective force fields used in classical molecular simulations need the input from *ab initio* and quantum-mechanical density functional theory methods. Recent DFT developments have been able to provide better descriptions of weak dispersion interactions that are being tested for gas adsorption and separation, and more work will be needed to assess and further develop improved functions. Preliminary but promising screening methodologies have already been implemented that allow rapid analyses of large groups of materials; this is another area where additional advances are foreseen. Finally, new techniques, especially innovative combination of molecular modeling methods that address different scales of length and time will be extremely useful in this field.

It is evident that the combination of material design, synthesis, characterization, calculational simulation, and finally implementation requires plentiful knowledge and expertise, which can only be afforded through extensive collaborations of scientists with different scientific backgrounds [18]. This should culminate in collaboration between scientists and engineers to figure out the solution to the CCS problem we are facing. Specifically, what the most promising materials in an industrial separation process for CO_2 capture are. In addition, the implementation costs for industrially relevant scale-up of new materials must be evaluated. The ease and cost of synthesis of MOFs in large scale for example, will be extremely significant in determining their applicability in future industry.

Acknowledgements

Appendix A. Supplementary data

Supplementary data associated with this article can be found, in the online version, at doi:10.1016/j.ccr.2011.02.012.

References

[1] S.A. Rackley, Carbon Capture and Storage, Elsevier, 2010.
[2] R.E. Hester, R.M. Harrison, Carbon Capture: Sequestration and Storage, RSC Pub, 2010.
[3] S.A. Roosa, A.G. Jhaveri, Carbon Reduction: Policies. Strategies and Technologies, The Fairmont Press, 2009.
[4] IPCC, IPCC Special Report on Carbon Dioxide Capture and Storage, Cambridge University Press, 2005.
[5] E.J. Wilson, D. Gerard, Carbon Capture and Sequestration: Integrating Technology, Monitoring, Regulation, Wiley, 2007.
[6] ESRL, ESRL's Global Monitoring Division, Trends in Atmospheric Carbon Dioxide, 2010.
[7] J. Bolhàr-Nordenkampf, Chemical Looping for Syngas and Power Generation with CO_2 Capture: Pilot Plant Study and Process Modeling, Suedwestdeutscher Verlag fuer Hochschulschriften, 2009.
[8] S. Mokhatab, W.A. Poe, J.G. Speight, Handbook of Natural Gas Transmission and Processing, Gulf Professional Pub, 2006.
[9] M. Tagliabue, D. Farrusseng, S. Valencia, S. Aguado, U. Ravon, C. Rizzo, A. Corma, C. Mirodatos, Chem. Eng. J. (Lausanne) 155 (2009) 553.

[10] R. Thiruvenkatachari, S. Su, H. An, X.X. Yu, Prog. Energy Combust. Sci. 35 (2009) 438.
[11] M. Hasib-ur-Rahman, M. Siaj, F. Larachi, Chem. Eng. Process. 49 (2010) 313.
[12] D. Wappel, G. Gronald, R. Kalb, J. Draxler, Int. J. Greenhouse Gas Control 4 (2010) 486.
[13] S. Choi, J.H. Drese, C.W. Jones, ChemSusChem 2 (2009) 796.
[14] J.R. Benemann, Energy Convers. Manage. 34 (1993) 999.
[15] K. Maeda, M. Owada, N. Kimura, K. Omata, I. Karube, Energy Convers. Manage. 36 (1995) 717.
[16] K.O. Kwak, S. Jung, S.Y. Chung, C.M. Kang, Y.I. Huh, S.O. Bae, Biochem. Eng. J. 31 (2006) 1.
[17] G.T. Rochelle, Science 325 (2009) 1652.
[18] D.M. D'Alessandro, B. Smit, J.R. Long, Angew. Chem., Int. Ed. 49 (2010) 6058.
[19] J.R. Li, R.J. Kuppler, H.C. Zhou, Chem. Soc. Rev. 38 (2009) 1477.
[20] A.D. Ebner, J.A. Ritter, Sep. Sci. Technol. 44 (2009) 1273.
[21] U.S.D.o., Energy, DOE/NETL's Carbon Capture R&D Program for Existing Coal-Fired Power Plants Energy, U. S. D. o., 2009.
[22] H. Herzog, J. Meldon, A. Hatton, Advanced Post-Combustion CO₂ Capture, Massachusetts Institute of Technology, Boston, MA, 2009.
[23] M.T. Ho, G. Leamon, G.W. Allinson, D.E. Wiley, Ind. Eng. Chem. Res. 45 (2006) 2546.
[24] G. Ferey, Chem. Soc. Rev. 37 (2008) 191.
[25] L. MacGillivray, Metal-Organic Frameworks: Design and Application, John Wiley & Sons, 2010.
[26] S.R. Batten, S.M. Neville, D.R. Turner, Coordination Polymers: Design. Analysis and Application, RSC Publishing, 2009.
[27] O.M. Yaghi, M. O'Keeffe, N.W. Ockwig, H.K. Chae, M. Eddaoudi, J. Kim, Nature 423 (2003) 705.
[28] S. Kitagawa, R. Kitaura, S. Noro, Angew. Chem., Int. Ed. 43 (2004) 2334.
[29] D. Zhao, D.Q. Yuan, D.F. Sun, H.C. Zhou, J. Am. Chem. Soc. 131 (2009) 9186.
[30] D. Yuan, D. Zhao, D. Sun, H.C. Zhou, Angew. Chem., Int. Ed. 49 (2010) 5357.
[31] Z.Q. Wang, S.M. Cohen, Chem. Soc. Rev. 38 (2009) 1315.
[32] J. Klinowski, F.A. Almeida Paz, P. Silva, J. Rocha, Dalton Trans. 40 (2011) 321.
[33] H. Furukawa, N. Ko, Y.B. Go, N. Aratani, S.B. Choi, E. Choi, A.O. Yazaydin, R.Q. Snurr, M. O'Keeffe, J. Kim, O.M. Yaghi, Science 329 (2010) 424.
[34] X.S. Wang, S.Q. Ma, P.M. Forster, D.Q. Yuan, J. Eckert, J.J. Lopez, B.J. Murphy, J.B. Parise, H.C. Zhou, Angew. Chem., Int. Ed. 47 (2008) 7263.
[35] U.S.E.I. Administration, International Energy Annual, 2008.
[36] R.J. Kuppler, D.J. Timmons, Q.R. Fang, J.R. Li, T.A. Makal, M.D. Young, D.Q. Yuan, D. Zhao, W.J. Zhuang, H.C. Zhou, Coord. Chem. Rev. 253 (2009) 3042.
[37] B.L. Chen, S.C. Xiang, G.D. Qian, Acc. Chem. Res. 43 (2010) 1115.
[38] J.P. Zhang, X.C. Huang, X.M. Chen, Chem. Soc. Rev. 38 (2009) 2385.
[39] X.M. Zhang, Coord. Chem. Rev. 249 (2005) 1201.
[40] M.P. Suh, Y.E. Cheon, E.Y. Lee, Coord. Chem. Rev. 252 (2008) 1007.
[41] S.L. Qiu, G.S. Zhu, Coord. Chem. Rev. 253 (2009) 2891.
[42] H. Zhao, Z.R. Qu, H.Y. Ye, R.G. Xiong, Chem. Soc. Rev. 37 (2008) 84.
[43] J.J. Perry, J.A. Perman, M.J. Zaworotko, Chem. Soc. Rev. 38 (2009) 1400.
[44] L.Q. Ma, C. Abney, W.B. Lin, Chem. Soc. Rev. 38 (2009) 1248.
[45] L.J. Murray, M. Dinca, J.R. Long, Chem. Soc. Rev. 38 (2009) 1294.
[46] A.U. Czaja, N. Trukhan, U. Muller, Chem. Soc. Rev. 38 (2009) 1284.
[47] A.M. Spokoyny, D. Kim, A. Sumrein, C.A. Mirkin, Chem. Soc. Rev. 38 (2009) 1218.
[48] G. Ferey, C. Serre, Chem. Soc. Rev. 38 (2009) 1380.
[49] M.D. Allendorf, C.A. Bauer, R.K. Bhakta, R.J.T. Houk, Chem. Soc. Rev. 38 (2009) 1330.
[50] M. Kurmoo, Chem. Soc. Rev. 38 (2009) 1353.
[51] J. Lee, O.K. Farha, J. Roberts, K.A. Scheidt, S.T. Nguyen, J.T. Hupp, Chem. Soc. Rev. 38 (2009) 1450.
[52] G.K.H. Shimizu, R. Vaidhyanathan, J.M. Taylor, Chem. Soc. Rev. 38 (2009) 1430.
[53] T. Uemura, N. Yanai, S. Kitagawa, Chem. Soc. Rev. 38 (2009) 1228.
[54] D. Zacher, O. Shekhah, C. Woll, R.A. Fischer, Chem. Soc. Rev. 38 (2009) 1418.
[55] T. Duren, Y.S. Bae, R.Q. Snurr, Chem. Soc. Rev. 38 (2009) 1237.
[56] R.E. Morris, P.S. Wheatley, Angew. Chem., Int. Ed. 47 (2008) 4966.
[57] S.Q. Ma, H.C. Zhou, Chem. Commun. 46 (2010) 44.
[58] R.Q. Zou, A.I. Abdel-Fattah, H.W. Xu, Y.S. Zhao, D.D. Hickmott, CrystEngComm 12 (2010) 1337.
[59] K. Kim, M. Banerjee, M. Yoon, S. Das, in: M. Schröder (Ed.), Functional Metal-Organic Frameworks: Gas Storage, Separation and Catalysis, Springer, Berlin/Heidelberg, 2010, p. 115.
[60] Y. Liu, W. Xuan, Y. Cui, Adv. Mater. 22 (2010) 4112.
[61] K.A. Cychosz, R. Ahmad, A.J. Matzger, Chem. Sci. 1 (2010) 293.
[62] S.T. Meek, J.A. Greathouse, M.D. Allendorf, Adv. Mater. 23 (2011) 249.
[63] X. Lin, N. Champness, M. Schröder, in: M. Schröder (Ed.), Functional Metal-Organic Frameworks: Gas Storage, Separation and Catalysis, Springer, Berlin/Heidelberg, 2010, p. 35.
[64] C. Janiak, J.K. Vieth, New J. Chem. 34 (2010) 2366.
[65] D. Liu, C. Zhong, J. Mater. Chem. 20 (2010) 10308.
[66] J.D. Figueroa, T. Fout, S. Plasynski, H. McIlvried, R.D. Srivastava, Int. J. Greenhouse Gas Control 2 (2008) 9.
[67] N. MacDowell, N. Florin, A. Buchard, J. Hallett, A. Galindo, G. Jackson, C.S. Adjiman, C.K. Williams, N. Shah, P. Fennell, Energy Environ. Sci. 3 (2011) 1645.
[68] C.A. Scholes, K.H. Smith, S.E. Kentish, G.W. Stevens, Int. J. Greenhouse Gas Control 4 (2010) 739.
[69] S. Smart, C.X.C. Lin, L. Ding, K. Thambimuthu, J.C.D. da Costa, Energy Environ. Sci. 3 (2010) 268.
[70] F.M. Orr, Energy Environ. Sci. 2 (2009) 449.
[71] S. Bachu, Prog. Energy Combust. Sci. 34 (2008) 254.
[72] C. Scholes, S. Kentish, G. Stevens, Sep. Purif. Rev. 38 (2009) 1.
[73] A.J. Hunt, E.H.K. Sin, R. Marriott, J.H. Clark, ChemSusChem 3 (2010) 306.
[74] T.L. Chew, A.L. Ahmad, S. Bhatia, Adv. Colloid Interface Sci. 153 (2010) 43.
[75] G. Pipitone, O. Bolland, Int. J. Greenhouse Gas Control 3 (2009) 528.
[76] H.W. Pennline, D.R. Luebke, K.L. Jones, C.R. Myers, B.I. Morsi, Y.J. Heintz, J.B. Ilconich, Fuel Process. Technol. 89 (2008) 897.
[77] H.Q. Yang, Z.H. Xu, M.H. Fan, R. Gupta, R.B. Slimane, A.E. Bland, I. Wright, J. Environ. Sci. (China) 20 (2008) 14.
[78] K.M.K. Yu, I. Curcic, J. Gabriel, S.C.E. Tsang, ChemSusChem 1 (2008) 893.
[79] E.J. Granite, T. O'Brien, Fuel Process. Technol. 86 (2005) 1423.
[80] J.E. Bara, D.E. Camper, D.L. Gin, R.D. Noble, Acc. Chem. Res. 43 (2010) 152.
[81] B. Feng, H. An, E. Tan, Energy Fuels 21 (2007) 426.
[82] C. Gough, Int. J. Greenhouse Gas Control 2 (2008) 155.
[83] Y.G. Zhang, J.Y.G. Chan, Energy Environ. Sci. 3 (2010) 408.
[84] A. Phan, C.J. Doonan, F.J. Uribe-Romo, C.B. Knobler, M. O'Keeffe, O.M. Yaghi, Acc. Chem. Res. 43 (2010) 58.
[85] H. de Coninck, T. Flach, P. Curnow, P. Richardson, J. Anderson, S. Shackley, G. Sigurthorsson, D. Reiner, Int. J. Greenhouse Gas Control 3 (2009) 333.
[86] S. Shackley, D. Reiner, P. Upham, H. de Coninck, G. Sigurthorsson, J. Anderson, Int. J. Greenhouse Gas Control 3 (2009) 344.
[87] P. Riemer, Energy Convers. Manage. 37 (1996) 665.
[88] C. Jones, E. Maginn, ChemSusChem 3 (2010) 863.
[89] C. Grande, R.P. Ribeiro, A. Rodrigues, ChemSusChem 3 (2010) 892.
[90] N. Hedin, L. Chen, A. Laaksonen, Nanoscale 2 (2010) 1819.
[91] S. Keskin, T.M. van Heest, D.S. Sholl, ChemSusChem 3 (2010) 879.
[92] Z.H. Xiang, D.P. Cao, J.H. Lan, W.C. Wang, D.P. Broom, Energy Environ. Sci. 3 (2010) 1469.
[93] G. Ferey, C. Serre, T. Devic, G. Maurin, H. Jobic, P.L. Llewellyn, G. De Weireld, A. Vimont, M. Daturi, J.-S. Chang, Chem. Soc. Rev. 40 (2011) 550.
[94] Y.B. Zhang, W.X. Zhang, F.Y. Feng, J.P. Zhang, X.M. Chen, Angew. Chem., Int. Ed. 48 (2009) 5287.
[95] A.R. Millward, O.M. Yaghi, J. Am. Chem. Soc. 127 (2005) 17998.
[96] K.S. Walton, A.R. Millward, D. Dubbeldam, H. Frost, J.J. Low, O.M. Yaghi, R.Q. Snurr, J. Am. Chem. Soc. 130 (2008) 406.
[97] J. Seo, H. Chun, Eur. J. Inorg. Chem. (2009) 4946.
[98] S. Couck, J.F.M. Denayer, G.V. Baron, T. Remy, J. Gascon, F. Kapteijn, J. Am. Chem. Soc. 131 (2009) 6326.
[99] F. Salles, A. Ghoufi, G. Maurin, R.G. Bell, C. Mellot-Draznieks, G. Ferey, Angew. Chem., Int. Ed. 47 (2008) 8487.
[100] N.A. Ramsahye, G. Maurin, S. Bourrelly, P.L. Llewellyn, C. Serre, T. Loiseau, T. Devic, G. Ferey, J. Phys. Chem. C 112 (2008) 514.
[101] Y. Liu, J.H. Her, A. Dailly, A.J. Ramirez-Cuesta, D.A. Neumann, C.M. Brown, J. Am. Chem. Soc. 130 (2008) 11813.
[102] A. Vimont, A. Travert, P. Bazin, J.C. Lavalley, M. Daturi, C. Serre, G. Ferey, S. Bourrelly, P.L. Llewellyn, Chem. Commun. (2007) 3291.
[103] P.L. Llewellyn, S. Bourrelly, C. Serre, Y. Filinchuk, G. Ferey, Angew. Chem., Int. Ed. 45 (2006) 7751.
[104] S. Bourrelly, P.L. Llewellyn, C. Serre, F. Millange, T. Loiseau, G. Ferey, J. Am. Chem. Soc. 127 (2005) 13519.
[105] C. Serre, F. Millange, C. Thouvenot, M. Nogues, G. Marsolier, D. Louer, G. Ferey, J. Am. Chem. Soc. 124 (2002) 13519.
[106] S.R. Miller, P.A. Wright, T. Devic, C. Serre, G. Ferey, P.L. Llewellyn, R. Denoyel, L. Gaberova, Y. Filinchuk, Langmuir 25 (2009) 3618.
[107] Z.Q. Wang, S.M. Cohen, J. Am. Chem. Soc. 131 (2009) 16675.
[108] J.T. Culp, M.R. Smith, E. Bittner, B. Bockrath, J. Am. Chem. Soc. 130 (2008) 12427.
[109] K.L. Mulfort, O.K. Farha, C.D. Malliakas, M.G. Kanatzidis, J.T. Hupp, Chem. -Eur. J. 16 (2010) 276.
[110] F.X. Coudert, C. Mellot-Draznieks, A.H. Fuchs, A. Boutin, J. Am. Chem. Soc. 131 (2009) 11329.
[111] H. Kim, D.G. Samsonenko, M. Yoon, J.W. Yoon, Y.K. Hwang, J.S. Chang, K. Kim, Chem. Commun. (2008) 4697.
[112] D. Tanaka, K. Nakagawa, M. Higuchi, S. Horike, Y. Kubota, L.C. Kobayashi, M. Takata, S. Kitagawa, Angew. Chem., Int. Ed. 47 (2008) 3914.
[113] J. Seo, R. Matsuda, H. Sakamoto, C. Bonneau, S. Kitagawa, J. Am. Chem. Soc. 131 (2009) 12792.
[114] R. Kitaura, K. Seki, G. Akiyama, S. Kitagawa, Angew. Chem., Int. Ed. 42 (2003) 428.
[115] S.Q. Ma, D.F. Sun, D.Q. Yuan, X.S. Wang, H.C. Zhou, J. Am. Chem. Soc. 131 (2009) 6445.
[116] S.Q. Ma, D.F. Sun, X.S. Wang, H.C. Zhou, Angew. Chem., Int. Ed. 46 (2007) 2458.
[117] T.K. Maji, G. Mostafa, R. Matsuda, S. Kitagawa, J. Am. Chem. Soc. 127 (2005) 17152.
[118] Y. Cheng, A. Kondo, H. Noguchi, H. Kajiro, K. Urita, T. Ohba, K. Kaneko, H. Kanoh, Langmuir 25 (2009) 4510.
[119] J. Rabone, Y.-F. Yue, S.Y. Chong, K.C. Stylianou, J. Bacsa, D. Bradshaw, G.R. Darling, N.G. Berry, Y.Z. Khimyak, A.Y. Ganin, P. Wiper, J.B. Claridge, M.J. Rosseinsky, Science 329 (2010) 1053.
[120] A. Kondo, A. Chinen, H. Kajiro, T. Nakagawa, K. Kato, M. Takata, Y. Hattori, F. Okino, T. Ohba, K. Kaneko, H. Kanoh, Chem. -Eur. J. 15 (2009) 7549.
[121] J.A. Botas, G. Calleja, M. Sanchez-Sanchez, M.G. Orcajo, Langmuir 26 (2010) 5300.
[122] J. An, N.L. Rosi, J. Am. Chem. Soc. 132 (2010) 5578.
[123] T.K. Maji, R. Matsuda, S. Kitagawa, Nat. Mater. 6 (2007) 142.

[124] A.O. Yazaydin, A.I. Benin, S.A. Faheem, P. Jakubczak, J.J. Low, R.R. Willis, R.Q. Snurr, Chem. Mater. 21 (2009) 1425.
[125] Z. Xiang, Z. Hu, D. Cao, W. Yang, J. Lu, B. Han, W. Wang, Angew. Chem., Int. Ed. 50 (2011) 491.
[126] A. Demessence, D.M. D'Alessandro, M.L. Foo, J.R. Long, J. Am. Chem. Soc. 131 (2009) 8784.
[127] D. Farrusseng, C. Daniel, C. Gaudillere, U. Ravon, Y. Schuurman, C. Mirodatos, D. Dubbeldam, H. Frost, R.Q. Snurr, Langmuir 25 (2009) 7383.
[128] R. Vaidhyanathan, S.S. Iremonger, G.K.H. Shimizu, P.G. Boyd, S. Alavi, T.K. Woo, Science 330 (2010) 650.
[129] R. Vaidhyanathan, S.S. Iremonger, K.W. Dawson, G.K.H. Shimizu, Chem. Commun. (2009) 5230.
[130] S. Bordiga, L. Regli, F. Bonino, E. Groppo, C. Lamberti, B. Xiao, P.S. Wheatley, R.E. Morris, A. Zecchina, Phys. Chem. Chem. Phys. 9 (2007) 2676.
[131] P.D.C. Dietzel, R.E. Johnsen, H. Fjellvag, S. Bordiga, E. Groppo, S. Chavan, R. Blom, Chem. Commun. (2008) 5125.
[132] C.M. Lu, J. Liu, K.F. Xiao, A.T. Harris, Chem. Eng. J. (Lausanne) 156 (2010) 465.
[133] S.S. Kaye, A. Dailly, O.M. Yaghi, J.R. Long, J. Am. Chem. Soc. 129 (2007) 14176.
[134] S.S. Han, S.H. Choi, A.C.T. van Duin, Chem. Commun. 46 (2010) 5713.
[135] P.L. Llewellyn, S. Bourrelly, C. Serre, A. Vimont, M. Daturi, L. Hamon, G. De Weireld, J.S. Chang, D.Y. Hong, Y.K. Hwang, S.H. Jhung, G. Ferey, Langmuir 24 (2008) 7245.
[136] L. Hamon, P.L. Llewellyn, T. Devic, A. Ghoufi, G. Clet, V. Guillerm, G.D. Pirngruber, G. Maurin, C. Serre, G. Driver, W. van Beek, E. Jolimaitre, A. Vimont, M. Daturi, G. Ferey, J. Am. Chem. Soc. 131 (2009) 17490.
[137] P.S. Barcia, L. Bastin, E.J. Hurtado, J.A.C. Silva, A.E. Rodrigues, B.L. Chen, Sep. Sci. Technol. 43 (2008) 3494.
[138] A.J. Fletcher, E.J. Cussen, T.J. Prior, M.J. Rosseinsky, C.J. Kepert, K.M. Thomas, J. Am. Chem. Soc. 123 (2001) 10001.
[139] F. Salles, H. Jobic, A. Ghoufi, P.L. Llewellyn, C. Serre, S. Bourrelly, G. Ferey, G. Maurin, Angew. Chem., Int. Ed. 48 (2009) 8335.
[140] F. Salles, H. Jobic, T. Devic, P.L. Llewellyn, C. Serre, G. Ferey, G. Maurin, ACS Nano 4 (2010) 143.
[141] O.J. Garcia-Ricard, A.J. Hernandez-Maldonado, J. Phys. Chem. C 114 (2010) 1827.
[142] Z.X. Zhao, Z. Li, Y.S. Lin, Ind. Eng. Chem. Res. 48 (2009) 10015.
[143] D. Saha, Z.B. Bao, F. Jia, S.G. Deng, Environ. Sci. Technol. 44 (2010) 1820.
[144] A.L. Myers, J.M. Prausnitz, AIChE J. 11 (1965) 121.
[145] E. Barea, G. Tagliabue, W.G. Wang, M. Perez-Mendoza, L. Mendez-Linan, F.J. Lopez-Garzon, S. Galli, N. Masciocchi, J.A.R. Navarro, Chem. -Eur. J. 16 (2010) 931.
[146] Z.X. Chen, S.C. Xiang, H.D. Arman, P. Li, S. Tidrow, D.Y. Zhao, B.L. Chen, Eur. J. Inorg. Chem. (2010) 3745.
[147] M. Radha Kishan, J. Tian, P.K. Thallapally, C.A. Fernandez, S.J. Dalgarno, J.E. Warren, B.P. McGrail, J.L. Atwood, Chem. Commun. 46 (2010) 538.
[148] B. Mu, P.M. Schoenecker, K.S. Walton, J. Phys. Chem. C 114 (2010) 6464.
[149] C.A. Fernandez, P.K. Thallapally, R.K. Motkuri, S.K. Nune, J.C. Sumrak, J. Tian, J. Liu, Cryst. Growth Des. 10 (2010) 1037.
[150] H.J. Park, M.P. Suh, Chem. Commun. 46 (2010) 610.
[151] S.K. Nune, P.K. Thallapally, A. Dohnalkova, C.M. Wang, J. Liu, G.J. Exarhos, Chem. Commun. 46 (2010) 4878.
[152] P. Kanoo, K.L. Gurunatha, T.K. Maji, J. Mater. Chem. 20 (2010) 1322.
[153] Y.X. Hu, S.C. Xiang, W.W. Zhang, Z.X. Zhang, L. Wang, J.F. Bai, B.L. Chen, Chem. Commun. (2009) 7551.
[154] B. Mu, F. Li, K.S. Walton, Chem. Commun. (2009) 2493.
[155] P.D.C. Dietzel, V. Besikiotis, R. Blom, J. Mater. Chem. 19 (2009) 7362.
[156] Z.J. Liang, M. Marshall, A.L. Chaffee, Energy Fuels 23 (2009) 2785.
[157] R. Banerjee, H. Furukawa, D. Britt, C. Knobler, M. O'Keeffe, O.M. Yaghi, J. Am. Chem. Soc. 131 (2009) 3875.
[158] H. Chun, J. Seo, Inorg. Chem. 48 (2009) 9980.
[159] Y.S. Bae, O.K. Farha, J.T. Hupp, R.Q. Snurr, J. Mater. Chem. 19 (2009) 2131.
[160] I. Senkovska, F. Hoffmann, M. Fröba, J. Getzschmann, W. Böhlmann, S. Kaskel, Micropor. Mesopor. Mater. 122 (2009) 93.
[161] M. Xue, Y. Liu, R.M. Schaffino, S. Xiang, X. Zhao, G.-S. Zhu, S.-L. Qiu, B. Chen, Inorg. Chem. 48 (2009) 4649.
[162] E. Neofotistou, C.D. Malliakas, P.N. Trikalitis, Chem. -Eur. J. 15 (2009) 4523.
[163] C. Volkringer, T. Loiseau, N. Haouas, F. Taulelle, D. Popov, M. Burghammer, C. Riekel, C. Zlotea, F. Cuevas, M. Latroche, D. Phanon, C. Knofelv, P.L. Llewellyn, G. Ferey, Chem. Mater. 21 (2009) 5783.
[164] Y.E. Cheon, J. Park, M.P. Suh, Chem. Commun. (2009) 5436.
[165] L. Bastin, P.S. Barcia, E.J. Hurtado, J.A.C. Silva, A.E. Rodrigues, B. Chen, J. Phys. Chem. C 112 (2008) 1575.
[166] Y.S. Bae, O.K. Farha, A.M. Spokoyny, C.A. Mirkin, J.T. Hupp, R.Q. Snurr, Chem. Commun. (2008) 4135.
[167] P.L. Llewellyn, S. Bourrelly, C. Serre, A. Vimont, M. Daturi, L. Hamon, G. De Weireld, J.-S. Chang, D.-Y. Hong, Y.K. Hwang, S.H. Jhung, G. Ferey, Langmuir 24 (2008) 7245.
[168] S. Cavenati, C.A. Grande, A.E. Rodrigues, Ind. Eng. Chem. Res. 47 (2008) 6333.
[169] S. Galli, N. Masciocchi, G. Tagliabue, A. Sironi, J.A.R. Navarro, J.M. Salas, L. Mendez-Linan, M. Domingo, M. Perez-Mendoza, E. Barea, Chem. -Eur. J. 14 (2008) 9890.
[170] M. Xue, S.Q. Ma, Z. Jin, R.M. Schaffino, G.S. Zhu, E.B. Lobkovsky, S.L. Qiu, B.L. Chen, Inorg. Chem. 47 (2008) 6825.
[171] J.R. Li, Y. Tao, Q. Yu, X.H. Bu, H. Sakamoto, S. Kitagawa, Chem. -Eur. J. 14 (2008) 2771.
[172] Y.S. Bae, K.L. Mulfort, H. Frost, P. Ryan, S. Punnathanam, L.J. Broadbelt, J.T. Hupp, R.Q. Snurr, Langmuir 24 (2008) 8592.
[173] S.R. Miller, G.M. Pearce, P.A. Wright, F. Bonino, S. Chavan, S. Bordiga, I. Margiolaki, N. Guillou, G. Feerey, S. Bourrelly, P.L. Llewellyn, J. Am. Chem. Soc. 130 (2008) 15967.
[174] B.L. Chen, S.Q. Ma, E.J. Hurtado, E.B. Lobkovsky, H.C. Zhou, Inorg. Chem. 46 (2007) 8490.
[175] B.L. Chen, S.Q. Ma, F. Zapata, F.R. Fronczek, E.B. Lobkovsky, H.C. Zhou, Inorg. Chem. 46 (2007) 1233.
[176] J.W. Yoon, S.H. Jhung, Y.K. Hwang, S.M. Humphrey, P.T. Wood, J.S. Chang, Adv. Mater. 19 (2007) 1830.
[177] S. Ma, X.-S. Wang, E.S. Manis, C.D. Collier, H.-C. Zhou, Inorg. Chem. 46 (2007) 3432.
[178] M.P. Suh, Y.E. Cheon, E.Y. Lee, Chem. -Eur. J. 13 (2007) 4208.
[179] H. Hayashi, A.P. Cote, H. Furukawa, M. O'Keeffe, O.M. Yaghi, Nat. Mater. 6 (2007) 501.
[180] P.L. Llewellyn, S. Bourrrelly, C. Serre, Y. Filinchuk, G. Ferey, Angew. Chem., Int. Ed. 45 (2006) 7751.
[181] H.R. Moon, N. Kobayashi, M.P. Suh, Inorg. Chem. 45 (2006) 8672.
[182] S. Surble, F. Millange, C. Serre, T. Duren, M. Latroche, S. Bourrelly, P.L. Llewellyn, G. Ferey, J. Am. Chem. Soc. 128 (2006) 14889.
[183] D.N. Dybtsev, H. Chun, S.H. Yoon, D. Kim, K. Kim, J. Am. Chem. Soc. 126 (2004) 32.
[184] S.-M. Zhang, Z. Chang, T.-L. Hu, X.-H. Bu, Inorg. Chem. 49 (2010) 11581.
[185] Z. Zhang, S. Xiang, Y.-S. Chen, S. Ma, Y. Lee, T. Phely-Bobin, B. Chen, Inorg. Chem. 49 (2010) 8444.
[186] Z. Zhang, S. Xiang, X. Rao, Q. Zheng, F.R. Fronczek, G. Qian, B. Chen, Chem. Commun. 46 (2010) 7205.
[187] J. Seo, N. Jin, H. Chun, Inorg. Chem. 49 (2010) 10833.
[188] P. Kanoo, T.K. Maji, Eur. J. Inorg. Chem. (2010) 3762.
[189] J.M. Gu, T.H. Kwon, J.H. Park, S. Huh, Dalton Trans. 39 (2010) 5608.
[190] J. An, S.J. Geib, N.L. Rosi, J. Am. Chem. Soc. 132 (2010) 38.
[191] Y.J. Zhang, T. Liu, S. Kanegawa, O. Sato, J. Am. Chem. Soc. 132 (2010) 912.
[192] D.C. Zhong, W.G. Lu, L. Jiang, X.L. Feng, T.B. Lu, Cryst. Growth Des. 10 (2010) 739.
[193] R. Grunker, I. Senkovska, R. Biedermann, N. Klein, A. Klausch, I.A. Baburin, U. Mueller, S. Kaskel, Eur. J. Inorg. Chem. (2010) 3835.
[194] P.D. Southon, L. Liu, E.A. Fellows, D.J. Price, G.J. Halder, K.W. Chapman, B. Moubaraki, K.S. Murray, J.F. Letard, C.J. Kepert, J. Am. Chem. Soc. 131 (2009) 10998.
[195] P.K. Thallapally, J. Tian, M.R. Kishan, C.A. Fernandez, S.J. Dalgarno, P.B. McGrail, J.E. Warren, J.L. Atwood, J. Am. Chem. Soc. 130 (2008) 16842.
[196] Y. Zou, S. Hong, M. Park, H. Chun, M.S. Lah, Chem. Commun. (2007) 5182.
[197] E.D. Bloch, D. Britt, C. Lee, C.J. Doonan, F.J. Uribe-Romo, H. Furukawa, J.R. Long, O.M. Yaghi, J. Am. Chem. Soc. 132 (2010) 14382.
[198] B. Zheng, J. Bai, J. Duan, L. Wojtas, M.J. Zaworotko, J. Am. Chem. Soc. 133 (2011) 748.
[199] A. Mallick, S. Saha, P. Pachfule, S. Roy, R. Banerjee, J. Mater. Chem. 20 (2010) 9073.
[200] L. Pan, K.M. Adams, H.E. Hernandez, X.T. Wang, C. Zheng, Y. Hattori, K. Kaneko, J. Am. Chem. Soc. 125 (2003) 3062.
[201] A.O. Yazaydin, R.Q. Snurr, T.-H. Park, K. Koh, J. Liu, M.D. LeVan, A.I. Benin, P. Jakubczak, M. Lanuza, D.B. Galloway, J.J. Low, R.R. Willis, J. Am. Chem. Soc. 131 (2009) 18198.
[202] O.K. Farha, Y.S. Bae, B.G. Hauser, A.M. Spokoyny, R.Q. Snurr, C.A. Mirkin, J.T. Hupp, Chem. Commun. 46 (2010) 1056.
[203] S.Q. Ma, X.S. Wang, E.S. Manis, C.D. Collier, H.C. Zhou, Inorg. Chem. 46 (2007) 3432.
[204] K. Sumida, S. Horike, S.S. Kaye, Z.R. Herm, W.L. Queen, C.M. Brown, F. Grandjean, G.J. Long, A. Dailly, J.R. Long, Chem. Sci. 1 (2010) 184.
[205] H.S. Choi, M.P. Suh, Angew. Chem., Int. Ed. 48 (2009) 6865.
[206] A.L. Myers, in: A. Liapis (Ed.), Fundamental of Adsorption, Engineering Foundation, 1986.
[207] S. Kim, J.R. Jinschek, H. Chen, D.S. Sholl, E. Marand, Nano Lett. 7 (2007) 2806.
[208] M. Murthi, R.Q. Snurr, Langmuir 20 (2004) 2489.
[209] R. Banerjee, A. Phan, B. Wang, C. Knobler, H. Furukawa, M. O'Keeffe, O.M. Yaghi, Science 319 (2008) 939.
[210] B. Wang, A.P. Cote, H. Furukawa, M. O'Keeffe, O.M. Yaghi, Nature 453 (2008) 207.
[211] J.Y. Lee, J.M. Roberts, O.K. Farha, A.A. Sarjeant, K.A. Scheidt, J.T. Hupp, Inorg. Chem. 48 (2009) 9971.
[212] S.Q. Ma, X.S. Wang, C.D. Collier, E.S. Manis, H.C. Zhou, Inorg. Chem. 46 (2007) 8499.
[213] L.J. Murray, M. Dinca, J. Yano, S. Chavan, S. Bordiga, C.M. Brown, J.R. Long, J. Am. Chem. Soc. 132 (2010) 7856.
[214] H.X. Deng, C.J. Doonan, H. Furukawa, R.B. Ferreira, J. Towne, C.B. Knobler, B. Wang, O.M. Yaghi, Science 327 (2010) 846.
[215] D. Britt, H. Furukawa, B. Wang, T.G. Glover, O.M. Yaghi, Proc. Natl. Acad. Sci. U.S.A. 106 (2009) 20637.
[216] N.A. Ramsahye, G. Maurin, S. Bourrelly, P.L. Llewellyn, T. Loiseau, C. Serre, G. Ferey, Chem. Commun. (2007) 3261.
[217] V. Finsy, L. Ma, L. Alaerts, D.E. De Vos, G.V. Baron, J.F.M. Denayer, Micropor. Mesopor. Mater. 120 (2009) 221.
[218] E. Quartapelle Procopio, F. Linares, C. Montoro, V. Colombo, A. Maspero, E. Barea, J.A.R. Navarro, Angew. Chem., Int. Ed. 49 (2010) 7308.

[219] B. Crittenden, W.J. Thomas, Adsorption Technology & Design, Butterworth-Heinemann, 1998, p. 187.
[220] A. Brunetti, F. Scura, G. Barbieri, E. Drioli, J. Membr. Sci. 359 (2010) 115.
[221] D. Aaron, C. Tsouris, Sep. Sci. Technol. 40 (2005) 321.
[222] H. Lin, B.D. Freeman, J. Mol. Struct. 739 (2005) 57.
[223] M.T. Ho, G.W. Allinson, D.E. Wiley, Ind. Eng. Chem. Res. 47 (2008) 1562.
[224] R.W. Baker, Ind. Eng. Chem. Res. 41 (2002) 1393.
[225] Z.P. Lai, G. Bonilla, I. Diaz, J.G. Nery, K. Sujaoti, M.A. Amat, E. Kokkoli, O. Terasaki, R.W. Thompson, M. Tsapatsis, D.G. Vlachos, Science 300 (2003) 456.
[226] J. Choi, H. Jeong, M. Snyder, J. Stoeger, R. Masel, M. Tsapatsis, Science 325 (2009) 590.
[227] R. Krishna, J.M. van Baten, J. Membr. Sci. 360 (2010) 323.
[228] J. Caro, M. Noack, P. Kolsch, R. Schafer, Micropor. Mesopor. Mater. 38 (2000) 3.
[229] E.E. McLeary, J.C. Jansen, F. Kapteijn, Micropor. Mesopor. Mater. 90 (2006) 198.
[230] A. Hussain, M.-B. Hagg, J. Membr. Sci. 359 (2010) 140.
[231] P. Scovazzo, D. Havard, M. McShea, S. Mixon, D. Morgan, J. Membr. Sci. 327 (2009) 41.
[232] H. Chen, A.S. Kovvali, S. Majumdar, K.K. Sirkar, Ind. Eng. Chem. Res. 38 (1999) 3489.
[233] H. Chen, G. Obuskovic, S. Majumdar, K.K. Sirkar, J. Membr. Sci. 183 (2001) 75.
[234] A.S. Kovvali, H. Chen, K.K. Sirkar, J. Am. Chem. Soc. 122 (2000) 7594.
[235] C.E. Powell, G.G. Qiao, J. Membr. Sci. 279 (2006) 1.
[236] R. Mahajan, W.J. Koros, Ind. Eng. Chem. Res. 39 (2000) 2692.
[237] C.M. Zimmerman, A. Singh, W.J. Koros, J. Membr. Sci. 137 (1997) 145.
[238] S. Shu, S. Husain, W.J. Koros, J. Phys. Chem. C 111 (2007) 652.
[239] M. Eddaoudi, J. Kim, N. Rosi, D. Vodak, J. Wachter, M. O'Keefe, O.M. Yaghi, Science 295 (2002) 469.
[240] J.L.C. Rowsell, O.M. Yaghi, Micropor. Mesopor. Mater. 73 (2004) 3.
[241] Y.Y. Liu, Z.F. Ng, E.A. Khan, H.K. Jeong, C.B. Ching, Z.P. Lai, Micropor. Mesopor. Mater. 118 (2009) 296.
[242] Y. Yoo, Z.P. Lai, H.K. Jeong, Micropor. Mesopor. Mater. 123 (2009) 100.
[243] H. Guo, G. Zhu, I.J. Hewitt, S. Qiu, J. Am. Chem. Soc. 131 (2009) 1646.
[244] R. Ranjan, M. Tsapatsis, Chem. Mater. 21 (2009) 4920.
[245] H. Bux, F.Y. Liang, Y.S. Li, J. Cravillon, M. Wiebcke, J. Caro, J. Am. Chem. Soc. 131 (2009) 16000.
[246] V.V. Guerrero, Y. Yoo, M.C. McCarthy, H.K. Jeong, J. Mater. Chem. 20 (2010) 3938.
[247] Y.S. Li, F.Y. Liang, H. Bux, A. Feldhoff, W.S. Yang, J. Caro, Angew. Chem., Int. Ed. 49 (2010) 548.
[248] Y. Liu, E. Hu, E.A. Khan, Z. Lai, J. Membr. Sci. 353 (2010) 36.
[249] M.C. McCarthy, V.V. Guerrero, G. Barnett, H.K. Jeong, Langmuir 26 (2010) 14636.
[250] A. Huang, H. Bux, F. Steinbach, J. Caro, Angew. Chem., Int. Ed. 49 (2010) 4958.
[251] Y.S. Li, F.Y. Liang, H.G. Bux, W.S. Yang, J. Caro, J. Membr. Sci. 354 (2010) 48.
[252] A. Huang, W. Dou, J. Caro, J. Am. Chem. Soc. 132 (2010) 15562.
[253] S. Takamizawa, Y. Takasaki, R. Miyake, J. Am. Chem. Soc. 132 (2010) 2862.
[254] J.G. Nyuyen, S.M. Cohen, J. Am. Chem. Soc. 132 (2010) 4560.
[255] Y.-S. Li, H.G. Bux, A. Feldhoff, G.-L. Li, W.S. Yang, J. Caro, Adv. Mater. 22 (2010) 3322.
[256] K.S. Park, Z. Ni, A.P. Cote, J.Y. Choi, R.D. Huang, F.J. Uribe-Romo, H.K. Chae, M. O'Keeffe, O.M. Yaghi, Proc. Natl. Acad. Sci. U.S.A. 103 (2006) 10186.
[257] Y. Hu, X. Dong, J. Nan, W. Jin, X. Ren, N. Xu, Y.M. Lee, Chem. Commun. 47 (2011) 737.
[258] L. Pan, M.B. Sander, X.Y. Huang, J. Li, M. Smith, E. Bittner, B. Bockrath, J.K. Johnson, J. Am. Chem. Soc. 126 (2004) 1308.
[259] K. Kusakabe, T. Kuroda, A. Murata, S. Morooka, Ind. Eng. Chem. Res. 36 (1997) 649.
[260] J.G. Won, J.S. Seo, J.H. Kim, H.S. Kim, Y.S. Kang, S.J. Kim, Y.M. Kim, J.G. Jegal, Adv. Mater. 17 (2005) 80.
[261] Y. Zhang, I.H. Musselman, J.P. Ferraris, K.J. Balkus Jr., J. Membr. Sci. 313 (2008) 170.
[262] R. Adams, C. Carson, J. Ward, R. Tannenbaum, W. Koros, Micropor. Mesopor. Mater. 131 (2010) 13.
[263] M.J.C. Ordonez, K.J. Balkus Jr., J.P. Ferraris, I.H. Musselman, J. Membr. Sci. 361 (2010) 28.
[264] A. Car, C. Stropnik, P. Klaus-Viktor, Desalination 200 (2006) 424.
[265] E.V. Perez, K.J. Balkus Jr., J.P. Ferraris, I.H. Musselman, J. Membr. Sci. 328 (2009) 165.
[266] W. Morris, B. Leung, H. Furukawa, O.K. Yaghi, N. He, H. Hayashi, Y. Houndonougbo, M. Asta, B.B. Laird, O.M. Yaghi, J. Am. Chem. Soc. 132 (2010) 11006.
[267] S.M. Kuznicki, V.A. Bell, S. Nair, H.W. Hillhouse, R.M. Jacubinas, C.M. Braunbarth, B.H. Toby, M. Tsapatsis, Nature 412 (2001) 720.
[268] S.S. Han, W.Q. Deng, W.A. Goddard, Angew. Chem., Int. Ed. 46 (2007) 6289.
[269] A. Kuc, T. Heine, G. Seifert, H.A. Duarte, Chem. -Eur. J. 14 (2008) 6597.
[270] S.S. Han, A.G. William III, J. Am. Chem. Soc. 129 (2007) 8422.
[271] Y.Y. Sun, K. Lee, Y.H. Kim, S.B. Zhang, Appl. Phys. Lett. 95 (2009).
[272] H. Wu, J.M. Simmons, Y. Liu, C.M. Brown, X.S. Wang, S. Ma, V.K. Peterson, P.D. Southon, C.J. Kepert, H.C. Zhou, T. Yildirim, W. Zhou, Chem. -Eur. J. 16 (2010) 5205.
[273] A. Pianwanit, C. Kritayakornupong, A. Vongachariya, N. Selphusit, T. Ploymeerusmee, T. Remsungnen, D. Nuntasri, S. Fritzsche, S. Hannongbua, Chem. Phys. 349 (2008) 77.
[274] Q. Xu, D.H. Liu, Q.Y. Yang, C.L. Zhong, J.G. Mi, J. Mater. Chem. 20 (2010) 706.

[275] A. Torrisi, C. Mellot-Draznieks, R.G. Bell, J. Chem. Phys. 130 (2009) 194703.
[276] A. Torrisi, C. Mellot-Draznieks, R.G. Bell, J. Chem. Phys. 132 (2010) 044705.
[277] D. Dubbeldam, H. Frost, K.S. Walton, R.Q. Snurr, Fluid Phase Equilib. 261 (2007) 152.
[278] C. Moller, M.S. Plesset, Phys. Rev. 46 (1934) 0618.
[279] S. Grimme, J. Comput. Chem. 27 (2006) 1787.
[280] C. Tuma, J. Sauer, Phys. Chem. Chem. Phys. 8 (2006) 3955.
[281] R.B. Rankin, J.C. Liu, A.D. Kulkarni, J.K. Johnson, J. Phys. Chem. C 113 (2009) 16906.
[282] L. Valenzano, B. Civalleri, S. Chavan, G.T. Palomino, C. Arean, S. Bordiga, J. Phys. Chem. C 114 (2010) 11185.
[283] S.F. Boys, F. Bernardi, Mol. Phys. 19 (1970) 553.
[284] A. Ikeda, Y. Nakao, H. Sato, S. Sakaki, J. Phys. Chem. A 111 (2007) 7124.
[285] F. Negri, N. Saendig, Theor. Chem. Acc. 118 (2007) 149.
[286] Q.Y. Yang, C.L. Zhong, J.F. Chen, J. Phys. Chem. C 112 (2008) 1562.
[287] R. Babarao, J. Jiang, J. Am. Chem. Soc. 131 (2009) 11417.
[288] D. Foguet-Albiol, T.A. O'Brien, W. Wernsdorfer, B. Moulton, M.J. Zaworotko, K.A. Abboud, G. Christou, Angew. Chem., Int. Ed. 44 (2005) 897.
[289] R.S. Mulliken, J. Chem. Phys. 23 (1955) 1833.
[290] B.H. Besler, K.M. Merz, P.A. Kollman, J. Comput. Chem. 11 (1990) 431.
[291] C.I. Bayly, P. Cieplak, W.D. Cornell, P.A. Kollman, J. Phys. Chem. 97 (1993) 10269.
[292] C.M. Breneman, K.B. Wiberg, J. Comput. Chem. 11 (1990) 361.
[293] C. Campañá, B. Mussard, T.K. Woo, J. Chem. Theory Comput. 5 (2009) 2866.
[294] M.P. Allen, D.J. Tildesley, Computer Simulation of Liquids, Clarendon Press, 1987.
[295] G.E. Norman, V.S. Filinov, High Temp. 7 (1969) 216.
[296] D. Frenkel, B. Smit, Understanding of Molecular Simulation: From Algorithms to Applications, Academic Press, 2002.
[297] N.A. Ramsahye, G. Maurin, S. Bourrelly, P. Llewellyn, T. Loiseau, G. Ferey, Phys. Chem. Chem. Phys. 9 (2007) 1059.
[298] Y. Iwai, H. Higashi, H. Uchida, Y. Arai, Fluid Phase Equilib. 127 (1997) 251.
[299] J.G. Harris, K.H. Yung, J. Phys. Chem. 99 (1995) 12021.
[300] G. Maurin, P.L. Llewellyn, R.G. Bell, J. Phys. Chem. B 109 (2005) 16084.
[301] Y.F. Chen, J.Y. Lee, R. Babarao, J. Li, J.W. Jiang, J. Phys. Chem. C 114 (2010) 6602.
[302] R. Babarao, J. Jiang, Langmuir 24 (2008) 6270.
[303] A.K. Rappe, C.J. Casewit, K.S. Colwell, W.A. Goddard, W.M. Skiff, J. Am. Chem. Soc. 114 (1992) 10024.
[304] S.L. Mayo, B.D.W.A.G. Olafson III, J. Phys. Chem. 94 (1990) 8897.
[305] W.L. Jorgensen, D.S. Maxwell, J. TiradoRives, J. Am. Chem. Soc. 118 (1996) 11225.
[306] H. Frost, T. Duren, R.Q. Snurr, J. Phys. Chem. B 110 (2006) 9565.
[307] S.S. Han, W.A. Goddard, J. Phys. Chem. C 112 (2008) 13431.
[308] W.Q. Deng, X. Xu, W.A. Goddard, Phys. Rev. Lett. 92 (2004).
[309] H. Jobic, D.N. Theodorou, Micropor. Mesopor. Mater. 102 (2007) 21.
[310] G.K. Papadopoulos, H. Jobic, D.N. Theodorou, J. Phys. Chem. B 108 (2004) 12748.
[311] A.I. Skoulidas, D.M. Ackerman, J.K. Johnson, D.S. Sholl, Phys. Rev. Lett. 89 (2002) 185901.
[312] D.M. Ackerman, A.I. Skoulidas, D.S. Sholl, J.K. Johnson, Mol. Simul. 29 (2003) 677.
[313] J. Karger, D. Ruthven, Diffusion in Zeolites and Other Microporous Solids, 1992.
[314] S. Keskin, J.C. Liu, J.K. Johnson, D.S. Sholl, Micropor. Mesopor. Mater. 125 (2009) 101.
[315] E. Haldoupis, S. Nair, D.S. Sholl, J. Am. Chem. Soc. 132 (2010) 7528.
[316] A.I. Skoulidas, D.S. Sholl, J. Phys. Chem. B 109 (2005) 15760.
[317] Q. Yang, C. Zhong, ChemPhysChem 7 (2006) 1417.
[318] Q. Yang, C. Zhong, J. Phys. Chem. B 110 (2006) 17776.
[319] S. Wang, Q. Yang, C. Zhong, Sep. Purif. Technol. 60 (2008) 30.
[320] Q. Yang, C. Xue, C. Zhong, J.-F. Chen, AIChE J. 53 (2007) 2832.
[321] C.-Y. Xue, Q.-Y. Yang, C.-L. Zhong, Mol. Simul. 35 (2009) 1249.
[322] R. Krishna, J.M. van Baten, Langmuir 26 (2010) 2975.
[323] J. Jiang, AIChE J. 55 (2009) 2422.
[324] R. Babarao, J. Jiang, Energy Environ. Sci. 2 (2009) 1088.
[325] R. Babarao, J.W. Jiang, Ind. Eng. Chem. Res. 50 (2010) 62.
[326] Q. Xu, C. Zhong, J. Phys. Chem. C 114 (2010) 5035.
[327] D. Liu, C. Zheng, Q. Yang, C. Zhong, J. Phys. Chem. C 113 (2009) 5004.
[328] J. Perez-Pellitero, H. Amrouche, F.R. Siperstein, G. Pirngruber, C. Nieto-Draghi, G. Chaplais, A. Simon-Masseron, D. Bazer-Bachi, D. Peralta, N. Bats, Chem. -Eur. J. 16 (2010) 1560.
[329] A. Sirjoosingh, S. Alavi, T.K. Woo, J. Phys. Chem. C 114 (2010) 2171.
[330] S. Bourrelly, C. Serre, A. Vimont, N.A. Ramsahye, G. Maurin, M. Daturi, Y. Filinchuk, G. Ferey, P.L. Llewellyn, Stud. Surf. Sci. Catal. 170A (2007) 1008.
[331] N.A. Ramsahye, G. Maurin, S. Bourrelly, P.L. Llewellyn, T. Devic, C. Serre, T. Loiseau, G. Ferey, Adsorption 13 (2007) 461.
[332] A. Ghoufi, G. Maurin, J. Phys. Chem. C 114 (2010) 6496.
[333] Y.F. Chen, R. Babarao, S.I. Sandler, J.W. Jiang, Langmuir 26 (2010) 8743.
[334] C. Zheng, D. Liu, Q. Yang, C. Zhong, J. Mi, Ind. Eng. Chem. Res. 48 (2009) 10479.
[335] R. Babarao, J. Jiang, S.I. Sandler, Langmuir 25 (2009) 6590.
[336] Q. Yang, Q. Xu, B. Liu, C. Zhong, S. Berend, Chin. J. Chem. Eng. 17 (2009) 781.
[337] Y. Liu, D. Liu, Q. Yang, C. Zhong, J. Mi, Ind. Eng. Chem. Res. 49 (2010) 2902.
[338] B. Liu, B. Smit, Langmuir 25 (2009) 5918.
[339] D.S. Sholl, S. Keskin, H. Chen, S.E. Jee, Prepr. Symp.—Am. Chem. Soc., Div. Fuel Chem. 52 (2007) 671.
[340] S. Keskin, D.S. Sholl, Ind. Eng. Chem. Res. 48 (2009) 914.

[341] T. Watanabe, S. Keskin, S. Nair, D.S. Sholl, Phys. Chem. Chem. Phys. 11 (2009) 11389.
[342] A. Torrisi, R.G. Bell, C. Mellot-Draznieks, Cryst. Growth Des. 10 (2010) 2839.
[343] W. Mu, D. Liu, Q. Yang, C. Zhong, Micropor. Mesopor. Mater. 130 (2010) 76.
[344] R. Krishna, J.M. van Baten, Langmuir 26 (2010) 3981.
[345] R. Krishna, J.M. van Baten, Langmuir 26 (2010) 8450.
[346] D. Dubbeldam, R. Krishna, R.Q. Snurr, J. Phys. Chem. C 113 (2009) 19317.
[347] Y. Liu, H. Liu, Y. Hu, J. Jiang, J. Phys. Chem. B 114 (2010) 2820.
[348] P.B. Balbuena, D. Berry, K.E. Gubbins, J. Phys. Chem. 97 (1993) 937.
[349] Y.E. Cheon, M.P. Suh, Chem. -Eur. J. 14 (2008) 3961.
[350] B. Arstad, H. Fjellvag, K.O. Kongshaug, O. Swang, R. Blom, Adsorption 14 (2008) 755.
[351] H. Kanoh, A. Kondo, H. Noguchi, H. Kajiro, A. Tohdoh, Y. Hattori, W.C. Xu, M. Moue, T. Sugiura, K. Morita, H. Tanaka, T. Ohba, K. Kaneko, J. Colloid Interface Sci. 334 (2009) 1.